Josip Juraj Strossmayer University of Osijek
University of Dubrovnik
Ruđer Bošković Institute

Postgraduate Interdisciplinary University Study Programme in Molecular Biosciences

Iva Bazina

SYSTEMIC EFFECT OF Tff3 PROTEIN DEFICIENCY IN LONG-TERM HIGH-FAT DIET MOUSE MODEL

PhD thesis

Osijek, 2023.

BASIC DOCUMENTATION CARD

Josip Juraj Strossmayer University of Osijek **PhD thesis**
University of Dubrovnik
Ruđer Bošković Institute
University Postgraduate Interdisciplinary Doctoral Study of Molecular biosciences

Scientific Area: Interdisciplinary Area of Science
Scientific Fields: Biology, Basic Medical Sciences

SYSTEMIC EFFECT OF Tff3 PROTEIN DEFICIENCY IN LONG-TERM HIGH-FAT DIET MOUSE MODEL

Iva Bazina

Thesis performed at: Laboratory for Neurodegenerative Disease Research, Division of Molecular Medicine, Ruđer Bošković Institute

Supervisor: Mirela Baus Lončar, PhD, Senior research associate Ruđer Bošković Institute

Short abstract:
The Tff3 protein exhibits ubiquitous expression and functions. It is involved in various physiological and pathophysiological processes, including metabolic and neurodegenerative diseases. A high-fat diet is known to induce features of both diseases. *Tff3*-/- mice and WT controls were subjected to long-term HFD, metabolic testing, as well as liver and hippocampal tissue analysis. The *Tff3*-/- genotype showed a protective effect on metabolic syndrome traits.

Number of pages: 123
Number of figures: 28
Number of tables: 7
Number of references: 237
Original in: English
Key words: Trefoil factor 3, metabolism, high-fat diet, neurodegeneration

Date of the thesis defense:

Reviewers:
1. Prof. dr. sc. Slavica Kvolik. PhD, Full Professor with tenure, Faculty of Medicine, Josip Juraj Strossmayer University of Osijek, president of commission
2. Silva Katušić Hećimović, PhD, Senior scientist, Ruđer Bošković Institute, Associate Professor, Josip Juraj Strossmayer University of Osijek, member
3. Prof. dr. sc. Ljubica Glavaš-Obrovac, PhD, Full Professor with tenure, Faculty of Medicine, Josip Juraj Strossmayer University of Osijek, member

Thesis deposited in: National and University Library in Zagreb, Ul. Hrvatske bratske zajednice 4, Zagreb; City and University Library of Osijek, Europska avenija 24, Osijek; Josip Juraj Strossmayer University of Osijek, Trg sv. Trojstva 3, Osijek

TEMELJNA DOKUMENTACIJSKA KARTICA

Sveučilište Josipa Jurja Strossmayera u Osijeku **Doktorska disertacija**
Sveučilište u Dubrovniku
Institut Ruđer Bošković
Poslijediplomski interdisciplinarni sveučilišni studij Molekularne bioznanosti

Znanstveno područje: Interdisciplinarno područje znanosti
Znanstvena polja: Biologija, Temeljne medicinske znanosti

SISTEMSKI UČINAK NEDOSTATKA Tff3 PROTEINA U MIŠJEM MODELU VISOKOMASNE PREHRANE

Iva Bazina

Disertacija je izrađena u: Laboratoriju za istraživanje neurodegenerativnih bolesti Zavoda za molekularnu medicinu Instituta Ruđer Bošković

Mentor: dr.sc. Mirela Baus Lončar, Viša znanstvena suradnica Instituta Ruđer Bošković

Kratki sažetak doktorske disertacije:
Tff3 protein je široko rasprostranjen protein s mnogo funkcija. Uključen je u brojne fiziološke I patofiziološke procese, uključujući one metaboličke i neurodegenerativne. Visokomasna prehrana može uzrokovati obilježja obiju patologija. Tff3-/- i WT miševi bili su izloženi visokomasnoj prehrani, povrgnuti metaboličkim testovima, te im je analizirano tkivo jetre i hipokampusa. *Tff3*-/- genotip pokazao je protektivni učinak na značajke metaboličkog sindroma.

Broj stranica: 123
Broj slika: 28
Broj tablica: 7
Broj literaturnih navoda: 237
Jezik izvornika: Engleski
Ključne riječi: Trefoil factor 3, metabolizam, visokomasna prehrana, neurodegeneracija

Datum obrane:

Stručno povjerenstvo za obranu:
1. prof. dr. sc. Slavica Kvolik, redovita profesorica Medicinskog fakulteta Sveučilišta Josipa Jurja Strossmayera u Osijeku, predsjednica
2. izv. prof dr. sc. Silva Katušić Hećimović, znanstvena savjetnica Instituta Ruđer Bošković u Zagrebu i izvanredna profesorica u naslovnom znanstveno-nastavnom zvanju Sveučilišta Josipa Jurja Strossmayera u Osijeku, članica
3. prof. dr. sc. Ljubica Glavaš-Obrovac, redovita profesorica Medicinskog fakulteta Sveučilišta Josipa Jurja Strossmayera u Osijeku, članica

Disertacija je pohranjena u: Nacionalnoj i sveučilišnoj knjižnici Zagreb, Ul. Hrvatske bratske zajednice 4, Zagreb;Gradskoj i sveučilišnoj knjižnici Osijek, Europska avenija 24, Osijek; Sveučilištu Josipa Jurja Strossmayera u Osijeku, Trg sv. Trojstva 3, Osijek

This doctoral dissertation was prepared in the Laboratory for Neurodegenerative Disease Research, Division of Molecular Medicine, Ruđer Bošković Institute, under mentorship of Mirela Baus Lončar, PhD, Senior research associate RBI, within the framework of the research project "Tff3 protein at intersection of metabolism and neurodegeneration" (HRZZ-IP-2016-06-2717). This research was funded by the Croatian Science Foundation

(grant IP-06-2016-2717) and the European Structural Funds 2014-2020 as financial support for PhD student I. Bazina.

Contents

1 Introduction

1.1 Trefoil factor family of proteins

Trefoil factor 3 (Tff3) 3 protein is a small secretory protein of the trefoil factor family. This small family of three owes its name to the characteristic trefoil-like spatial conformation, which consists of six disulphide-linked cysteine residues in a 38- or 39-amino-acid sequence (1–4) known as the trefoil (1) or p (4) domain. The trefoil domain enables resistance to digestion by proteases (5–7), which is important for secretion into the gastrointestinal environment, the major site of their activity (8–10). TFFs are predominantly secreted in the mucosa covering the normal epithelium. Goblet cells scattered through the epithelia are the main site of TFF synthesis. Proteins from the trefoil factor family are involved in maintaining mucosal integrity and their accumulation is rapidly increased at the margins of gastrointestinal tract injury (11–14). Normal repair of the epithelium requires restitution and regeneration, with restitution (Figure 1) being the critical first phase required to restore epithelial continuity (15).

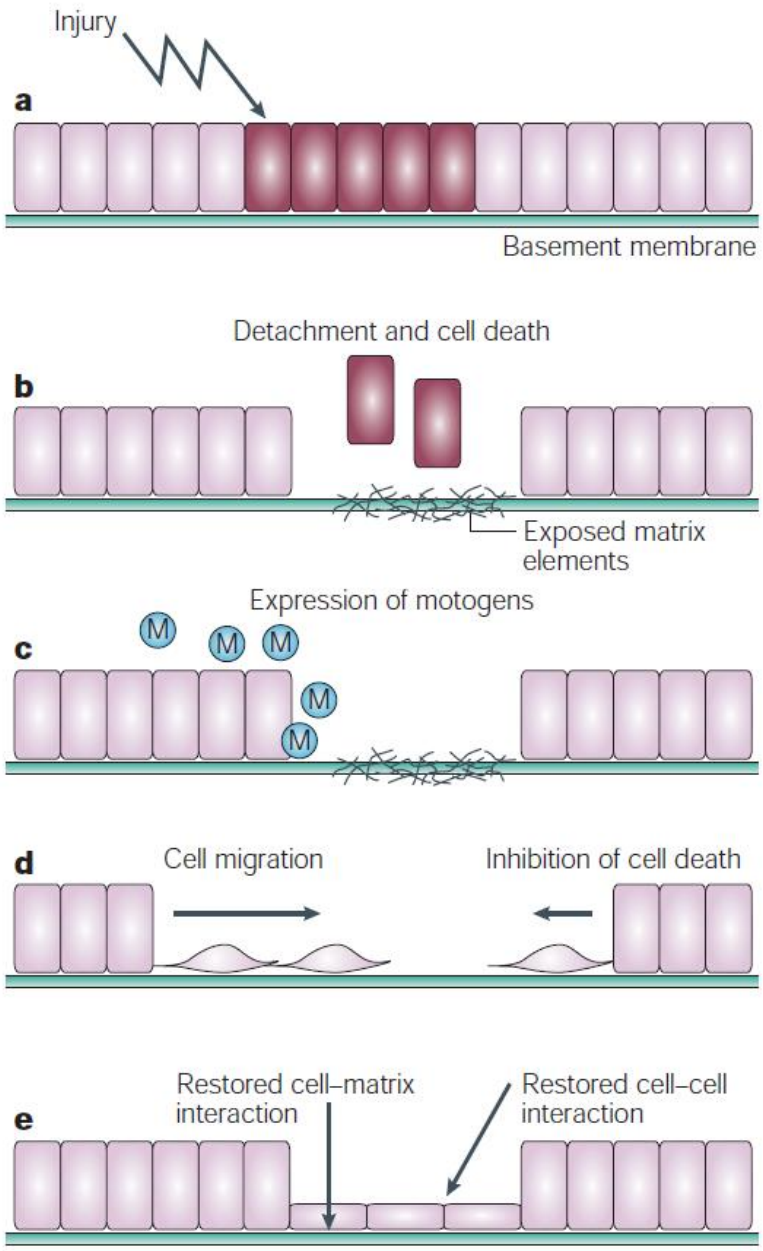

Figure 1. Key steps of restitution. Injury to mucosal epithelial cells (a) results in cell detachment and death (b). Elements required for rapid repair (motogens-M) are expressed by adjacent cells and exposed matrix elements (c). The remaining surviving epithelial cells migrate to the site of injury, accompanied by inhibition of cell death caused by detachment (d). Finally, cell-cell and cell-matrix interactions restructure (e).

Material from: Taupin, D., Podolsky, D. Trefoil factors: initiators of mucosal healing. *Nat Rev Mol Cell Biol* **4**, 721–732 (2003). https://doi.org/10.1038/nrm1203 (16)

Reproduced with permission from Springer Nature (license number: 5466331380060)

The trefoil family includes three members, known since 1997 by the standardized nomenclature TFF1-3 (17). The abbreviation for the human trefoil factor protein is TFF, for the murine Tff, and gene names are written in italics (*TFF* and *Tff*). TFF1, formerly known as pS2 (18), and TFF3, formerly ITF (7), have a single trefoil domain, whereas TFF2, formerly PSP (5), has two. Tff3 and Tff1 have an additional free cysteine residue that is critical for dimer formation. They can form both homodimers and heterodimers with each other (19). Tff family genes are mapped to murine chromosome 17q (20,21) and human chromosome 21q22.3 (22) and are evolutionarily conserved (23,24), suggesting an important function in the organism. Functions of the trefoil protein family are summarized in Figure 2.

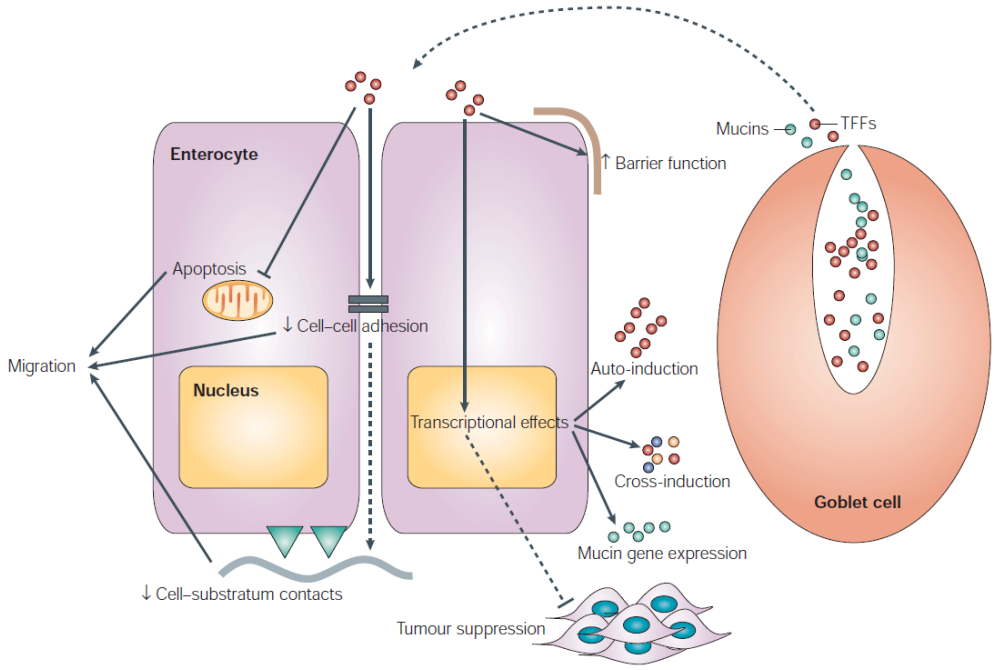

Figure 2. Functions of trefoil protein family. Secretion of trefoil protein (red circles) is coordinated with secretion of mucins (green circles). Secreted TFFs can act extracellularly (enhancing barrier function) or intracellularly (transcriptional and signaling role). They have a role in apoptosis, migration, tumor suppression, and cell adhesion. *TFF* expression can be regulated through auto-induction and cross induction of other TFFs.

Material from: Taupin, D., Podolsky, D. Trefoil factors: initiators of mucosal healing. *Nat Rev Mol Cell Biol* **4**, 721–732 (2003). https://doi.org/10.1038/nrm1203 (16)

Reproduced with permission from Springer Nature (license number: 5466331380060)

1.1.1 Trefoil factor 3 protein

Tff3 was first described in primary cell cultures of rat enterocytes in 1991 (7). Its main function is the maintenance of the intestinal mucosa, which was first described in 1996 (15). Whole-body Tff3 knockout (*Tff3*-/-) mice were much more sensitive to mild injury of the colonic epithelium with ulceration than wild-type (WT) controls. Half of them developed bloody diarrhea and died, whereas only 10% of WT mice developed bloody diarrhea and 5% died. Treatment with recombinant TFF3 restored normal restitution. Restitution (Figure 2) starts rapidly in response to small surface lesions of epithelium (25). It involves cell dedifferentiation, cytoskeletal reorganization, anoikis blocking, migration and cell redifferentiation at the site of injury (16,25). TFF3 can reduce adhesion between cells (17,26) and inhibit apoptosis (6,27), thereby promoting epithelial cell survival and migration. It has also been associated with cell proliferation and differentiation (7,28). Tff3 has been repeatedly shown to be involved in maintaining the intestinal barrier by reducing intestinal permeability (29–35).

Tff3 is the most prevalent of the three trefoil factors. The colon is the predominant site of expression for Tff3 (9,12,15,24), but it is present throughout the body. TFF3 has been found in the liver (9,12,36–42), brain (43–48) and cerebrospinal fluid, biliary tree (9,49–51), pancreas (9,12,52–54), lymphoid tissue (9,55–57), small intestine (9,12,24), stomach (4,9,12,24,42,55,58), esophagus (9,12), salivary glands (9,59) and saliva (59), respiratory tract (9,60–62), breast (9,63) and breast milk (64), uterus (9,58,65), prostate (9), urinary tract (9,66–68) and urine (67,69,70), bone (71), cartilage (72,73), eye (74,75) and tears (76), ear (77,78), and nasal mucosa (79,80).

Given its ubiquitous distribution, it is not surprising that TFF3 is involved in many pathologies. As expected, it plays an important role in inflammatory bowel diseases (81). In cancers, including gastric, colon, lung, thyroid, and breast cancers, it is markedly upregulated and plays an important role in tumor progression (82). Resistance to tumor cell apoptosis, proliferation, angiogenesis, and metastasis are hallmarks of cancer progression. TFF3 is involved in all four via the mitogen-activated protein kinase

(MAPK)/ERK, PI3K/AKT, STAT3, and hypoxia-inducible factor (HIF)-1α signaling pathways (83). In addition, it is involved in metabolic and neurological pathophysiology, which will be discussed in detail in a separate section below.

1.1.2 Interactive proteins and receptors of Tff3

Several binding partners of Tff3 were discovered early: mucin2 (MUC2) (84), IgG Fc-binding protein (FCGBP) and deleted in malignant brain tumor 1 protein (DMBT1). MUC2 and Tff3 are colocalized, secrete together, and are components of mucus (85). Tffs can migrate more rapidly to the injury site in association with MUC 2 (86). The TFF3–FCGBP complexes may play a role in the innate immune defense of mucosal epithelial cells (87,88). The role of the DMBT1-Tff3 interaction is still unclear (89). Tff3 may exert its pro-invasive role indirectly through the thromboxane A2 receptor (TXA2-R) and PG-R receptors (90,91). Tff3 has been identified as a low affinity ligand for C-X-C chemokine receptors (CXCR) 4 and 7 (92) and protease activated receptor 2 (PAR-2) (93). CXCR receptors mediated cell migration and PAR-2 cytokine trafficking. Recent advances in receptor research showed that LINGO2 was a key to Tff3 reactivity (94). Their interaction induced EGFR signaling, which is involved in wound healing and immunity.

1.1.3 Trefoil factor 3 in the context of metabolism

Numerous research articles show a clear link of Tff3 to metabolism. The first association between Tff3 and metabolism was established in Tally-Ho mice, a polygenic mouse model of diabesity, a term coined to describe a phenotype characterized by obesity and diabetes (41). In the livers of 7-week-old mice, representing an early stage of pathology, Tff3 mRNA was virtually undetectable, whereas it remained transcriptionally active in the livers of the control group. A reduction in Tff3 expression was also found in other genetic (obese mice - ob/ob and diabetic mice - db/db) and dietary (DIO) models of obesity

(36,37), as well as in the model of hepatic steatosis. It has been shown that food intake can regulate the expression of Tff3 in the small intestine, as it was significantly upregulated in fasting mice compared to fed mice and then reduced by feeding (42). In contrast, in a human study, food intake decreased serum Tff3 levels, as did insulin administration in patients with type 1 diabetes (93). In the same study, treatment with insulin and glucose resulted in a reduction of Tff3 in the HT -29 colon cell line.

The expression of hepatic Tff3 was significantly decreased in NAFLD mouse models (db/db, ob/ob, and DIO obese mice), suggesting that Tff3 is a potential marker gene for NAFLD (36). Tff3 reduction was followed by lower expression of genes involved in beta-oxidation and an apparent fatty liver phenotype that was alleviated by adenovirus-mediated restoration of Tff3 expression (Ad-Tff3). This was likely accomplished by binding of Tff3 to *Pparα* promoter, as evidenced by Chromatin immunoprecipitation (ChIP) assay. In contrast, adenovirus-mediated knockdown of Tff3 (Ad-shTff3) in C57BL/6J mice resulted in an obvious fatty liver phenotype.

It has been reported several times that overexpression or administration of recombinant TFF3 in mice results in improved glucose tolerance and insulin sensitivity, as well as decreased expression of genes involved in gluconeogenesis (G6pc, PEPCK, PGC1a) (37,42). Body weight, fasting insulin, triglyceride, cholesterol and leptin levels are not affected by TFF3 treatment (42). Tff3 was identified as a downstream target gene of UDP-galactose 4-epimerase (GALE), the final enzyme of galactose metabolism (40). Gale-overexpressing mice had suppressed expression of Tff3 in the liver. Restoration of Tff3 expression ameliorates the impaired glucose metabolism characteristic of this strain of mice.

Overall, the different mouse models show a reduction of Tff3 in the liver during metabolic stress and an alleviation of symptoms by restoring Tff3, suggesting a protective effect of Tff3 *in vivo.*

Adenoviral overexpression of Tff3 in primary mouse hepatocyte culture resulted in inhibition of gluconeogenesis genes. In mouse and human pancreatic cells, it led to increased proliferation of beta cells (95). The expression of *Tff3* in rat pancreatic cell cultures and INS -1 (beta cell model) was stimulated with growth hormone, which stimulates beta cell proliferation (52). Co-localization of Tff3 and insulin in beta cells has also been reported (52).

Valuable data on the physiological function of the Tff3 protein have been obtained using Tff3 knockout mice (38,96). Given the protective effects of Tff3 described in the above paragraph, one would expect that a whole-body Tff3 knockout would have adverse effects, but in the context of glucose metabolism, this is not the case. Whole-body Tff3 knockout mice of mixed genetic background (Sv129/C57Bl6) exhibited improved glucose tolerance and insulin sensitivity compared with controls (38). These mice had increased numbers of small lipid vesicles in the liver compared with control mice (WT), but no obvious signs of hepatic steatosis. They also showed decreased accumulation of Pparγ and Sirt-1 proteins (involved in the regulation of lipid metabolism) and a different fatty acid composition. The mice of both genotypes had similar body weights. In another study, *Tff3*-/- mice of the same strain but without age specification had significantly lower body weight than their WT counterparts (96). MicroRNA analysis identified 21 deregulated miRNAs in the blood of the same mouse strain compared with WT mice. The majority of deregulated miRNAs were associated with the glycolysis/gluconeogenesis pathway.

Presently, only one study of Tff3 has been performed in the context of metabolism in humans (93). In this work, patients suffering from type 1 diabetes had lower serum Tff3 levels than healthy controls. Tff3 levels increased in healthy donors after consumption of food and in patients after administration of insulin.

1.1.4 Trefoil factor 3 and the central nervous system

As mentioned earlier, Tff3 is found in most regions of the brain. The mRNA expression of Tff3 was first detected in the rat hypothalamus and at very low levels in the cortex, brainstem and cerebellum (97). Localization detected by *in situ* hybridization was confirmed by immunohistochemistry only in the hypothalamus. Subsequently, it was detected in the human hypothalamus and pituitary gland and classified as a new neuropeptide (98). Later studies confirmed its localization in the hypothalamic-pituitary axis and reported co-localization with oxytocin (47,99,100). Its presence in the posterior lobe of the pituitary gland suggests a probable release into the bloodstream (47). Systemic screening of the adult human brain with three well-characterized TFF3 antibodies revealed localization of the Tff3 protein in neurons of the cerebral cortex, hippocampus, amygdala, basal ganglia, thalamus, cerebellum, brainstem, and midbrain (44). In mouse brain Tff3 expression is expressed in hippocampus, temporal cortex (46), and cerebellum (46,101), with the cerebellum being the predominant site of expression (46). It has also been detected in the developing brain of mice (46) and humans (44), suggesting a possible developmental role.

Most research reports neuronal localization of Tff3 (44–46). Arnold et al (48) found Tff3 in astrocytes in rat primary cortical cell cultures, and its transcription was reduced by incubation with LPS. Fu et al. (45) detected Tff3 in astrocytes, and they showed Tff3 expression in neurons and microglia of rat primary cortical and hippocampal cell cultures. They even showed co-localization of Tff3 with Iba1 and Map2, cell markers for microglia and neurons, respectively. Co-localization with Map2 was confirmed *in vivo* in rat cerebellum tissue. Because microglia are in an activated state in cell cultures, Tff3 expression in microglia is thought to be activated when inflammation occurs. Although Tff3 is widely expressed and most likely plays an important role in brain physiology, its function still remains unexplored.

In vivo data show that intraperitoneal (i.p.) administration of Tff3 has an antidepressant effect on behavioral tests in mice (102). The level of Tff3 in the basolateral amygdala

increased half an hour after i.p. injection, suggesting that it can cross the blood-brain barrier. Negatively charged liposomes loaded with Tff3 were successfully transported across the blood-brain barrier *in vitro* and by monocytes, and showed antidepressant-like effects *in vivo* in mice and rats (103). Rat model of depression caused by olfactory bulbectomy exhibits behaviors comparable to those of depression patients (104). Intraperitoneal injection of recombinant TFF3 over a 7-day period improved performance of these rats on standard behavioral tests. Bulbectomy of the olfactory organ resulted in a decrease in BDBF (brain-derived neurotrophic factor), pPERK1, and pCREB levels, which were restored by treatment with Tff3 in the CA1 region of the hippocampus. They showed that BDNF was a key mediator of this effect. In addition to depression, pharmacological effects of Tff3 have also been studied in anxiety (105), learning and retention (102), and addiction (106) research. TFF3 showed a dose-dependent anxiolytic or anxiogenic effect, with lower doses being anxiolytic and higher doses being anxiogenic (105). Mice pre-treated with recombinant TFF3 showed better performance on tests of learning and retention of novel objects (102). In mice with morphine dependence, naloxone induced withdrawal symptoms were alleviated upon TFF3 administration, possibly through decreased activation of hypothalamic-pituitary activity (107).

Altered expression of Tff3 has been associated with various neuropsychiatric pathologies in the brain. Schizophrenia patients had increased *TFF3* gene expression in peripheral blood mononuclear cells (108). Tff3 gene expression is downregulated in the prefrontal cortex of mouse model of alcoholism (109). *TFF3* expression is increased in dopaminergic neurons of midbrain, main source of dopamine in mammals (110). Loss of midbrain dopaminergic neurons is a hallmark of Parkinson's disease. Kriks et al. showed significantly increased Tff3 expression *in vitro* in dopaminergic neurons derived from ES cells. Later, a significant reduction was found in the serum of PD patients compared to healthy controls (111). This was particularly pronounced in male patients and correlated significantly with disease severity.

Analysis of potential biomarkers of neurodegeneration in CSF of Alzheimer disease patients detected TFF3 protein as the most promising candidate (112). TFF3 protein

levels in the CSF of AD patients were significantly reduced compared to healthy controls, and Tff3 levels correlated with the extent of whole brain atrophy, hippocampal atrophy, and ventricular expansion.

Mouse model of Tff3 protein deficiency (*Tff3-/-*) on mixed genetic background (C57Bl6J /Sv129) contributed to research of Tff3 in nervous system. When this strain was developed, it was characterized as "grossly indistinguishable" from the WT mouse and did not exhibit any noticeable developmental problems (15). However, *Tff3-/-* mice were later found to show signs of accelerated presbycusis and hearing loss at advanced ages, suggesting a role for neurosensory signaling (113). They had no morphological changes in the middle compared to WT mice. Tff3 protein was detected in cochlea. The search for possible interaction partners pointed to Y2H-HLA-B-associated transcript 3 (Bat3 or Bag6), a protein known for its role in regulating apoptosis induced by endoplasmic reticulum stress.

Tff3 is not only synthesized in the brain but can also reach there from the periphery (114). In response to experimental cerebral ischemia/reperfusion injury in WT mice, Tff3 levels were upregulated in the liver and subsequently in serum. Tff3 was shown to cross the blood-brain barrier and accumulate at the site of injury. In addition, *Tff3-/-* mice exhibited significantly higher neuronal death than WT mice, which was mitigated by the application of recombinant Tff3 through attenuation of caspase-3 activity. Another study also showed more pronounced brain infarct volume in Tff3-/- mice than WT mice (115).

1.2 Mouse model

First developed *Tff3-/-* mouse model was maintained on mixed genetic background (C57BL6J/Sv129) (15). This implies that research results may be influenced by genetic heterogeneity due to unpredictable combinations on different loci and possible additional mutations (116). In many scientific papers, the mouse model used is simply referred to

as C57BL/6, which is not sufficient because this strain has branched into more than 20 different sub-strains with genetic and phenotypic differences (117).

The most used substrains are C57BL/6J and C57BL/6N. The C57BL/6 J mouse has a multiexon deletion of the nicotinamide nucleotide transhydrogenase (Nnt) gene and exhibits impaired insulin secretion and glucose homeostasis (118). Nnt is an important mitochondrial protein, one of several enzymes that catalyze the generation of NADPH (119). An adequate supply of NADPH to mitochondria is essential for ATP synthesis, and thus for insulin release (120). Loss of Nnt activity in 6J mice results in a decreased ability to detoxify reactive oxygen species, thus impairing various processes and immunological responses. Recently, it was reported that granzyme A (GZMA)-deficient mice on mixed 6N/6J gene background showed improvement in arthritic symptoms that was not due to the absence of GZMA but to the presence of Nnt, as knockout mice on mixed background expressed Nnt but the 6J control mice did not (121). This highlights the importance of considering the influence of genetic background.

The mouse model used in this study is a newly developed congenic *Tff3-/-* strain on a C57BL/6N genetic background (39). It was generated by crossing males of the existing mixed background *Tff3−/−*/C57BL6/J/SV129 strain with C57BL6/N females using the speed congenics method (122). The end result was mice that differed from the WT control only in the protein of interest and a small portion around it.

1.3 Aims of the research

Metabolic and neurodegenerative diseases, especially Alzheimer's disease and diabetes, are among the greatest public health burdens of today. They are multifactorial diseases with complex pathogenesis for which no developmental mechanism or means of prevention and treatment are known. Underlying both diseases are disorders of insulin signaling and energy metabolism, as well as common molecular pathways (123). The overall structural and functional integrity of the central nervous system is impaired under

conditions of insulin resistance (124). Additionally, magnetic resonance imaging shows similarities between brain atrophies in type 2 diabetes and early Alzheimer's disease patients (125). Epidemiological data show that type 2 diabetes is a risk factor for the development of AD (126) and excessive body weight is a risk factor for both diseases Induction of nonalcoholic fatty liver disease (NAFLD) by a high-fat diet worsened neurodegenerative symptoms in AD mouse model after 2,5 months, and only one year of HFD treatment was sufficient to induce AD traits in WT mice (127).

In this study, male and female *Tff3-/-*/C57BL/6N mice and corresponding WT controls were exposed to high levels of HFD for 8 months. The aim was to elicit the features of the metabolic syndrome and to determine whether the absence of Tff3 causes a difference in the response to this stress. In addition, to determine how this stress affects the hippocampus, whether it leads to disruption of hippocampal integrity, and whether this is different in *Tff3-/-* and WT animals

1.3.1 Hypothesis

1. Long-term HFD exposure will decrease *Tff3* expression in WT animals.
2. Metabolic status (body weight, glucose homeostasis, fatty liver phenotype) will be improved in *Tff3-/-* mice compared with WT.
3. The gene expression profile affected by stress imposed on mice by HFD will be favorable in *Tff3-/-* mice.
4. The absence of Tff3 in *Tff3-/-* mice will cause greater changes in hippocami in response to HFD.

2 Materials and methods

2.1 Animals

A mouse strain lacking trefoil factor family 3 (Tff3) protein on C57BL/6NCrl (Charles River) genetic background (*Tff3-/-*/C57BL/6NCrl), developed from an existing mixed background strain (C57BL/6J/SV129) using a 'speed congenics' approach and a corresponding C57BL/6NCrl (WT) strain were used in all experiments. Mixed background *Tff3*$^{-/-}$ males were crossed with C57BL6/NCrl females, offspring was genotyped, and heterozygote *Tff3*−/+males were analyzed for 500 SNP polymorphisms (ENVIGO) to identify the *Tff3*-/+ male most similar to the C57BL6/NCrl strain. This approach was used for five consecutive back crossings to identify the male carrier with 99.99% resemblance to the C57BL6/NCrl strain regarding relevant SNP loci. Resulting offspring were set up to mate according to a brother x sister scheme, homozygous *Tff3*−/− male and female mice (F0 generation) were detected and used to start a new *Tff3*−/−/C57BL6/NCrl strain. This new strain differs from WT mice only in the *Tff3* region and a small surrounding fragment, ensuring that the observed phenotype is a consequence of Tff3 protein inactivation. The mice were raised at the Facility for laboratory animals of the Ruđer Bošković Institute as part of the project "Tff3 protein at intersection of metabolism and neurodegeneration" (HRZZ-IP-2016-06-2717), funded by the Croatian Science Foundation. Animal breeding and all experimental procedures were performed in accordance with the Animal Welfare Law (NN 102/17, 32/19) and Ordinance on the Protection of Animals Used for Scientific Purposes (NN 55/13, 39/17, 116/19). The research was approved by the Bioethics Committee of the Ruđer Bošković Institute and by the National Council of the Ministry of Agriculture of the Republic of Croatia (CLASS: UP/I-322-01 /19-01 /14 RN: 525-10/0255-19-3 Zagreb, July 5, 2019, and CLASS: UP/I-322-01/16-01/81, RN: 525-10/0543-21-6 Zagreb, February 18, 2021). Animals were kept under standard conditions, i.e., 12-hour light-dark cycle, temperature of 22°C and humidity of 60%.

2.2 High fat diet treatment

A group of animals consisting of 10 male WT, 10 male *Tff3-/-*, 10 female WT, and 10 female *Tff3-/-* mice was fed a high-fat diet (HFD) (E15742-34(E15742-34, ssniff-Spezialdiäten GmbH, Germany) from weaning at 4 weeks of age until sacrifice 36 weeks later. The diet consisted of 24.4% crude protein, 34.6% crude fat, 6.0% crude fiber, 5.5% crude ash, 0.1% starch, and 9.4% sugar. In addition, an equally composed control group was fed a standard diet (SD) (4RF21, Mucedola, Italy).

2.3 Metabolic tests

Intraperitoneal glucose and insulin tolerance tests were performed halfway through HFD treatment and at the end of treatment on 10 animals per group (WT male, *Tff3-/-* male, WT female, *Tff3-/-* female), both HFD and SD animals, with two weeks between tests for recovery. Animals were weighed immediately before testing and appropriate doses of glucose or insulin were administered.

2.3.1 Intraperitoneal glucose tolerance test

The intraperitoneal glucose tolerance test (IPGTT) was performed according to the protocol of the International Mouse Phenotyping Resource of Standardised Screens (128) at 21 (17 weeks of HFD) and 36 (32 weeks of HFD) weeks of age. Before the test, mice were kept fasting for 16 hours, with water available ad libitum, from 6:00 pm to 10:00 am. Glucose levels were measured with a glucometer (Accu-Chek® Performa, Roche, Switzerland) from a venous blood drop taken at the beginning of the test (0 minutes) before glucose application and 15, 30, 60, and 120 minutes after application by cutting the tail tip. Sterile glucose (2 g/kg D (+)-Glucose, CELLPURE® (Carl Roth GmbH,

Germany) 1XPBS (phosphate-buffered saline, 137 mM NaCl, 2.7 mM KCl, 4.3 mM Na_2HPO_4, 1,4 mM KH_2PO_4, pH 7.4) was injected intraperitoneally.

2.3.2 Intraperitoneal insulin tolerance test (IPITT)

Mice were given two weeks to recover from the IGTT before the intraperitoneal insulin tolerance test (IPITT) was performed at 23 (19 weeks on HFD) and 38 (34 weeks on HFD) weeks of age. The test followed the guidelines of the National Mouse Metabolic Phenotyping Center (129). The test was carried out after a 4-hour fasting period, from 8:00 am to 12:00 pm. Glucose levels were measured from tail vein blood before administration of insulin, at 0 minutes, 0.75 IU/kg of insulin (Humulin® R, Eli Lilly, Canada) in sterile 1X PBS was injected intraperitoneally and glucose levels were measured 15,30,45,60, and 120 minutes after injection.

2.4 Tissue sample collection

Mice were sacrificed at 40 weeks of age, that is, after 38 weeks of HFD treatment, in two different ways.

2.4.1 Fresh frozen tissue

Half of the mice, 5 per group (WT♂, *Tff3-/-*♂, WT♀, *Tff3-/-* ♀,), were anesthetized with isoflurane (Isofluran-Piramal, Piramal Healthcare, UK). Once animals were under deep anesthesia, as confirmed by toe pinch method, blood was collected from the jugular vein for subsequent biochemical analysis, followed by cervical dislocation. The head was detached from the body and a midline incision was made through the skin from the neck to the nose to expose the skull. The remaining tissue was removed to gain access to the foramen magnum, through which two lateral incisions were made, taking care not to

damage the brain. A third incision was made along the midline and the skull was removed. The brain was removed, divided into two hemispheres, and the hippocampus was isolated. The skin and abdominal wall were cut open, and the liver was carefully separated from the other organs and removed. The tissues were rinsed in 1X PBS, snap frozen in liquid nitrogen, and stored at -80 °C until further processing.

2.4.2 Perfusion for morphological analysis

The other half of the animals (5 per group) were anesthetized with isoflurane to the point of surgical plane of anesthesia and whole-body transcardial perfusion fixation was performed. Before perfusion, 1X PBS and 4% paraformaldehyde (4% PFA, dissolved in 1XPBS, pH 7.4,) (Carl Roth GmbH, Germany) were prewarmed to 37 °C in a bath. A perfusion system (see Figure 3) was set up as follows: A perfusion line (Original Perfusor® Line PVC, B. Braun, Germany) from a bottle containing 1X PBS and a line from a bottle containing 4% PFA converged at a valve (Discofix®C 3-way stopcock, B. Braun, Germany). From there, a common line ran through the pump to the infusion set with bubble trap (Medicina Trgovina, Croatia) and then to the rounded tip cannula (Braun, Germany) attached to the end of the line. The system was primed with warm 1X PBS, ensuring no bubbles were present. The integument and abdominal wall were cut open, and the liver was carefully separated from the diaphragm, which was cut, as were the ribs on both sides. The sternum was lifted to expose the heart. A small incision was made at the posterior end of the left ventricle, a cannula was inserted through the incision into the ascending aorta, and the outlet in the right atrium was cut open. The flow rate was set at 5 ml/min. Whole body was first perfused with sterile 1xPBS to clear the organs of blood so that it would not fix. A clear liver was used as an indicator of successful perfusion. Following clearance, 4% PFA was passed through the system. Fixation tremors served as evidence of successful fixation. After fixation, the liver and the brain were placed in fresh 4%PFA, 10% formalin, or Ito's fixative, depending on which procedure they were intended for.

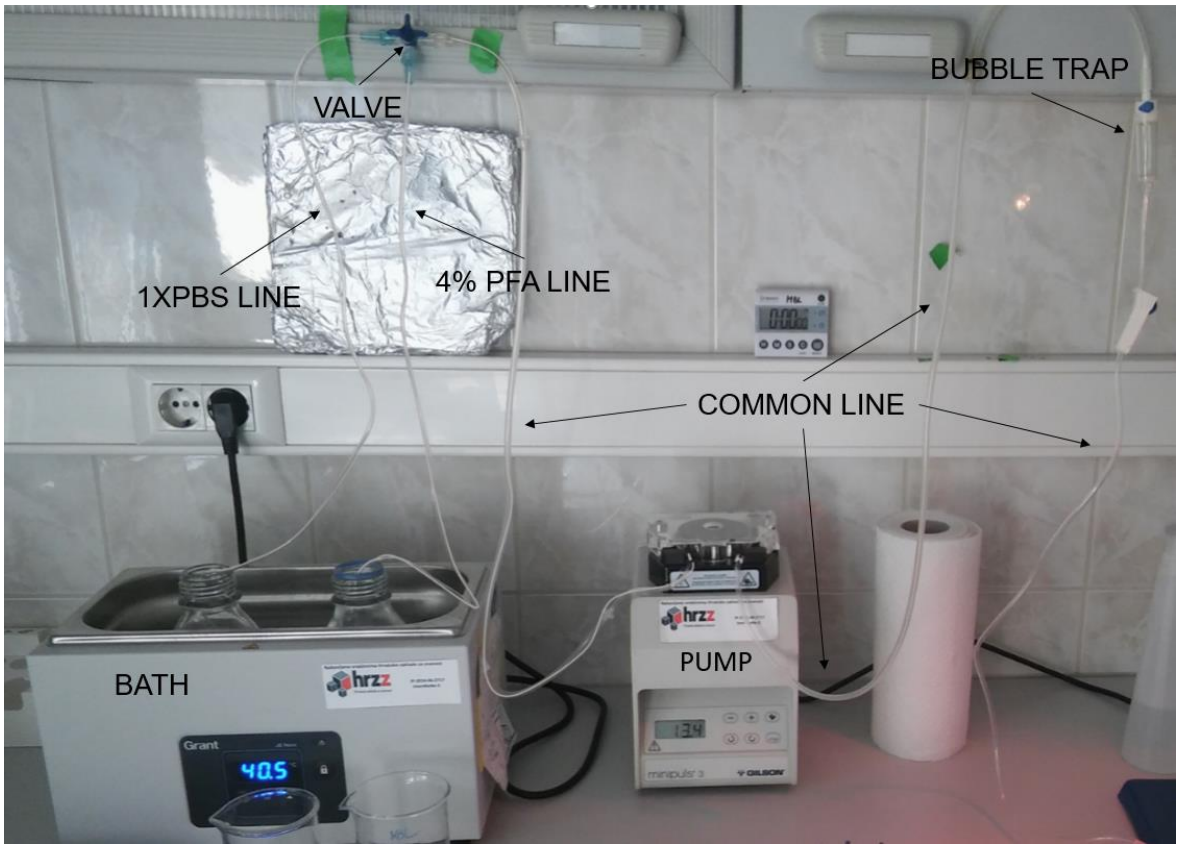

Figure 3. Perfusion system setup. A perfusion line from a bottle containing 1X PBS and a line from a bottle containing 4% PFA converges at a valve. From there, a common line runs through the pump to the infusion set with bubble trap and then to the rounded tip cannula attached to the end of the line.

2.5 Blood biochemistry

Blood samples taken before sacrifice were collected in tubes without anticoagulants, left at room temperature for at least one hour to clot, and centrifuged at 1500 g for 15 minutes in the Eppendorf 5415R refrigerated centrifuge. Supernatant serum was collected in clean tubes and stored at -80 °C. Serum levels of total cholesterol, high-density lipoprotein (HDL), low-density lipoprotein (LDL), triglycerides (TG), glucose, aspartate transaminase (AST), alanine transaminase (ALT), urea, total proteins (TP), uric acid, alkaline phosphatase, and C-reactive protein (CRP) were determined using Architect c8000 clinical chemistry analyzer (Abbot, USA).

2.6 Quantitative polymerase chain reaction (qPCR)

2.6.1 Total RNA isolation and cDNA synthesis

Frozen liver tissues from mice of both genotypes, both sexes and both diets (5 per group) were homogenized with mortar and pestle, and total RNA isolated using the NucleoSpin RNA kit (MACHEREY-NAGEL, Germany) according to the manufacturer's instructions. Briefly, the homogenized tissue was lysed with lysis buffer supplemented with 2-mercaptoethanol (Sigma-Aldrich, USA), the lysate was filtered, mixed with ethanol, and transferred to the RNA binding column. The DNA was digested, and the RNA was washed and eluted. RNA concentration and purity were checked using NanoPhotometer® N60 (Implen GmbH, Germany). A260/ A280 values of ~2.0 and A260/A230 of 2.0-2.2 were acceptable. RNA was then transcribed into cDNA using the High-Capacity cDNA Reverse Transcription Kit (Applied Biosystems, Germany) according to the manufacturer's protocol. The reaction was performed in the Veriti™ 96-Well Fast Thermal Cycler (Applied Biosystems, Germany) in the presence of RNase inhibitor (Applied Biosystems, Germany) with the following cycling conditions: 10 min at 25 ˚C, 120 min at 37 ˚C, 5 min at 85 ˚C. The reaction mixture consisted of 10 µl RNA (1,5 µg) and 10 µl of reverse transcription (RT) mastermix, shown in Table 1.

Table 1. Master mix for reverse transcription for a single reaction. Taken and adapted from the High Capacity cDNA Reverse Transcription Kit user guide

Component	Volume (µl)
10X RT Buffer	2.0
25X dNTP Mix (100 mM)	0.8
10X RT Random Primers	2.0
MultiScribe™ Reverse Trascriptase	1.0
RNase Inhibitor	1.0
Nuclease-free H_2O	3.2
Total per reaction	10

2.6.2 Amplification of cDNA

Amplification of cDNA was carried out on the StepOne™ Real-Time PCR System (Applied Biosystems, Germany) utilizing SYBR Green (Thermo Fischer Scientific, USA) detection chemistry. Cycling conditions consisted of 3 minutes of initial denaturation and polymerase activation at 95°C, followed by 40 amplification cycles, each of which included 1 minute of denaturation at 95°C, 30 seconds of annealing at a specific temperature for each primer determined by optimization, and 30 seconds of DNA elongation at 72°C. Fluorescence levels of SYBR Green were measured during the elongation step of each cycle. SYBR Green binds to DNA by intercalating between DNA bases in the minor groove of the double strand, lowering its energy and releasing the excess energy as fluorescence. The fluorescence signal is directly proportional to the number of amplified DNA copies. A passive reference dye (Reference Dye for Quantitative PCR, Sigma-Aldrich, USA) was used to normalize the fluorescence signal between wells.

Primers (Macrogen, South Korea) (Table 2) were designed using the PrimerQuest™ Tool software (Integrated DNA Technologies, USA) and the reactions were optimized to

ensure optimal specificity and efficiency. Amplification of the same cDNA was performed at a range of annealing temperatures and in reaction mixtures (Table 3.) with $MgCl_2$ concentrations of 2.5 mM, 3 mM and 3.5 mM. PCR products were then subjected to melting curve analysis. Amplification of a single product in samples that generated a single peak on a dissociation curve was confirmed by a single band on polyacrylamide gel electrophoresis. Finally, reaction efficiencies were determined by generating standard curves using serial DNA dilutions. Primer efficiencies between 90 and 110% were acceptable.

The number of cycles required for the fluorescent signal to exceed background noise, or cycle threshold (C_T), a value needed to determine relative gene expression, was recorded using StepOneSoftware (v 2.3) (Applied Biosystems, SAD). The C_T value is inversely proportional to the amount of target DNA in the sample, meaning that the higher the amount of target DNA, the lower the C_T.

Table 2. Oligonucleotides used for qPCR analysis

Gene name	Gene Symbol	Accession No.	Primer Sequence Forward (5′-3′) Reverse (5′-3′)	Optimized qPCR Conditions (Annealing Temp/MgCl)
Cytokines				
chemokine (C-C motif) receptor 2	Ccr2	NM_009915.2	GGTCTGGTTGGGTTGTAAA GTCTTTGAGGCTTGTTGCTATG	59°C; 3 mM
mouse CD68 antigen	*Cd68*	NM_001291058.1	CTCTTGCTGCCTCTCATCATT CTGGTAGGTTGATTGTCGTCTG	58 °C; 2,5 mM
C-X-C motif chemokine ligand 1	*Cxcl1*	NM_008176.3	GTGTCAACCACTGTGCTAGT CACACATGTCCTCACCCTAATAC	61 °C; 3.5 mM
atypical chemokine receptor 3	*Cxcr7*	NM_001271607.1	GACCATGTAGGCCTCAGATTAG CAGCCGAGACTGGCATAAA	63 °C; 3.5 mM
interleukin 1 alpha	*Il-1α*	NM_010554.4	CCTTACACCTACCAGAGTGATTT CCTTACACCTACCAGAGTGATTT	65 °C; 3 mM
interleukin 1 beta	*Il-1β*	NM_008361.4	ATGGGCAACCACTTACCTATTT GTTCTAGAGAGTGCTGCCTAATG	64 °C; 3 mM
interleukin 6	*Il-6*	NM_031168.2	GATAAGCTGGAGTCACAGAAGG TTGCCGAGTAGATCTCAAAGTG	59 °C; 3.5 mM
interleukin 14	*Il-14*	NM_001005506.3	CCTCACTTCAGCTACCTCTTAAA CTACAAGTGGATGGAGGGAAAG	61 °C; 3.5 mM
-monocyte chemoattractant protein-1	*Mcp1*	NM_011333.3	CCTGGATCGGAACCAAATGA CGGGTCAACTTCACATTCAAAG	62 °C; 3 mM
tumor growth factor beta	*Tgfα*	NM_031199.4	CTTTAGGAAGGACCTGGGTTG GTGTGTCCAGGCTCCAAATA	66 °C; 3 mM
tumor necrosis factor alpha	*Tnfα*	NM_013693.3	GTCTCAGAATGAGGCTGGATAAG CATTGCACCTCAGGGAAGAA	63 °C; 2.5 mM

Fatty Acid Metabolism				
abhydrolase domain containing 5	*Cgl58*	NM_026179.2	ATGCTGTGGAATGAGGACATAG CATAGTGAGTGGCTGGTGAAA	59°C; 2,5mM
carbohydrate response element binding protein	*Chreb*	NM_021455.5	CAGCTGCGGGATGAAATAGA CAAAGCGCTGATGTGTGATG	61°C; 2,5mM
carnitine palmitoyltransferase I	*Cpt1α*	NM_013495.2	TCGAAACCCAGTGCCTTAAC AAGCAGCACCCTCACATATC	58°C 2,5 mM
cytochrome P450, family 21, subfamily a, polypeptide	*Cyp21*	NM_009995.2	CTGGGTCGGAGCTTCATTT GTCTTGACTCTCTTCCCTTGAC	59°C; 3,5mM
diacylglycerol O-acyltransferase 1	*Dgat1*	NM_010046.3	CCAACCATCTGATCTGGCTTAT GACTCAGCATTCCACCAATCT	65°C; 3mM
glycerol kinase	*Glyk*	BC003767.1	GCACTAGAAGCTGTTTGTTTCC GCTGGTCATTCCTCCATCTAC	58°C; 2,5 mM
hydroxymethylglutaryl-CoA synthase	*Hmgcs2*	NM_008256.4	CCTGTGAAGAGGGAGATGAAAG GCCCACAGTCTGAGAATAAGC	64°C; 3 mM
fatty acid binding protein 1	*Fabp1*	NM_017399.5	AAGTCAAGGCAGTCGTCAAG TGGTATTGGTGATTGTGTCTCC	59°C; 3,5mM
fat storage-inducing transmembrane protein 2	*Fitm2*	NM_173397.4	GACAGGAGGACAATGGCTAAT CCACACCAAAGGTACCTAGTAAG	56°C; 2,5mM
insulin receptor substrate 1	*Irs1*	NM_010570.4	GTCAGGGACACTCTTGACTAAC TGCCAAGGAAAGACAGGATAAA	61°C; 2,5mM
insulin receptor substrate 2	*Irs2*	NM_001081212.2	CTGCTGCTCACTTTCCTATCA CCTGCCTCTTGGTTCCTTATC	61°C; 2,5mM
Pparγ coactivator	*Pgc1α*	NM_001127330.2	GCCTAAGTTTGAGTTTGCTGTG GCGGTCTCCACTGAGAATAATG	58°C 2,5 mM
peroxisome proliferator activated receptor alpha VI	*Pparα*	NM_011144.6	GCTCGTACAGGTCATCAAGAAG CTGCCATCTCAGGAAAGATCAG	59°C 2,5 mM

peroxisome proliferator activated receptor gamma	*Pparγ*	NM_001127330.2	GCCTAAGTTTGAGTTTGCTGTG GCGGTCTCCACTGAGAATAATG	59°C 2,5 mM
sterol regulatory element binding transcription factor 1	*Srebpf1*	NM_011480.4	AGCCCTCCACCAGGTAATAA GGGTTCCCAGTCTACTCACTAA	61°C; 2,5mM
Reference (housekeeping) genes				
actin beta	*Actβ*	NM_007393.5	GCAAGCAGGAGTACGATGAG CCATGCCAATGTTGTCTCTT	61 °C; 3.5mM
beta 2 microglobulin	*β2m*	NM_009735.3	CCTGCAGAGTTAAGCATGACAGT TCATGATGCTTGATCACATGTCT	60 °C; 3 mM

Table.3 Composition of qPCR master mix for a single reaction.

Component	Volume (µl)		
10X M-buffer (800mM KCl, 100mMTris-HCl, pH 8.3)	15.25		
dNTPs (5mM each) (Carl Roth GmbH, Germany)	1		
$MgCl_2$ (25 mM) (Sigma-Aldrich, USA)	2.5	3	3.5
Taq DNA polymerase (Sigma-Aldrich, USA)	1		
SYBR Green I (1000X) (Sigma-Aldrich, USA)	0.0025		
Reference Dye for Quantitative PCR (100X)	0.25		
mQ H_2O	15.75	14.75	15.25
Primer mix (5µM each)	1		
cDNA (37.5ng)	1		
Total per reaction	25		

2.7 Protein detection by Western blot

2.7.1 Protein isolation

Hippocampal and liver tissues were homogenized using a mortar and pestle and proteins were isolated using RIPA buffer (50 mM Tris-HCl, pH8, 150 mM NaCl, 1 mM EDTA, 1% NP40, 1% sodium deoxycholate, 0.1% SDS) supplemented with phosphatase (PhosSTOP, Roche, Switzerland) and protease (cOmplete™, Mini Protease Inhibitor Cocktail, Roche, Switzerland) inhibitors. Proteins were sonicated three times for 30 seconds at an amplitude of 50 using 1mm probe (bbi-8535 620). Samples were then centrifuged at 4°C for 20 minutes at maximum speed. The supernatant was collected and stored at -80°C.

2.7.2 Protein concentration

Protein concentration was measured using the Pierce™ BCA Protein Assay Kit (Thermo Fischer, USA), according to the manufacturer's instructions. In brief, 25 µl of Albumin standard (Thermo Fisher Scientific, USA) in serial dilution and samples were pipetted into a 96-well plate and 200µl of working reagent (reagent A:B, 50:1) was added. The microplate was covered and incubated at 37 °C for 30 minutes. Absorbance was measured at 570 nm using a spectrophotometer (Multiskan® EX, Thermo Fisher Scientific, USA).

2.7.3 Protein separation by polyacrylamide gel electrophoresis

Proteins were mixed with 5x Laemmli loading buffer (60mM Tris-HCl, pH 6.8, 25% glycerol, 2% SDS, 0,1% bromophenol blue) in a 1:5 ratio, the reducing agent DTT (dithiothreitol, dissolved in sodium acetate, Sigma) in a 1:10 ratio, and water. The proteins

were denatured at 92 °C for 5 min. Per well, 10 µg of protein in the mixture was loaded onto Tris-glycine SDS-polyacrylamide gel. The gel composition is shown in Table 4. The marker ROTI®Mark BI-PINK (Carl Roth GmbH, Germany) served as a protein size marker. Proteins were separated by size by polyacrylamide gel electrophoresis at a constant voltage of 100 V at room temperature in running buffer (25 mM Tris base, pH 8,3, 192 mM glycine, 0.1% SDS) using the Mini-PROTEAN Tetra vertical electrophoresis system (Bio-Rad Laboratories, USA

Table 4. Composition of Tris-glycine SDS-Polyacrylamide Gel for protein separation

Component	5% stacking gel Volume (ml)		12% resolving gel Volume (ml)	
reH_2O	2.18		4.3	
40% acrylamide/bis-acrylamide solution (29:1) (Acros Organics, USA)	0.38		3	
Tris Base (Fisher Scientific, USA)	1.5 M (pH 8.8)	0.38	1.0 M (pH 6.8)	2.5
10% SDS (Acros Organics, USA)	0.03		0.1	
10% ammonium persulfate (Carl Roth GmbH, Germany)	0.03		0.1	
TEMED (Carl Roth GmbH, Germany)	0.0003		0.004	

2.7.4 Protein transfer

After successful separation of the proteins, they were transferred to a polyvinylidene difluoride (PVDF) membrane (Bio-Rad Laboratories, USA). The gel and activated (in methanol) PVDF membrane were equilibrated in transfer buffer (25 mM Tris base, pH 8,3, 192 mM glycine, 20% methanol) and sandwiched between four sheets of buffer-soaked filter paper and fiber pads in a gel holder cassette. Transfer was performed in the Mini-PROTEAN system at a constant current of 100 mA for 16 hours at 4 °C.

2.7.5 Amido Black staining

To check whether the proteins were transferred to the membrane and whether the gel was uniformly loaded, the membrane was stained with Amido black 10B (Sigma-Aldrich, USA). It was washed in 1xPBS for 10 minutes, incubated in Amido black (0,1% amido black, 20% methanol, 2% acetic acid, dH_2O), for 2 minutes, incubated in Amido black destain solution (45% methanol, 7% acetic acid, dH_2O) two times for 30 minutes, washed in reH_2O four times for 2 minutes, and finally incubated in Tris Buffered Saline (TBS, 150 mM NaCl, 20 mM Tris Base, pH 8,0) with 0,1% TWEEN® 20 (Sigma-Aldrich, USA) (TBS-t) for 10 minutes.

2.7.6 Probing and visualization of the signal

The membrane was blocked with 0.2% Tropix® I-BLOCK™ Protein-Based Blocking Reagent (Applied Biosystems, USA) (0.2% I-Block™, 1X PBS, 0.05% TWEEN® 20, dH_2O) for 1 hour to prevent non-specific binding of the antibody to the membrane. The following step was incubation with a primary antibody (Table 5.) overnight on a rocking platform at 4°C. The next day, the membrane was transferred to a rocking platform at room temperature, washed three times for 10 minutes in 1X TBS-t, incubated with a

secondary antibody (Goat anti-rabbit IgG-HRP #170-6515; Bio-Rad Laboratories, USA), and washed again three times for 10 minutes in 1X TBS-t.

Table 5. List of used antibodies

Antibody	WB/IF	Dilution (WB/IF)	Manufacturer (stock number)
Anti-Pparγ	+/-	1:1000/-	Santa Cruz Biotechnology, Inc., USA (sc-7196)
Anti-Il-6	+/-	1:1000/-	Abcam, UK (ab208113)
Anti-Cxcl1	+/-	1:1000/-	Abcam, UK (ab)
Anti-GFAP	+/+	1:1000/1:500	Abcam, UK (ab7260)
Anti-Iba1	+/+	1:500/1:300	Abcam, UK (ab178846)
Anti-NeuN	+/+	1:1000/1:500	Abcam, UK (ab177487)
Anti-SNAP25	+/-	1:1000/-	Abcam, UK (ab109105)

Protein bands labelled by the antibodies were visualized using Pierce™ ECL Western Blotting Substrate (Thermo Fisher Scientific, USA). Peroxide solution and Luminol Enhancer solution were mixed in a 1:1 ratio, the membrane incubated with it for 1 minute, and visualized using the Uvitec Alliance Q9 Mini Chemiluminescence Imaging System. Normalization of the bands was done by Amido Black staining.

2.8 Morphological analysis

After perfusion, livers were kept in 10% buffered formalin (Shandon Formal-Fixx 10% neutral buffered formalin; Thermo Scientific GmbH, Austria). Specimens were then dehydrated and embedded in paraffin blocks according to a standard protocol (The Tissue-Tek® TEC™ 5 Tissue Embedding Console System, Sakura Finetek Europe). Histological sections of 5 μm were cut using a Leica SM 2000R microtome (Leica

Biosystems, Germany), stained with hematoxylin and eosin (HE) and a Masson-Goldner kit (Merck SA, Germany), and coverslipped using the Gemini AS automated slide stainer and ClearVue coverslipper (Thermo Fisher Scientific, USA). Lipid accumulation was visualized with Oil Red O staining. Formalin-fixed liver samples were frozen in liquid nitrogen. 10 µm cryosections were cut using a Leica CM 1800 cryostat (Leica Biosystems, Germany) at -17 °C and mounted on Thermo Scientific™ Superfrost® Plus slides (Gerhard Menzel B.V. & Co. KG, Germany) and stored at -80 °C until further processing. Cryosections were thawed and air-dried, then rinsed with deionized water and stained with Oil Red O (Merck SA, Germany) staining solution (0.5% Oil Red O in isopropanol) for 10 min. The nuclei were counterstained with hematoxylin. After rinsing with tap water, sections were mounted with aqueous mounting medium (Aquatex®; Merck SA, Germany). A Nikon Microphot FXA microscope with a DS -Fi1 camera and Imaging Software NIS Elements BR 4.6 (Nikon instruments Europe B.V., The Netherlands) was used for histological examination.

2.8.1 Ultrastructural analysis of liver

Liver tissues were immersion fixed in Ito's fixative (2.5% PFA, 2.5% glutaraldehyde, 80mM cacodylate buffer, pH 7.4) immediately after perfusion and dissection. Following fixation, they were postfixed in osmium tetroxide (OsO_4), dehydrated in a graded ethanol series and embedded in EPON™ epoxy resin (Miller-Stephenson Chemical Co., USA). 1 µm thick sections were cut using an ultramicrotome (Ultracut E; Reichert Jung, Austria) and stained with toluidine blue to determine the area of interest. Toluidine blue stained slides were examined with a Biorevo BZ-9000 microscope (Keyence, Germany). Ultrathin sections of the tissue were then sliced and stained with uranyl acetate and lead citrate. The sections were viewed with a transmission electron microscope JEM-1400Plus (JEOL (Deutschland) GmbH, Germany).

2.9 Fatty Acids Analyses

The fatty acid composition of the liver was analyzed by gas chromatography. Briefly, 0.25 g of the homogenized sample was transmethylated in situ using 0.5 M NaOH in methanol followed by 14% BF3 (boron trifluoride) in methanol according to the method of Park and Goins method (130). Fatty acid methyl esters (FAME) were extracted with hexane. An Agilent 6890 GC equipped with a DB-Fatwax UI chromatography column (30 m length; 0.25 mm i.d., 0.25 m film thickness; Agilent Technologies, USA) and a FID detector was used for FAME separation.

2.10 Immunofluorescence of the brain

2.10.1 Tissue sections preparation.

Isolated brain tissue fixed in 4% PFA was dehydrated in 15% PBS/sucrose solution until it sank, followed by 30% PBS/sucrose solution also until it sank, to prevent ice crystal formation in the tissue when water freezes. The tissue was embedded in OCT in a mold and frozen in isopentane and chilled with liquid nitrogen. Frozen samples were stored at -80°C until further use. 16µm thick sagittal brain sections were cut with a cryotome (Leica), placed on slides, and stored at –80°C until staining.

2.10.2 Detection of specific epitopes

The frozen slides were thawed and dried under the hood for at least one hour. Tissue was surrounded by hydrophobic barrier pen (Dako, Denmark). All subsequent steps were conducted in the dark in a box lined with wet paper. The tissues were incubated in 0.5% Triton™ X-100 in 1X TBS for 30 minutes to permeabilize them. The next step was blocking in 10% goat serum (Sigma-Aldrich, USA) for 1 hour. Incubation with the primary

antibodies (see Table 6 for details) was performed overnight at 4°C, followed by washing three times for 10 minutes in TBS-t. Secondary antibody was applied (Goat Anti-Mouse IgG H&L (Alexa Fluor® 488), ab150113, Abcam, UK) for 3 to 5 hours at room temperature, washed again three times for ten minutes in 1X TBS-t. Sections were counterstained with DAPI (2µg/ml, Carl Roth GmbH, Germany) for 10 minutes, and washed briefly in reH_2O to remove all TBS salts. All antibodies were diluted with 10% goat serum, and DAPI was diluted with 1XTBS-t. Finally, the slides were dried and mounted with ROTI®Mount FluorCare (Carl Roth GmbH, Germany). The protocol described above was followed for all antibodies except DCX, for which an antigen retrieval step was required. For this step, slides were briefly dipped in 1X TBS-t after drying and incubated in pre-warmed sodium citrate buffer (10 mM sodium citrate, 0.05% TWEEN® 20, pH 6.0) in a 95°C bath for 20 minutes. Tissues were then washed three times for ten minutes in TBS -t, followed by the blocking step and the remaining steps as previously described. Slides were examined using an Olympus BX51TF microscope and Olympus Stream Essentials software (Olympus, Japan).

2.11 Statistical evaluation

Blood glucose values from the IPGTT and IPITT, as well as body weight measurements were analyzed using two-way ANOVA, followed by Tukey multiple comparison post hoc analysis. The results of biochemical analysis of the blood sera were also analyzed by the two-way ANOVA, and in this case a Bonferoni post hoc test was performed. Relative gene expression was determined using the software REST © (ΔΔCt method) and normalized to most stable housekeeping genes. Several common housekeeping genes were tested and β-actin (*Actβ*) and β2-microglobulin (β*2m*) were chosen as appropriate referent genes.

Liver fat and fatty acid content were analyzed using general linear models (GLM) of the SAS/STAT module (SAS Institute Inc., Cary, NC, USA), with the differences determined by Tukey–Kramer post hoc test, genotype being the main effect, separately for male and

female mice. All graphical representations were created using GraphPad Prism version 8.0.0 (GraphPad Software, USA).

3 Results

3.1 Weight comparison

At 21 weeks of age, all animal groups (HFD WT male, HFD WT female, HFD *Tff3-/-*male, HFD *Tff3-/-* female, SD WT male, SD WT female, SD *Tff3-/-* male, SD *Tff3-/-*female) were weighed after a 16-hour fast. Male HFD *Tff3-/-* mice had significantly lower body weight than male HFD WT mice at 21 weeks of age or after 17 weeks of HFD (Figure 4a). This difference decreased with longer HFD exposure. Significance was lost at 36 weeks of age or after 32 weeks of HFD treatment (Figure 4a), when weight was reassessed. There were no genotype-related differences between SD mice (Figure 4b), suggesting that the absence of Tff3 protein does not cause differences in dietary habits or energy intake.

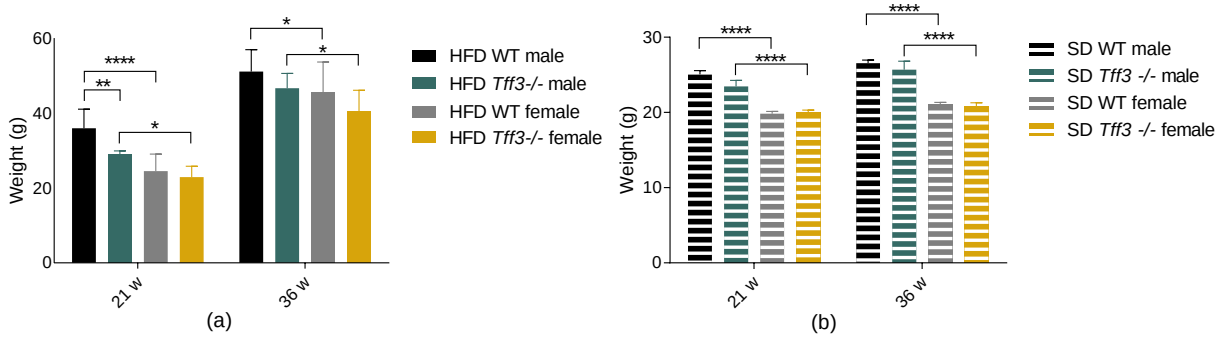

Figure 4. The effects of the absence of Tff3 on the body weight of HFD and SD mice of both sexes. (a) Body weight of 21-week-old (21w) and 36-week-old (36w) mice fed HFD from weaning. (b) Body weight of 21- and 36-week-old mice fed SD. Data are presented as mean and standard deviation (SD) (n~10 per group). Two-way ANOVA followed by Tukey post hoc test was used for statistical analysis. Significant differences are marked with * $p \leq 0.05$, ** $p \leq 0.01$, **** $p \leq 0.0001$.

3.2 The effect of Tff3 deficiency on metabolic homeostasis

To evaluate metabolic homeostasis under the stress of HFD exposure, metabolic tests were performed. The results of the metabolic tests are presented in two ways. First, two detailed figures are shown for each test (Figures 5,6,8, and 9), one representing genotype differences (Figures 5 and 8) and one representing sex differences (Figures 6 and 9). These figures include graphical representations of glucose levels comparing HFD- and SD -fed mice both at midpoint and at the end of the experiment. To make this large amount of data clearer, the area under the curve (AUC), which represents the overall trend of glucose excursion, was calculated and plotted for each curve (Figures 7 and 10). In this way, an overview of all results for each test is summarized in a single figure to facilitate comparison.

3.2.1 Intraperitoneal glucose tolerance test (IPGTT)

The intraperitoneal glucose tolerance test (IPGTT) was performed on both HFD and SD WT and *Tff3-/-* animals of both sexes (~10 per group) at 21 weeks of age and at 36 weeks of age (Figures 5 and 6). For the HFD group, this was after 17 and 32 weeks of HFD. At 21 weeks of age, HFD *Tff3-/-* males showed faster glucose clearance from the blood compared with HFD WT males at 15, 30, and 60 minutes after glucose administration (Figure 5a). At 36 weeks of age, this changed, with HFD WT males showing faster glucose clearance than HFD *Tff3-/-* males at the 30’ time point (Figure 5e), and significantly so at 60’. In contrast to their HFD counterpart SD males showed no difference in glucose clearance from blood at 21 weeks of age (Figure 5c), but at 36 weeks of age, SD *Tff3-/-* male mice showed lower blood glucose levels than SD WT males at 15’, 30’ and 60’ time points (Figure 5f).

On the other hand, HFD *Tff3-/-* and HFD WT females showed nearly identical glucose tolerance at both 21 and 36 weeks of age (Figures 5b and 5f), while SD *Tff3-/-* females

differed from SD WT females only in having lower glucose levels 30' after glucose injection at 21 weeks of age (Figure 5d).

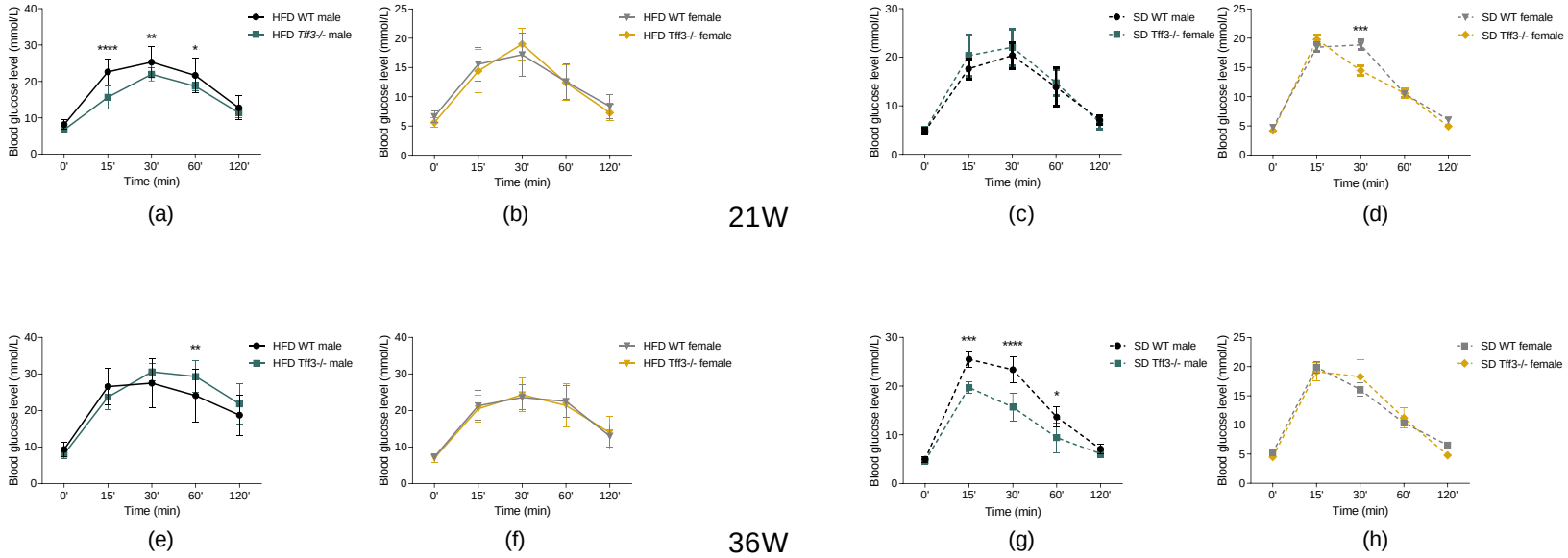

Figure 5. Intraperitoneal glucose tolerance test (IPGTT) performed in HFD and SD animals after 17 weeks of treatment (21 weeks of age) and 32 weeks of treatment (36 weeks of age) – genotype comparison. Blood glucose levels (mmol/L) at different time points (0, 15, 30, 60, and 120 minutes) after glucose injection were recorded and presented as comparison between 21-week-old (a) HFD WT and *Tff3-/-* males, (b) HFD WT and *Tff3-/-* females, (c) SD WT and *Tff3-/-* males, (d) SD WT and *Tff3-/-* females, and 36-week-old (e) HFD WT and *Tff3-/-* males, (f) HFD WT and *Tff3-/-* females, (g) SD WT and *Tff3-/-* males, (h) SD WT and *Tff3-/-* females. Data are expressed as mean and SD (n~10 per group). Two-way ANOVA followed by Tukey post hoc test was used for statistical analysis. Significant differences are marked with * $p \leq 0.05$, ** $p \leq 0.01$, *** $p \leq 0.001$, **** $p \leq 0.0001$

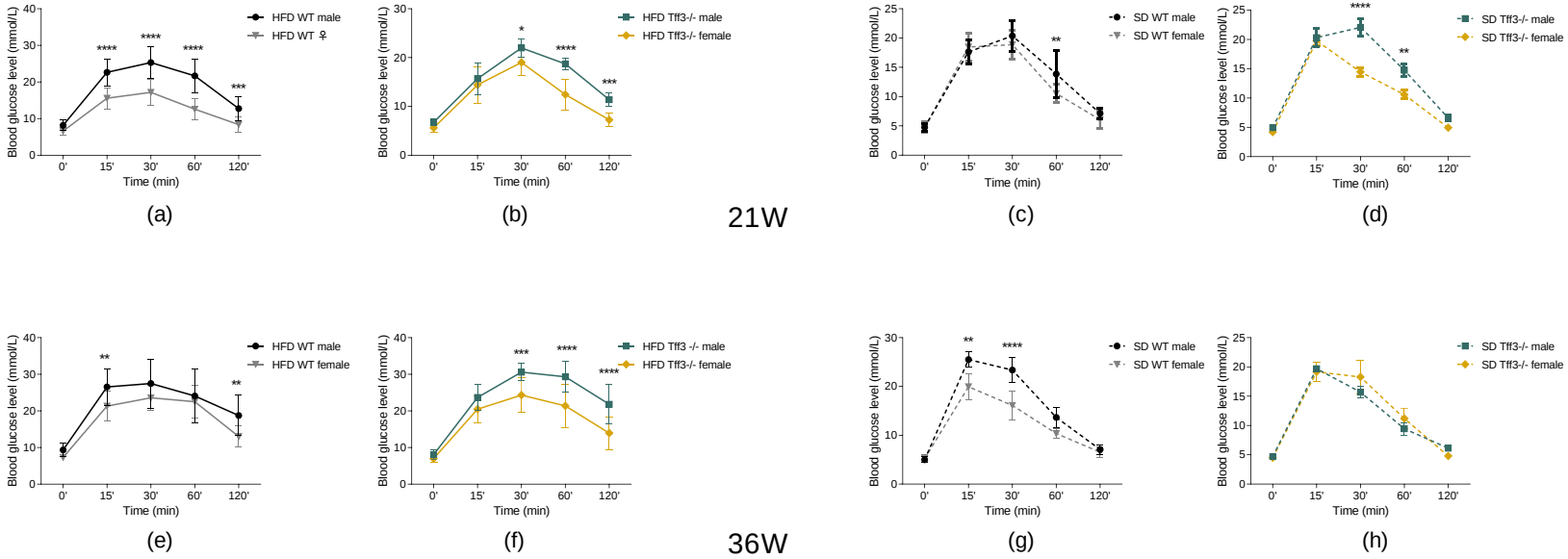

Figure 6. Intraperitoneal glucose tolerance test (IPGTT) performed on HFD and SD animals after 17 weeks of treatment (21 weeks of age) and 32 weeks of treatment (36 weeks of age) – sex comparison. Blood glucose levels (mmol/L) at different time points (0, 15, 30, 60, and 120 minutes) after glucose injection were recorded and presented as comparison between 21-week-old (a) HFD WT males and females, (b) HFD *Tff3-/-*males and females, (c) SD WT males and females, (d) SD *Tff3-/-*males and females, and 36-week-old (e) HFD WT males and females, (f) HFD *Tff3-/-*males and females, (g) SD WT males and females, (h) SD *Tff3-/-*males and females. Data are expressed as mean and SD (n~10 per group). Two-way ANOVA followed by Tukey post hoc test was used for statistical analysis. Significant differences are marked with * $p \leq 0.05$, ** $p \leq 0.01$, *** $p \leq 0.001$, **** $p \leq 0.0001$

Overall, male HFD *Tff3-/-* mice had better glucose utilization compared with HFD WT male at 21 weeks of age (Figure 7a), but the difference narrowed by 36 weeks of age (Figure 7b). In comparison, the situation was almost reversed in male SD mice, which showed virtually no difference at 21 weeks of age (Figure 7c), but the difference increased over time. At 36 weeks of age, SD *Tff3-/-* males had significantly better glucose tolerance than SD WT males (Figure 7d). Female mice of both genotypes had similar glucose tolerance throughout on both diets (Figure 7).

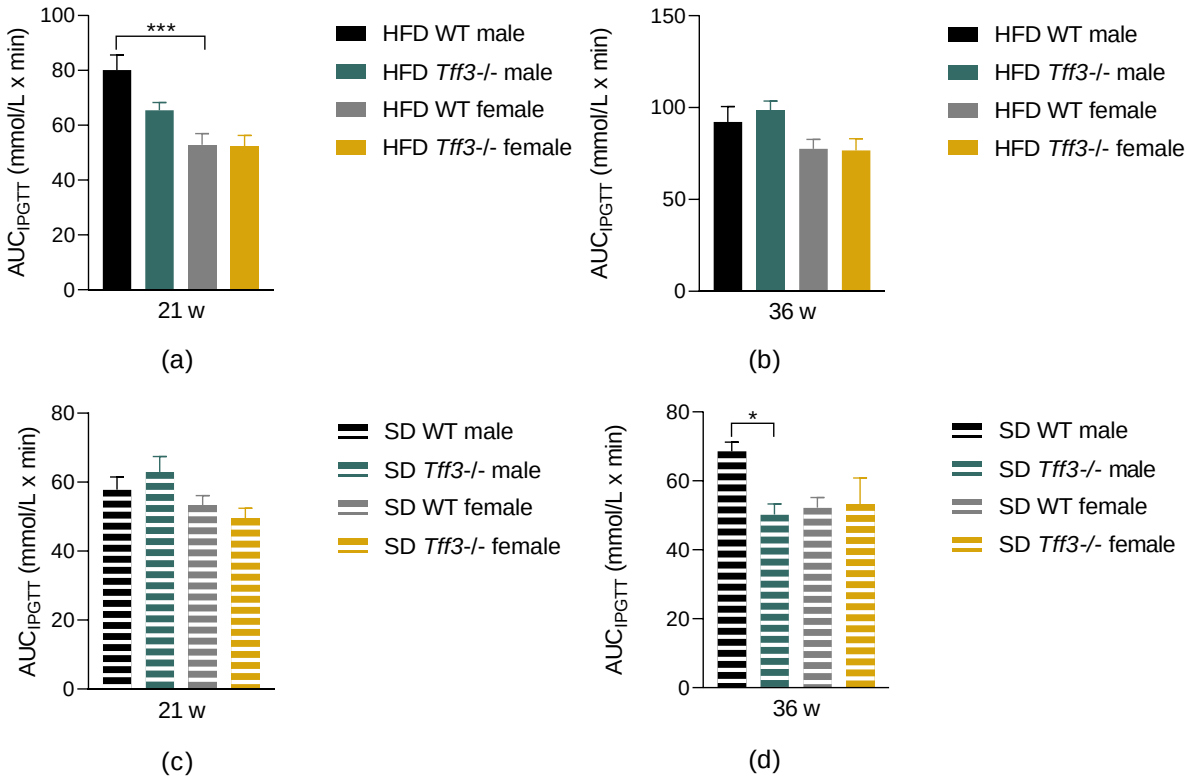

Figure 7. Area under the curve (AUC) of glucose tolerance for all animal groups. To summarize the results of all IPGTTs in one place, the AUCs (AUC$_{IPGTT}$) were calculated and plotted for the animals of each diet and age. (a) AUC$_{IPGTT}$ of 21-week-old HFD mice, (b) AUC$_{IPGTT}$ of 36-week-old HFD mice, (c) AUC$_{IPGTT}$ from 21-week-old SD mice, and (d) AUC$_{IPGTT}$ from 36-week-old SD mice. Data are given as mean and SD. Two-way ANOVA followed by Tukey post hoc test was used for statistical analysis. Significant differences are indicated by * $p \leq 0.05$, *** $p \leq 0.001$.

3.2.2 Intraperitoneal insulin tolerance test (IPITT)

Intraperitoneal insulin tolerance test was performed on HFD animals of both genotypes (WT and *Tff3*) and sexes (male and female) (n~10 per group) after 19 and 34 weeks of HFD treatment (23 and 38 weeks of age). The tests were also performed on age- and sex-matched SD-fed animals. At both 23 (Figure 8a) and 38 (Figure 8e) weeks of age, HFD WT males and HFD *Tff3-/-* males had similar blood glucose levels during testing. On the contrary, SD *Tff3-/-* males had significantly lower blood glucose levels than SD WT males at all the time points of the test at 23 weeks of age (Figure 8c). By 38 weeks of age the difference persisted only at the 60' time point (Figure 8g).

HFD *Tff3-/-* females exhibited slightly better glucose utilization than HFD WT females at the 60' and 120' time points at 23 weeks of age (Figure 8b), but their blood glucose levels equalized by 38 weeks of age (Figure 8d). In SD female mice, the situation was similar, except that the differences exist at the beginning and end of the test at 23 weeks of age (Figure 8h).

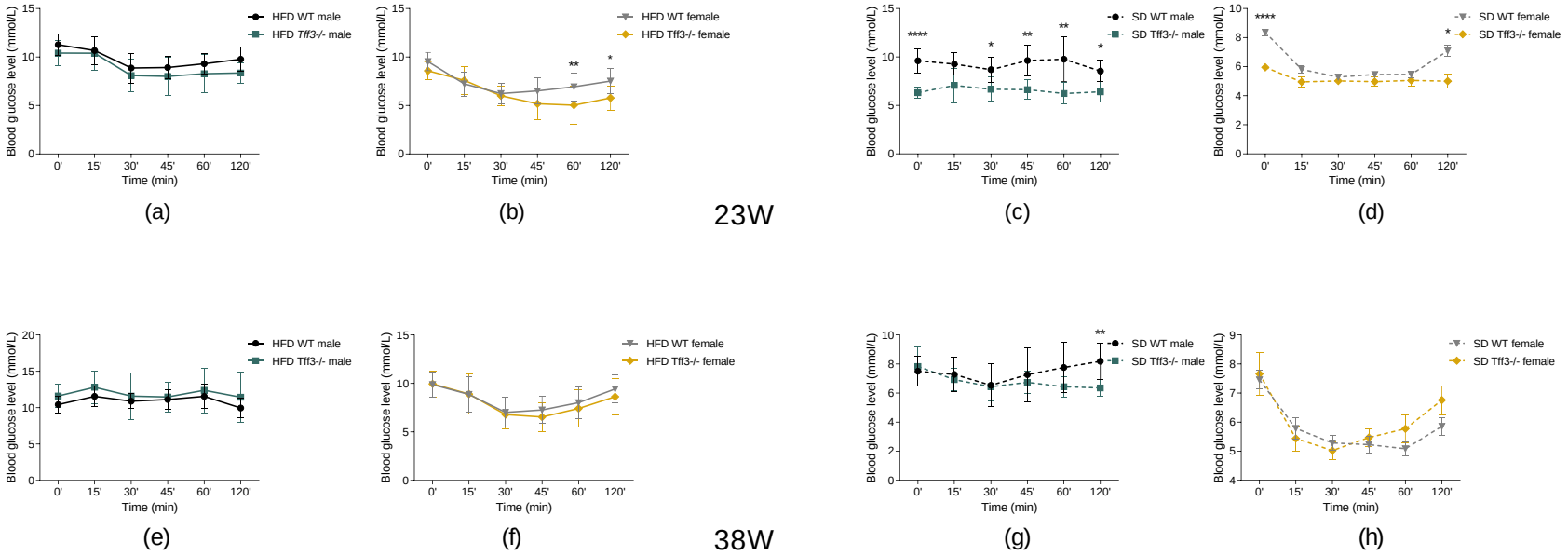

Figure 8. Intraperitoneal insulin tolerance test (IPITT) performed on HFD and SD animals after 19 weeks of treatment (23 weeks of age) and 34 weeks of treatment (38 weeks of age)- genotype comparison. Blood glucose levels (mmol/L) at different time points (0, 15, 30, 60, and 120 minutes) after insulin injection were recorded and presented as comparison between 23-week-old (a) HFD WT and *Tff3-/-* males, (b) HFD WT and *Tff3-/-* females, (c) SD WT and *Tff3-/-* males, (d) SD WT and *Tff3-/-* females, and 38-week-old (e) HFD WT and *Tff3-/-* males, (f) HFD WT and *Tff3-/-* females, (g) SD WT and *Tff3-/-* males, (h) SD WT and *Tff3-/-* females. Data are expressed as mean and SD (n~10 per group). Two-way ANOVA followed by Tukey post hoc test was used for statistical analysis. Significant differences are marked with * $p \leq 0.05$, ** $p \leq 0.01$, *** $p \leq 0.001$, **** $p \leq 0.0001$

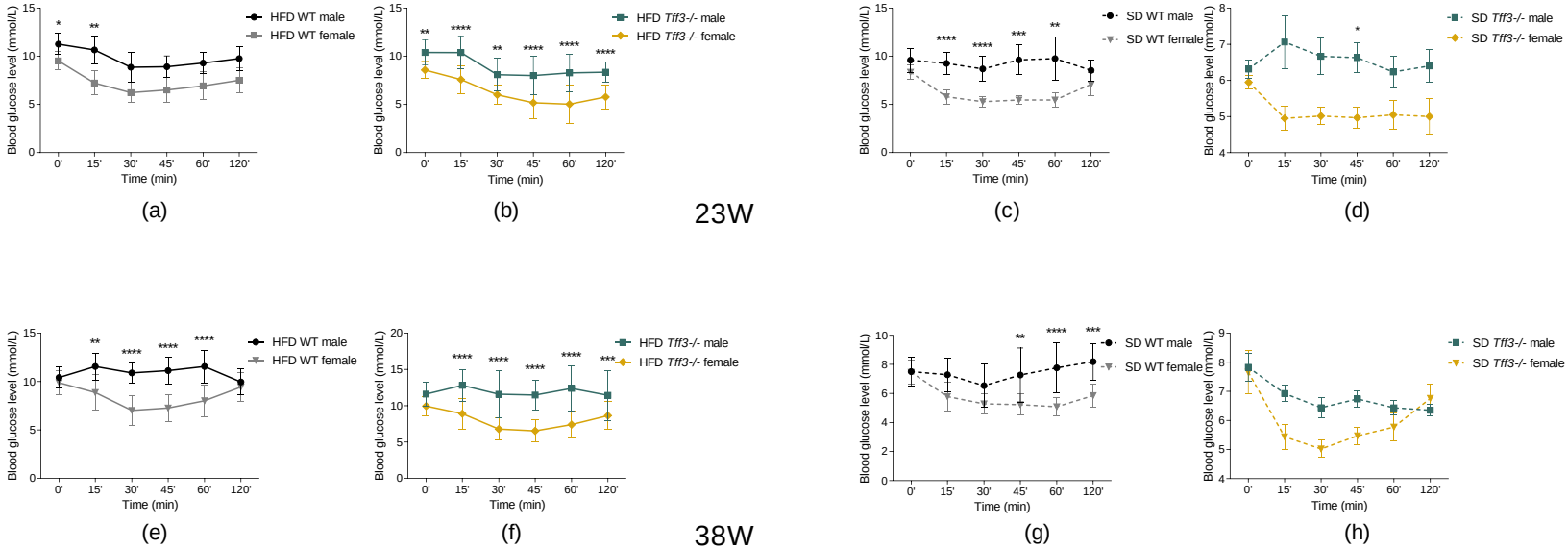

Figure 9. Intraperitoneal insulin tolerance test (IPITT) performed on HFD and SD animals after 19 weeks of treatment (23 weeks of age) and 34 weeks of treatment (38 weeks of age) – sex comparison. Blood glucose levels (mmol/L) at different time points (0, 15, 30, 60, and 120 minutes) after insulin injection were recorded and presented as comparison between 23-week-old (a) HFD WT males and females, (b) HFD *Tff3-/-* males and females, (c) SD WT males and females, (d) SD *Tff3-/-*males and females, and 38-week-old (e) HFD WT males and females, (f) HFD *Tff3-/-*males and females, (g) SD WT males and females, (h) SD *Tff3-/-*males and females. Data are expressed as mean and SD (n~10 per group). Two-way ANOVA followed by Tukey post hoc test was used for statistical analysis. Significant differences are marked with * $p \leq 0.05$, ** $p \leq 0.01$, *** $p \leq 0.001$, **** $p \leq 0.0001$

In summary, male HFD mice of the two genotypes had similar insulin tolerance, regardless of the age (Figures 10a and 10b), unlike SD male mice. SD *Tff3-/-* males showed faster glucose clearance than SD WT males at 23 weeks of age (Figure10c), but this difference narrowed at 38 weeks of age (Figure 10d). Both HFD and SD female mice of the two genotypes showed similar insulin tolerance (Figure 10).

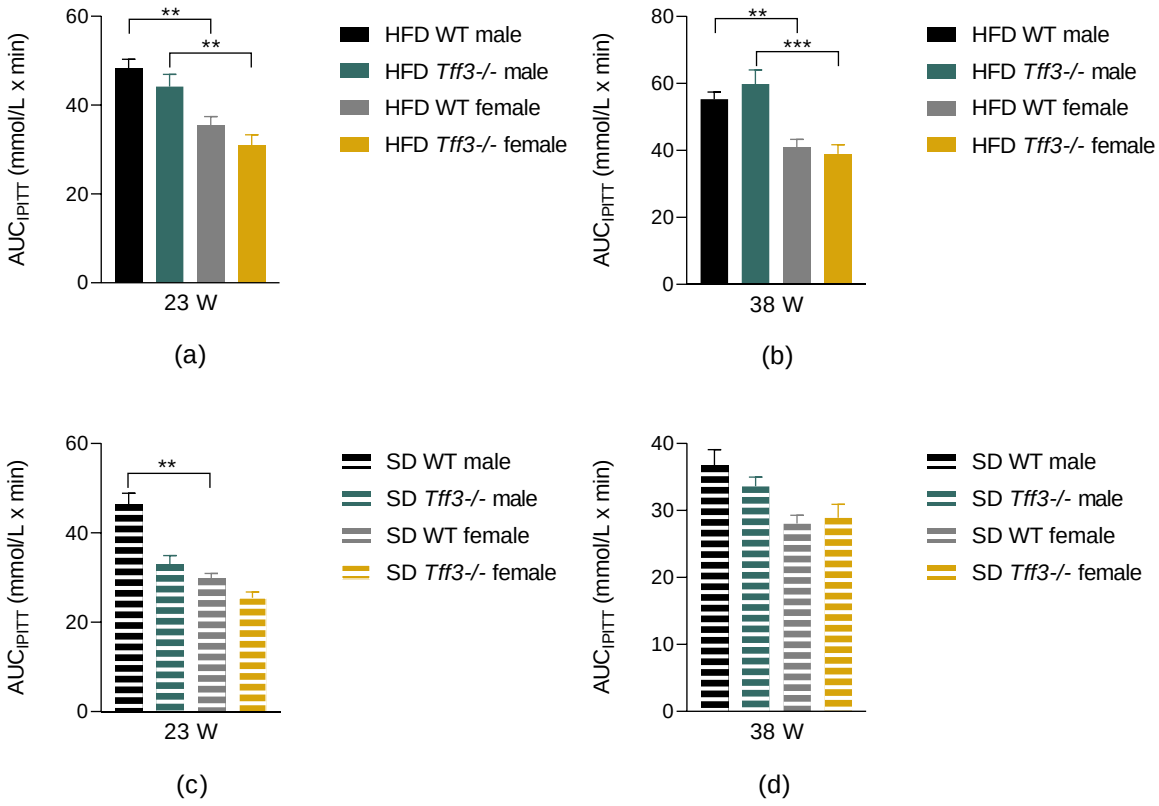

Figure 10. Area under the curve (AUC) of insulin tolerance for all animal groups. To summarize the results of all IPITTs in one place, the AUCs (AUC_{IPITT}) were calculated and plotted for the animals of each diet and age. (a) AUC_{IPITT} of 21-week-old HFD mice, (b) AUC_{IPITT} of 36-week-old HFD mice, (c) AUC_{IPITT} of 21-week-old SD mice, and (d) AUC_{IPITT} of 36-week-old SD mice. Data are given as mean and SD. Two-way ANOVA followed by Tukey post hoc test was used for statistical analysis. Significant differences are indicated by ** $p \leq 0.01$, *** $p \leq 0.001$.

Outside the scope of this work, but worth noting, male and female mice responded differently to glucose or insulin overload. Female mice of both genotypes and diet exposure showed faster glucose utilization in both IPGTT and ITT (Figures 6 and 9).

3.3 The effect of HFD intake and sex on Tff3 expression in the liver

Because major differences were noticed in the effect of Tff3 deficiency on general metabolic state of mice of different sex and diet treatment, *Tff3* expression in the liver of 40-week-old WT mice was examined (Figure 11). HFD intake reduced *Tff3* expression in the livers of male mice (Figure 11a), whereas there was no major difference in *Tff3* expression HFD and SD female mice (Figure 11b). This is probably because female mice, both HFD- and SD-fed, showed exceptionally low *Tff3* expression (Figure 11).

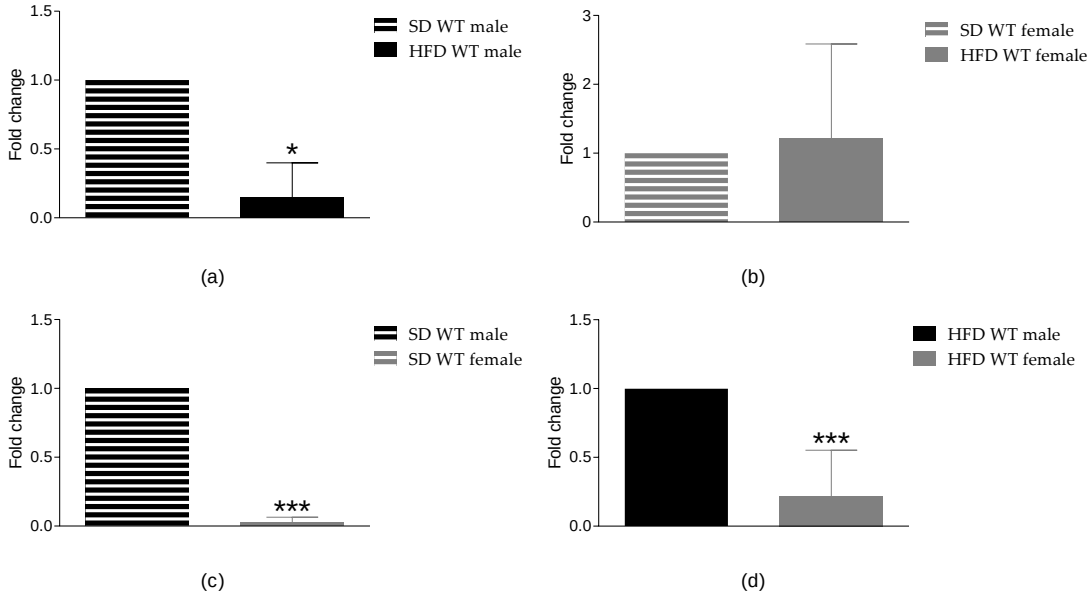

Figure 11. Influence of HFD and sex on Tff3 -/- expression in the liver. Gene expression was analyzed by qPCR using the SYBR green detection system and presented as comparison between SD (a) WT male mice on HFD and SD, (b) WT female mice on HFD and SD WT, (c) WT male and female mice on SD, and (d) WT male and female mice on HFD. The obtained Ct values were analyzed using REST © software (n=5 mice per group). Results are expressed as fold change mean and standard error of the mean (SEM). Significant differences are indicated by * $p \leq 0.05$, *** $p \leq 0.001$.

3.4 Blood serum biochemistry of HFD animals

To assess the general health status of the HFD animals, biochemical analysis of blood serum collected immediately before sacrifice (at 40 weeks of age, after 36 weeks of HFD) was performed. Levels of low-density lipoprotein (LDL), high-density lipoprotein (HDL), total cholesterol, aspartate aminotransferase (AST), alanine aminotransferase (ALT), alkaline phosphatase (ALP), blood glucose, C-reactive protein (CRP), urea, triglycerides, and total protein were determined (Figure 12). Genotype-related differences were found only in male mice. Male HFD *Tff3-/-* mice had lower LDL, total cholesterol, ALT, and ALP levels compared with male HFD WT mice.

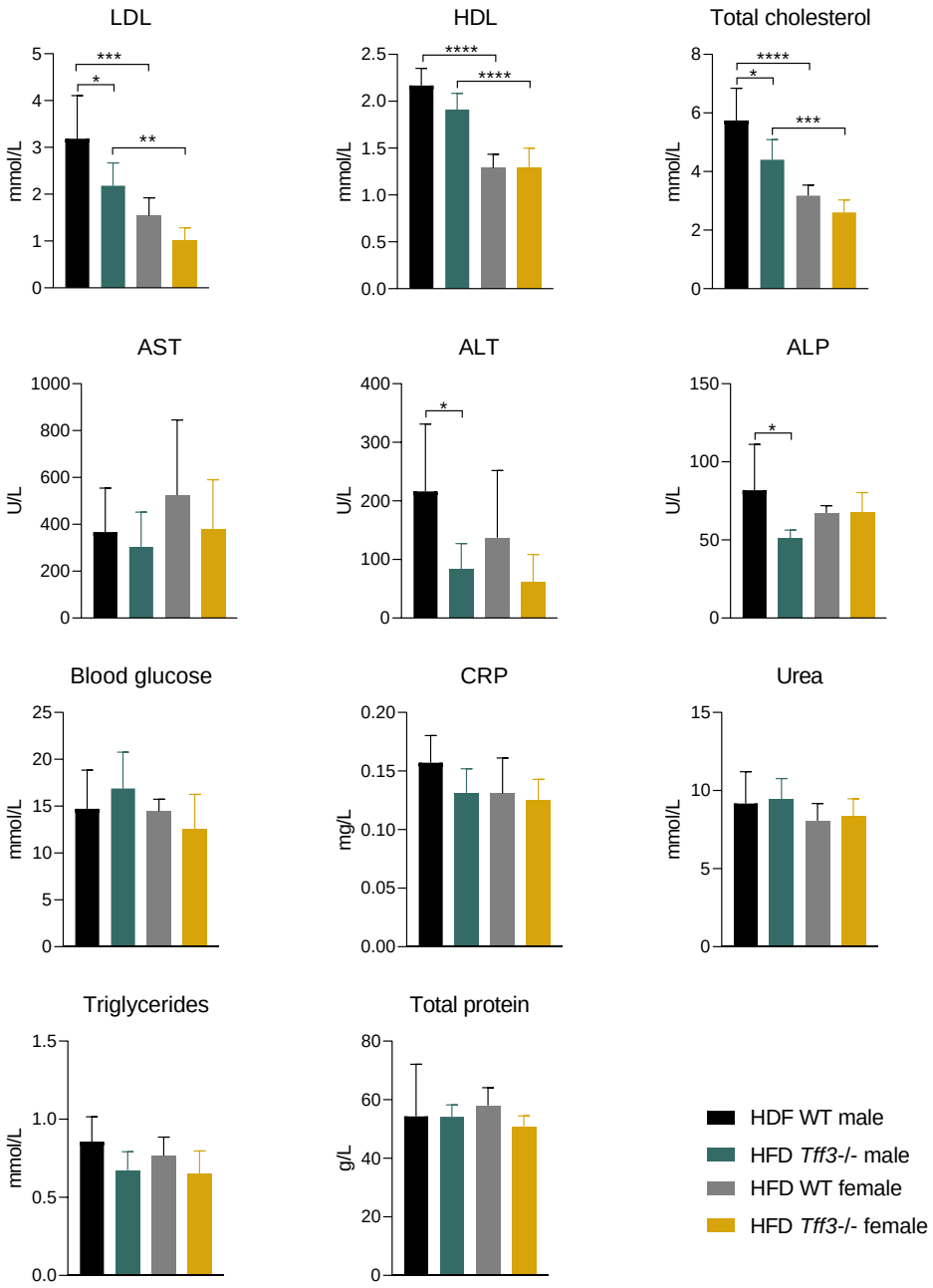

Figure 12. The effect of Tff3 deficiency on blood serum biochemistry of animals after 36 weeks of HFD. The levels of low-density lipoprotein (LDL), high-density lipoprotein (HDL), total cholesterol, aspartate aminotransferase (AST), alanine aminotransferase (ALT), alkaline phosphatase (ALP), blood glucose, C-reactive protein (CRP), urea, triglycerides, and total protein were determined for all groups of animals (n~10 per group) and presented as mean and SD. Two-way ANOVA followed by Tukey post hoc test was used for statistical analysis. Significant differences are marked with * $p \leq 0.05$, *** $p \leq 0.001$, **** $p \leq 0.0001$

3.5 Effect of Tff3 protein deficiency in the liver of mice on long-term high-fat diet

3.5.1 Liver morphology

Because consumption of HFD may have deleterious effects on the liver, histomorphological analysis of the livers of HFD animals was performed by hematoxylin and eosin (H&E) staining. It revealed numerous hepatocytes with unstained vacuoles in the cytoplasm and peripherally located nuclei, which is characteristic of macrovesicular steatosis. Signs of hepatic steatosis were obviously reduced in the livers of HFD *Tff3-/-* animals of both sexes compared with HFD WT animals as illustrated by the representative images shown in Figure 13 (upper panel). Such lipid accumulation was also seen in livers stained with Oil Red O (Figure 13, lower panel). This was quantified by measuring the total lipid content, which is described in Section 3.5.2.

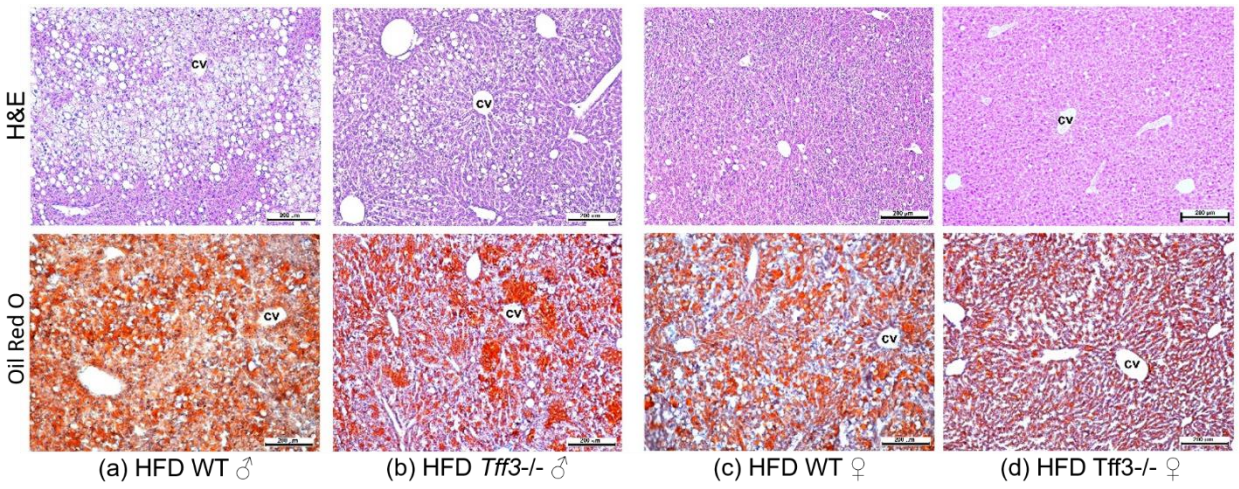

Figure 13. The effect of Tff3 deficiency on liver histomorphology of 40-week-old animals fed HFD. Liver sections were stained with hematoxylin and eosin (upper panel) and Oil Red O (lower panel). Scale bar 200 μm, H&E- hematoxylin – eosin staining, cv-central vein

Lipid droplets were also visualized on an ultrastructural level using electron microscopy (Figure 14).

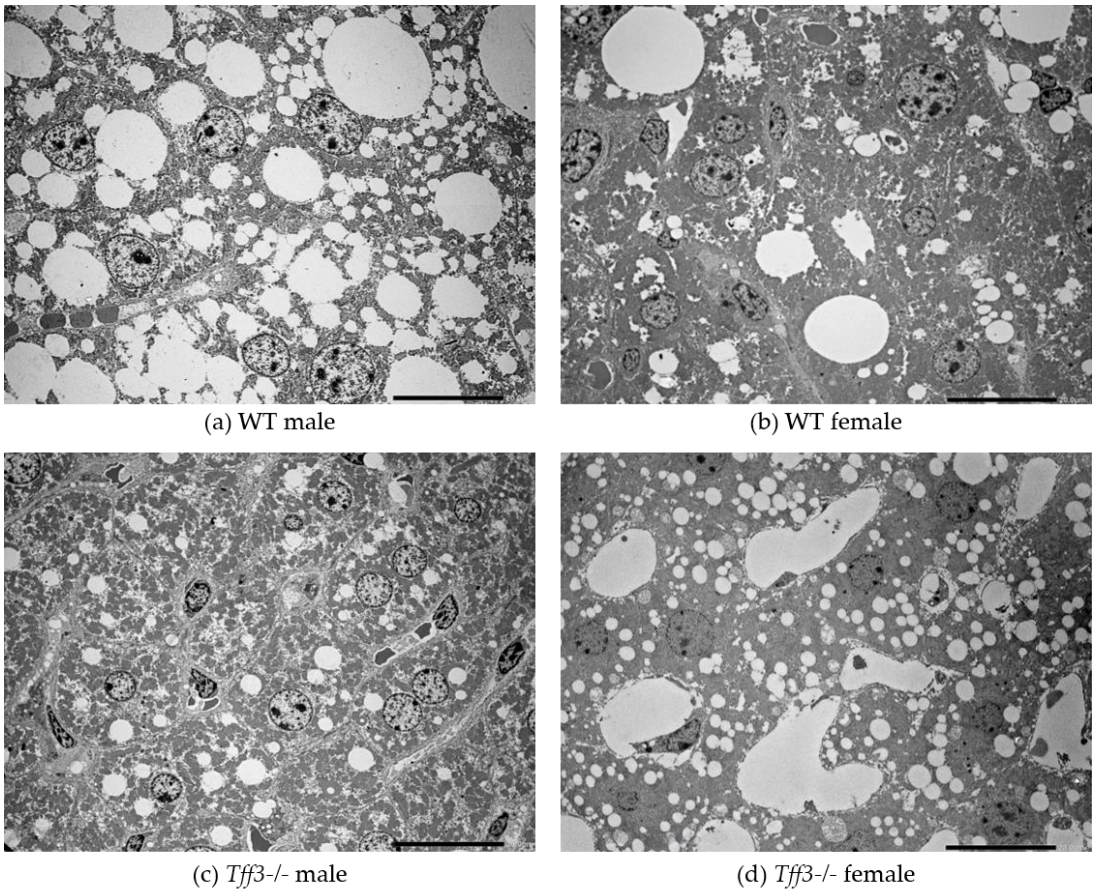

Figure 14. Ultrastructural analysis of HFD mice of both genotypes and sexes. TEM-images of liver sections from 40-week-old (a) HFD WT males; (b) HFD WT females; (c) HFD *Tff3-/-* males; (d) HFD *Tff3-/-* females. Scale bar 20µm.

Additionally, livers from SD-fed controls were stained (Figure 15). As expected, no conspicuous signs of hepatic steatosis were observed on the H&E-stained sections (Figure 15, upper panel). However, the Oil Red O-stained cryosections revealed more prominent staining of lipid droplets in WT males compared to SD exposed *Tff3* males and females of both genotypes.

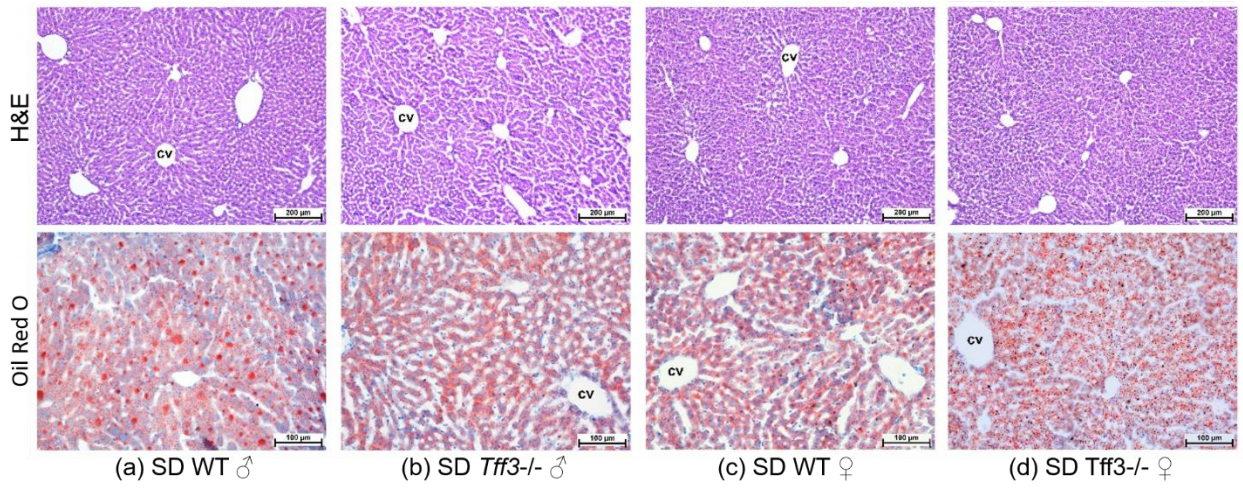

Figure 15. The effect of Tff3 deficiency on the histomorphology of livers from 40-week-old SD- fed animals. Liver sections were stained with hematoxylin and eosin (upper panel) and Oil Red O (lower panel). Scale bar 200 μm, H&E- hematoxylin-eosin staining, cv-central vein

3.5.2 Total fat and liver fatty acid content

Total fat content and specific content of main fatty acids were determined in the livers of all animal groups (Tables 6 and 7). HFD *Tff3-/-* mice showed a significant, nearly twofold, reduction of total liver fat content compared to HFD WT mice (Table 6). No relevant genotype-related differences were observed between specific fatty acids (Table 6).

Table 6. Fat and fatty acid content in the liver of 40-week-old mice on HFD.

Main fatty acids (g /100 g of total FA)	HFD WT male	HFD *Tff3-/-* male	HFD WT female	HFD *Tff3-/-* female
C 14:0	0.47	0.45	0.44	0.45
C 16:0	24.74	24.84	24.18	24.25
C 16:1	5.26	4.46	3.74	3.22
C 18:0	3.51	4.69	5.53	6.83
C 18:1	43.04	38.00	41.16	33.19
C 18:2, n-6	11.40	12.98	12.38	14.72
C 18:3, n-6	0.28	0.30	0.37	0.51
C 18:3, n-3	0.27	0.34	0.32	0.47
C 20:1, n-9	1.05	0.86	0.54	0.33
C 20:3, n-6	0.74	0.78	0.54	0.33
C 20:4, n-6	3.72	5.26	5.13	7.21
C 20:5, n-3	0.17	0.25	0.22	0.34
C 22:4, n-6	0.48	0.51	0.30	0.43
C 22:5, n-6	0.23	0.25	0.15	0.24
C 22:5, n-3	0.41	0.50	0.29	0.45
C 22:6, n-3	2.95	4.17	3.91	5.78
∑ SFA [1]	29.28	30.63	30.58	32.07
∑ MUFA [2]	49.75	43.68	45.70	37.00
∑ PUFA [3]	20.49	25.18	23.43	30.51
n-6/n-3 PUFA[4]	4.59: 1	3.92: 1	4.26: 1	3.28: 1
Fat content (g/100 g liver)	22.17 ± 1.18 *	14.37 ± 1.67	17.21 ± 1.87[#]	8.64 ± 1.25

[1] Saturated fatty acids. [2] Monounsaturated fatty acids. [3] Polyunsaturated fatty acids. [4] Ratio of omega -6 and omega -3 polyunsaturated fatty acids

Results are given for major fatty acid content in g of each FA per 100 g of total FA and for total fat content in g of fat per 100 g of liver tissue. Results are presented as mean and as mean ±SD (for fat content) and were analyzed using general linear models (GLM) procedures of the

SAS/STAT module (SAS Institute Inc., Cary, NC, USA), the differences being determined by a Tukey–Kramer multiple comparison test, taking into consideration the genotype as the main effect, separately for male and female mice. Statistical significance was considered at $p \leq 0.05$. * - WT male vs *Tff3-/-* male; # - WT female vs *Tff3-/-* female

Total liver fat content was also significantly reduced in SD *Tff3-/-* animals of both sexes (Table 7). In this group, genotype-related differences were found between some major fatty acids (Table 7). Interestingly, total liver fat content in female mice was noticeably higher for SD- than HFD-fed animals.

Table 7. Fat and fatty acid content in the liver of 40-week-old mice on SD.

Main fatty acids (g /100 g of total FA)	SD WT male	SD *Tff3-/-* male	SD WT female	SD *Tff3-/-* female
C 14:0	0.60	0.55	0.74	0.66
C 16:0	22.94*	25.43	22.71#	24.27
C 16:1	7.28	5.88	5.74	5.44
C 18:0	3.68	5.46	3.84	5.59
C 18:1	25.68*	21.15	31.55#	28.18
C 18:2, n-6	23.35	21.56	21.81	18.40
C 18:3, n-6	0.51	0.42	0.71	0.56
C 18:3, n-3	1.06	0.94	0.92	0.74
C 20:1, n-9	0.33	0.28	0.24	0.22
C 20:3, n-6	0.58	0.72	0.35	0.58
C 20:4, n-6	4.85	6.88	4.05	5.88
C 20:5, n-3	0.77	0.80	0.49	0.71
C 22:4, n-6	0.16	0.20	0.16	0.19
C 22:5, n-6	0.09	0.11	0.08	0.08
C 22:5, n-3	0.61	0.67	0.39	0.50
C 22:6, n-3	6.27	7.72	5.02	6.89
∑ SFA [1]	28.03*	32.26	28.09#	31.24
∑ MUFA [2]	33.35*	27.37	37.58#	33.90
∑ PUFA [3]	38.46	40.17	34.16	34.67
n-6/n-3 PUFA[4]	3.39: 1	2.92: 1	3.80: 1	2.91: 1
Fat content (g/100 g liver)	15.0 ± 1.72*	9.9 ± 1.88	19.7 ± 1.72#	13.9 ± 1.88

[1] Saturated fatty acids. [2] Monounsaturated fatty acids. [3] Polyunsaturated fatty acids. [4] Ratio of omega -6 and omega -3 polyunsaturated fatty acids

Results are given for major fatty acid content in g of each FA per 100 g of total FA and for total fat content in g of fat per 100 g of liver tissue. Results are presented as mean and as mean ±SD (for fat content) and were analyzed using general linear models (GLM) procedures of the

SAS/STAT module (SAS Institute Inc., Cary, NC, USA), the differences being determined by a Tukey–Kramer multiple comparison test, taking into consideration the genotype as the main effect, separately for male and female mice. Statistical significance was considered at $p \leq 0.05$. * - WT male vs *Tff3-/-* male; # - WT female vs *Tff3-/-* female

3.5.3 Influence of Tff3 deficiency on expression of liver genes

Several genes involved in inflammation, fatty acid metabolism, apoptosis, ER stress, and oxidative stress, pathophysiological processes known to be induced by HFD intake and involved in hepatic steatosis, were also monitored.

Among markers of fatty acid metabolism, both male (Figure 16a) and female (Figure 16b) HFD *Tff3-/-* mice exhibited decreased expression of peroxisome proliferator-activated receptor gamma (*Pparγ*) compared with HFD WT mice of the same sex.

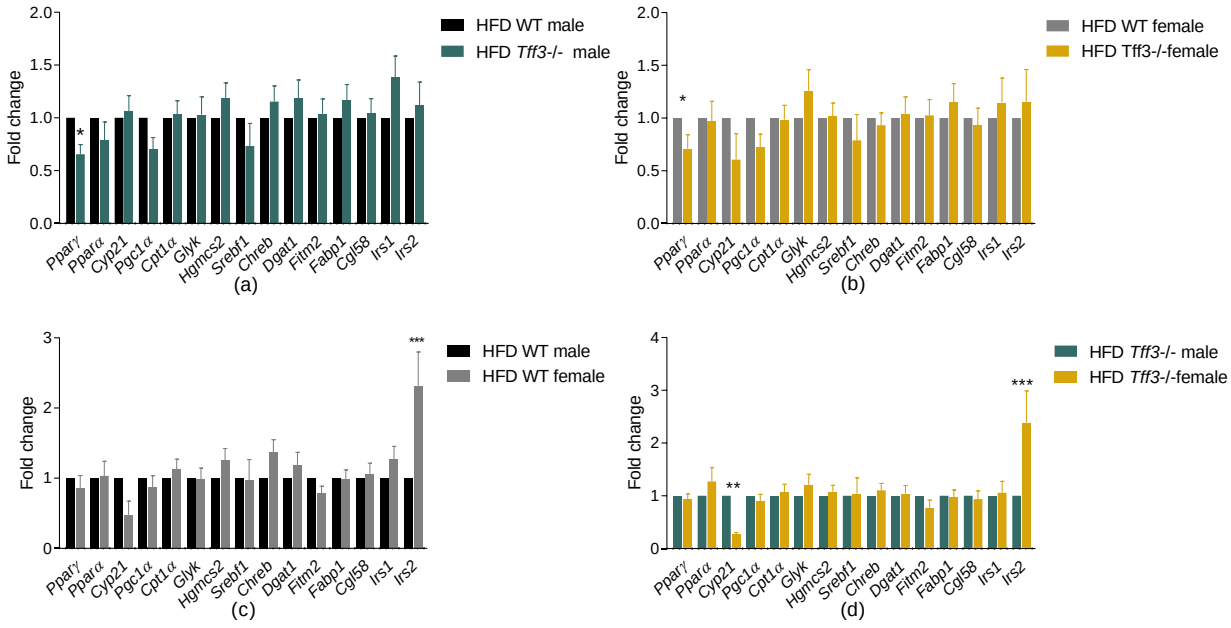

Figure 16. The effect of long-term HFD exposure on the expression of fatty acid metabolism markers in the livers of 40-week-old HFD WT and *Tff3-/-*. Gene expression was analyzed by qPCR using the SYBR green detection system and presented relative to the corresponding WT mice in (a) HFD *Tff3-/-* male and (b) HFD *Tff3-/-* female mice and relative to the corresponding male mice in (c) HFD WT female and (d) HFD *Tff3-/-* female mice. The obtained C_t values were analyzed using REST © software (n=5 mice per group). Results are expressed as fold change mean and standard error of the mean (SEM).* $p \leq 0.05$, ** $p \leq 0.01$;

Pparγ-peroxisome proliferator activated receptor gamma; *Pparα*- peroxisome proliferator activated receptor alpha *Cyp21*- cytochrome P450, family 21, subfamily a, polypeptide 1; *Pgc1α*- peroxisome proliferator-activated receptor-gamma coactivator 1alpha; *Cpt1α*- carnitine palmitoyltransferase I; *Glyk*-glycerol kinase; *Hgmcs2*- 3-hydroxy-3-methylglutaryl-CoA synthase 2; *Srebf1*- sterol regulatory element binding transcription factor 1; *Chreb*- carbohydrate response element binding protein; *Dgat1*- diacylglycerol O-acyltransferase 1; *Fitm2*-fat storage-inducing transmembrane protein 2; *Fabp1*-fatty acid binding protein 1; *Cgl58*- alpha/beta-hydrolase domain containing 5; *Irs1*-insulin receptor substrate 1; *Irs2*- insulin receptor substrate 2

Inflammatory marker expression analysis revealed significant upregulation of interleukin 6 (*Il-6*) in the livers of male HFD *Tff3-/-* compared with male HFD WT mice (Figure 17a). In female mice, HFD *Tff3-/-* mice exhibited lower expression of C-X-C motif chemokine ligand 1 (*Cxcl1*) and chemokine (C-C motif) receptor 2 (*Ccr2*) compared with HFD WT mice (Figure 17b).

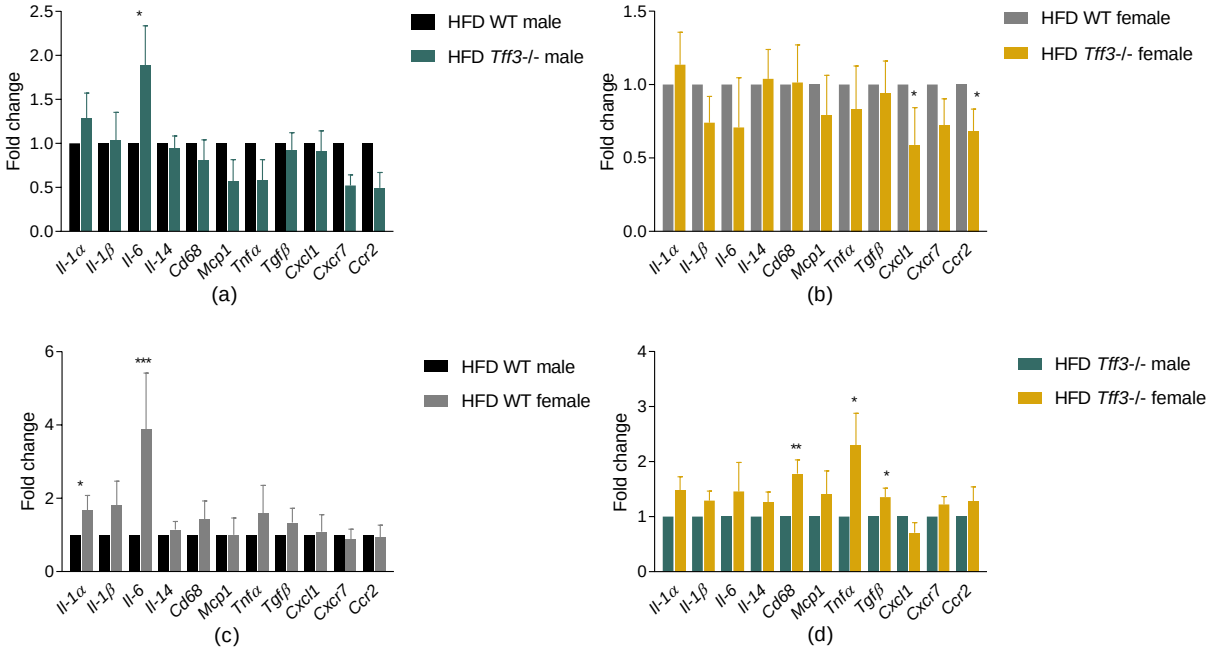

Figure 17. The effect of long-term HFD exposure on the expression of inflammatory markers in the livers of 40-week-old HFD WT and *Tff3-/-*. Gene expression was analyzed by qPCR using the SYBR green detection system and presented relative to the corresponding WT mice in (a) HFD *Tff3-/-* male and (b) HFD *Tff3-/-* female mice and relative to the corresponding male mice in (c) HFD WT female and (d) HFD *Tff3-/-* female mice. The obtained C_t values were analyzed using REST © software (n=5 mice per group). Results are expressed as fold change mean and standard error of the mean (SEM). * $p \leq 0.05$, ** $p \leq 0.01$; *** $p \leq 0.001$.

Il-1α- interleukin 1 alpha*; Il-1β*- interleukin 1 beta; *Il-6*- interleukin 6; *Il-14*- interleukin 14; *Cd68*- mouse CD68 antigen; *Mcp1*; *Tnfα*- tumor necrosis factor alpha, *Tgfβ*- tumor growth factor beta; *Cxcl1*- C-X-C motif chemokine ligand 1; *Cxcr7*- atypical chemokine receptor 3; *Ccr2*- chemokine (C-C motif) receptor 2

A single apoptosis marker differed significantly between female mice, HFD *Tff3-/-* females had higher expression of BCL2-Associated Athanogene 6 (*Bag6*) than HFD WT females (Figure 18b).

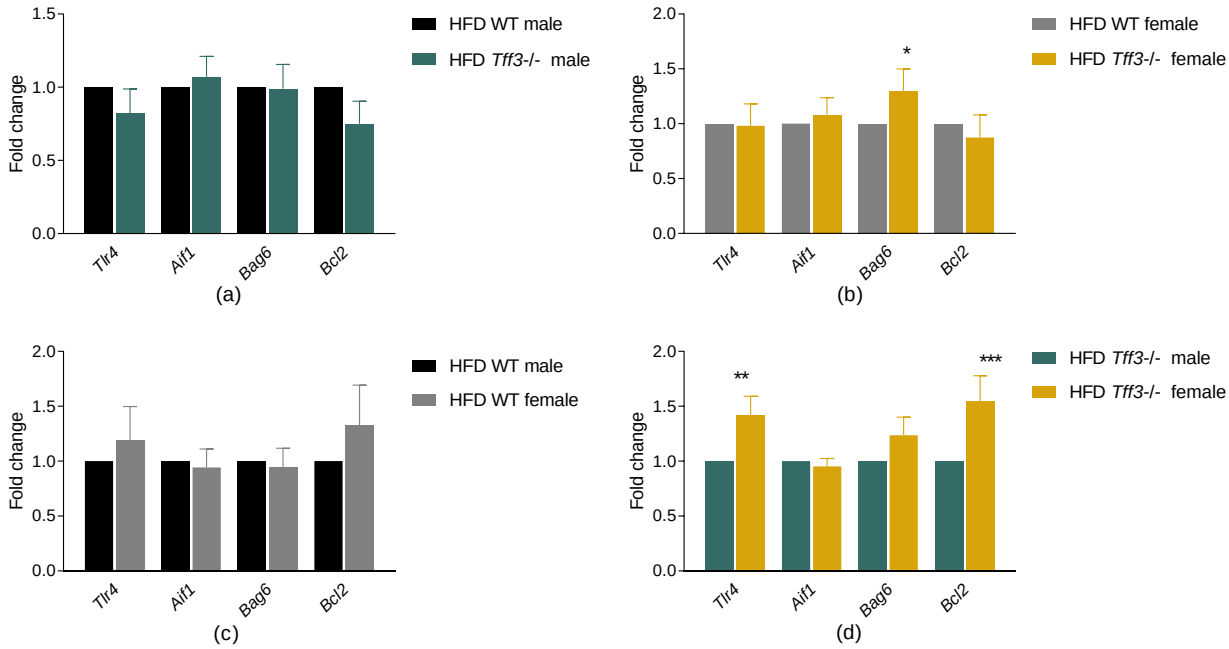

Figure 18. The effect of long-term HFD exposure on the expression of apoptosis markers in the livers of 40-week-old HFD WT and *Tff3-/-*. Gene expression was analyzed by qPCR using the SYBR green detection system and presented relative to the corresponding WT mice in (a) HFD *Tff3-/-* male and (b) HFD *Tff3-/-* female mice and relative to the corresponding male mice in (c) HFD WT female and (d) HFD *Tff3-/-* female mice. The obtained C_t values were analyzed using REST © software (n=5 mice per group). Results are expressed as fold change mean and standard error of the mean (SEM). * $p \leq 0.05$, ** $p \leq 0.01$; *** $p \leq 0.001$.

Tlr4 – toll-like receptor 4; *Aif1* – allograft inflammatory factor 1, *Bag6* - BCL2-associated athanogene 6, *Bcl2* - BCL2 apoptosis regulator

Among markers of endoplasmic reticulum stress (ERS), spliced X-box binding protein 1 (*sXbp1*) was upregulated in male HFD *Tff3-/-* mice compared with the corresponding WT mice (Figure 19a), whereas there were no differences between female mice (Figure 19b).

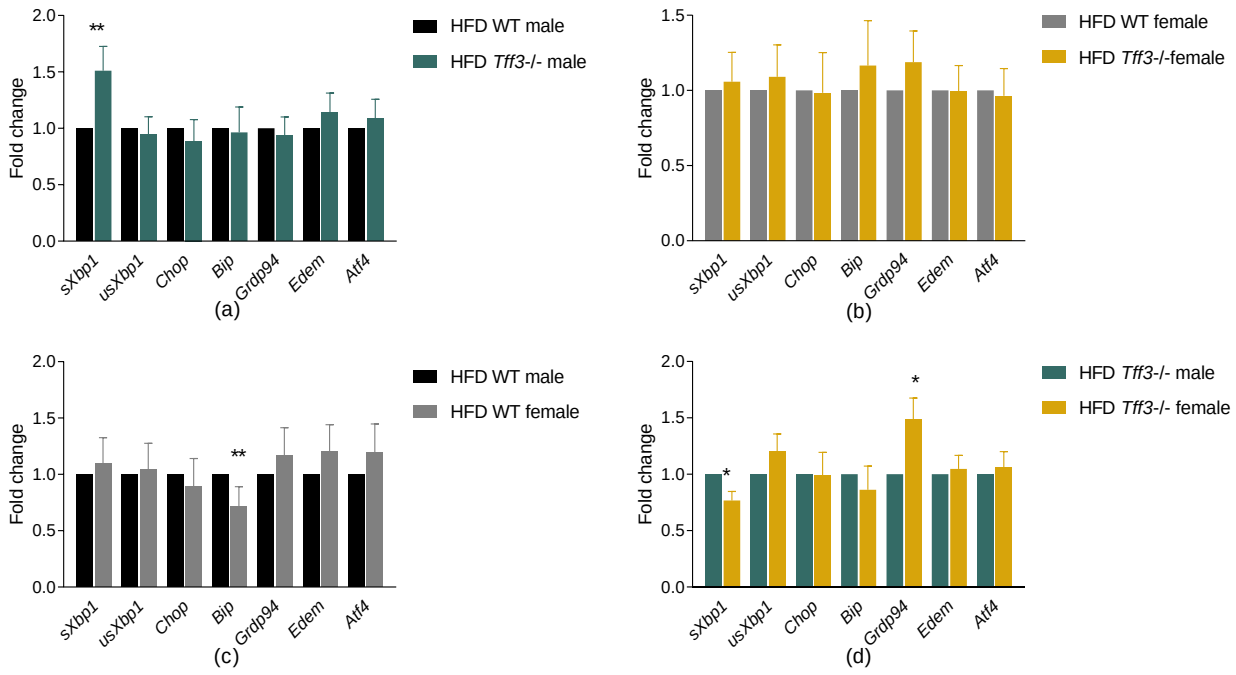

Figure 19. The effect of long-term HFD exposure on the expression of ERS markers in the livers of 40-week-old HFD WT and *Tff3-/-*. Gene expression was analyzed by qPCR using the SYBR green detection system and presented relative to the corresponding WT mice in (a) HFD *Tff3-/-* male and (b) HFD *Tff3-/-* female mice and relative to the corresponding male mice in (c) HFD WT female and (d) HFD *Tff3-/-* female mice. The obtained C_t values were analyzed using REST © software (n=5 mice per group). Results are expressed as fold change mean and standard error of the mean (SEM). * $p \leq 0.05$, ** $p \leq 0.01$.
Results are expressed as fold change mean and standard error of the mean (SEM). * $p \leq 0.05$, ** $p \leq 0.01$.

Oxidative stress markers showed no differences between genotypes (Figures 20a and 20b).

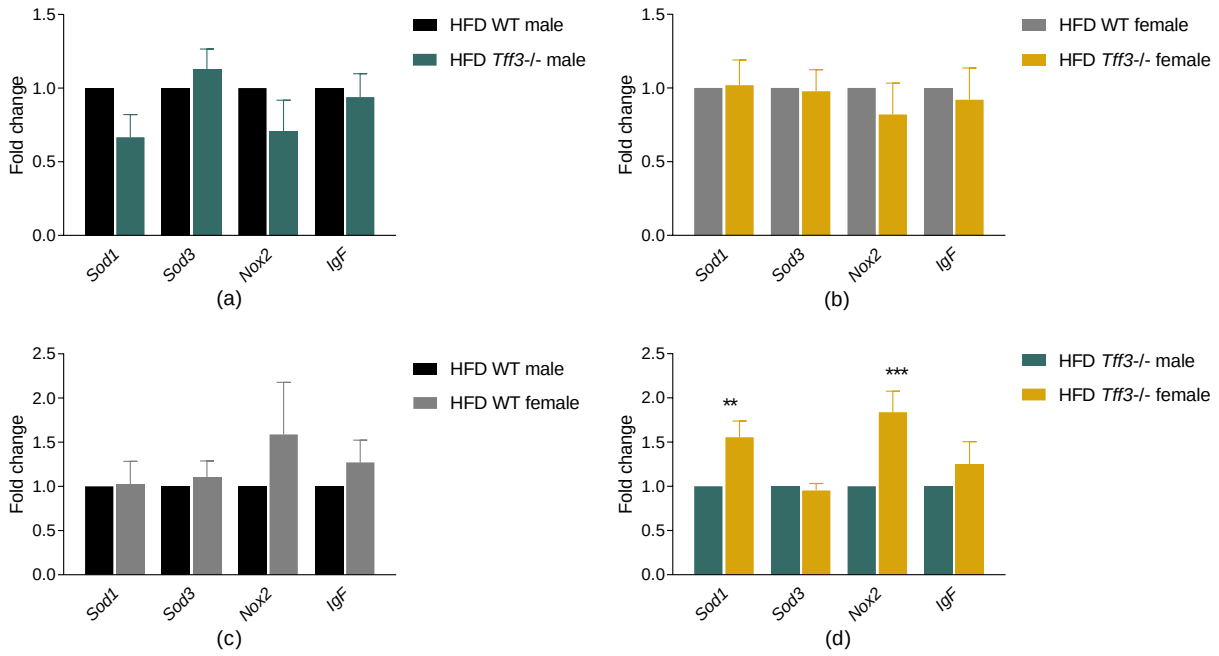

Figure 20. The effect of long-term HFD exposure on the expression of oxidative stress markers in the livers of 40-week-old HFD WT and *Tff3-/-*. Gene expression was analyzed by qPCR using the SYBR green detection system and presented relative to the corresponding WT mice in (a) HFD *Tff3-/-* male and (b) HFD *Tff3-/-* female mice and relative to the corresponding male mice in (c) HFD WT female and (d) HFD *Tff3-/-* female mice. The obtained C_t values were analyzed using REST © software (n=5 mice per group). Results are expressed as fold change mean and standard error of the mean (SEM). ** $p \leq 0.01$; *** $p \leq 0.001$.

Genes significantly altered in *Tff3-/-* animals compared to WT mice in HFD model were not affected in SD -fed animals (Figure 21).

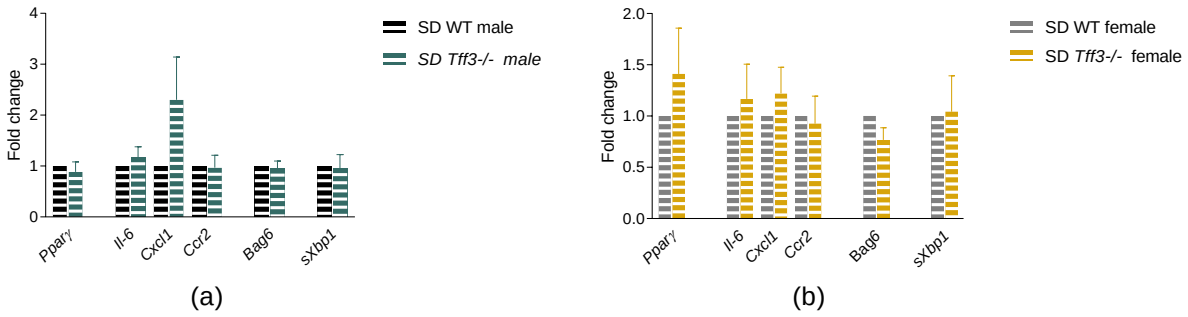

Figure 21. Gene expression of genes that showed genotype-related differences after HFD exposure showed no differences in the livers of SD-fed mice. Gene expression was analyzed by qPCR using the SYBR green detection system and presented as comparison between SD (a) WT and *Tff3-/-* male mice and (b) WT and *Tff3-/-* female mice. The obtained C_t values were analyzed using REST © software (n=5 mice per group). Results are expressed as fold change mean and standard error of the mean (SEM).

As evidenced by above presented data, male and female mice exhibited different expression profiles of genes included in monitored pathways. Graphical representations of exact differences between sexes are shown in Figures 16-20c and 16-20d

3.5.4 Protein accumulation of Pparγ and Il-6 and Cxcl1 in the liver of HFD-fed mice

To see if the changes observed on mRNA level were present on protein level western blot analysis of the protein accumulation of Pparγ and Il-6 protein (Figure 22a) in male and Pparγ and Cxcl1 (Figure 22b) protein in female livers were done. In 40-week-old mice protein levels of Pparγ were downregulated and Il-6 upregulated in the livers of HFD *Tff3-/-* male mice compared to their WT counterpart (Figure 22a). Protein levels showed the same trend observed at gene expression level, but the differences did not reach significance. The same is true for female mice, where Pparγ and Cxcl1 levels were downregulated in the livers of *Tff3-/-* mice compared to WT mice, following the trend of mRNA expression.

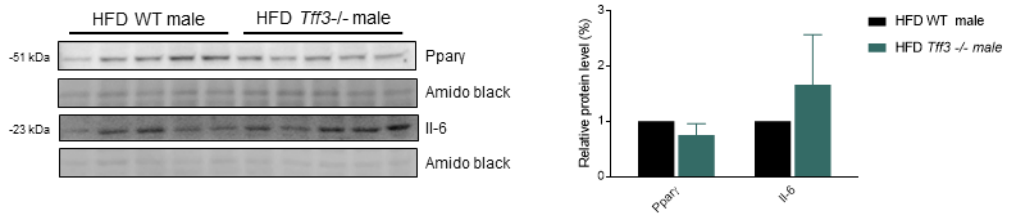

(a)

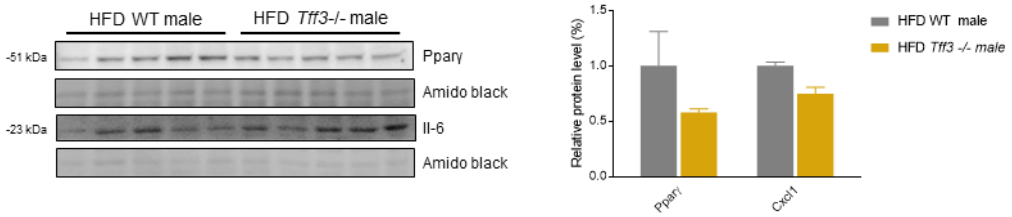

(b)

Figure 22. Protein accumulation of (a) Pparγ and Il-6 in the livers of 40-week-old male *Tff3-/-* and WT mice fed HFD and (b) Pparγ and Cxcl1 in the livers of 40-week-old female *Tff3-/-* and WT mice fed HFD. Blots showing relative protein levels in the livers of HFD WT and HFD *Tff3-/-* mice are on the left. Amido black staining was used as loading control. Associated quantification of proteins by densitometry is shown on the right. ImageJ was used to obtain the relative protein levels and they were normalized against the Amido black signal. Unpaired two-tailed Student's t- test was used for statistical analysis, and the results are shown as mean and SD.

3.6 Effect of Tff3 deficiency in the hippocampus of HFD- and SD-fed mice

3.6.1 Visualization and quantification of hippocampal cell markers

To determine whether the absence of Tff3 has a marked effect on the hippocampus of mice with long-term HFD treatment, the major cell types were labeled and visualized. Fluorescent labeling was used to determine if there were differences in the spatial arrangement and morphology of the cells. Astrocytes were labeled with glial fibrillary acidic protein (GFAP), microglia with ionized calcium binding adaptor molecule 1 (Iba1),

and mature neurons with neuronal nuclear protein (NeuN). The same cell markers were used on the hippocampus of SD -fed animals from all groups to rule out any effects of Tff3 deficiency alone. Proteins were also quantified by WB.

The astrocytes of the male HFD mice (Figure 23a, left panel) appeared to be activated compared with the male SD mice (Figure 23a, left panel), as indicated by larger somas and cell processes. The two genotypes were similar in terms of astrocyte morphology (Figure 23a, left panel) and GFAP quantity (Figure 24a). Both male HFD mice showed activation of microglia (Figure 23a, middle panel), as evidenced by swollen cell bodies and thicker, shorter processes compared with the male mice from SD (Figure 23a, middle panel). The male HFD-*Tff3-/-* mice appear to have slightly fewer activated microglia than their WT counterparts (Figure 23a, middle panel). Activation of microglia is usually followed by an increase in Iba1 accumulation, which is not visible here in the protein content of the HFD-*Tff3-/-* mice (Figure 24a). Visualization of neurons (Figure 23a, lower panel) and quantification of NeuN (Figure 24) showed no significant differences.

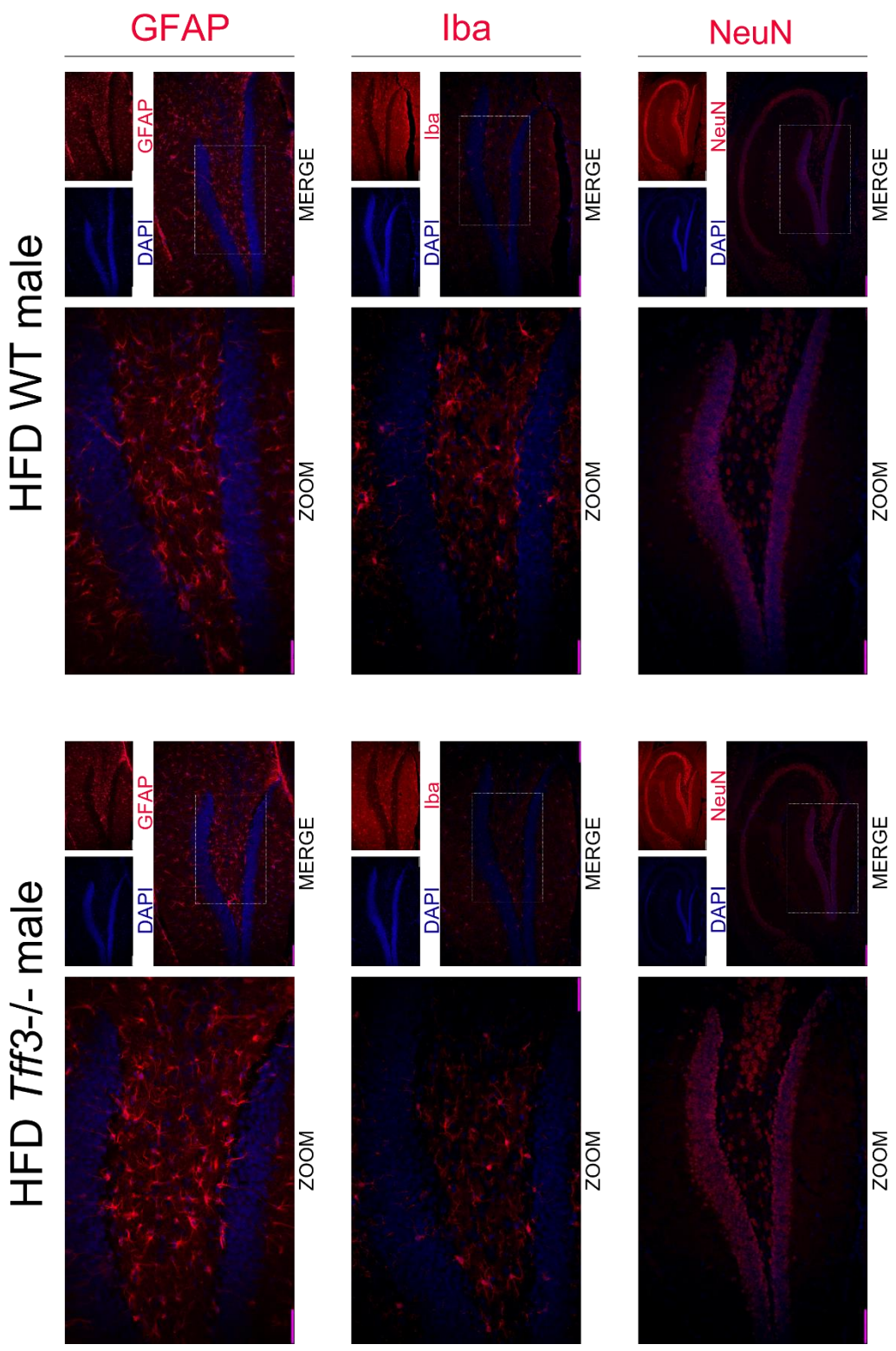

Figure 23. Caption on page 62.

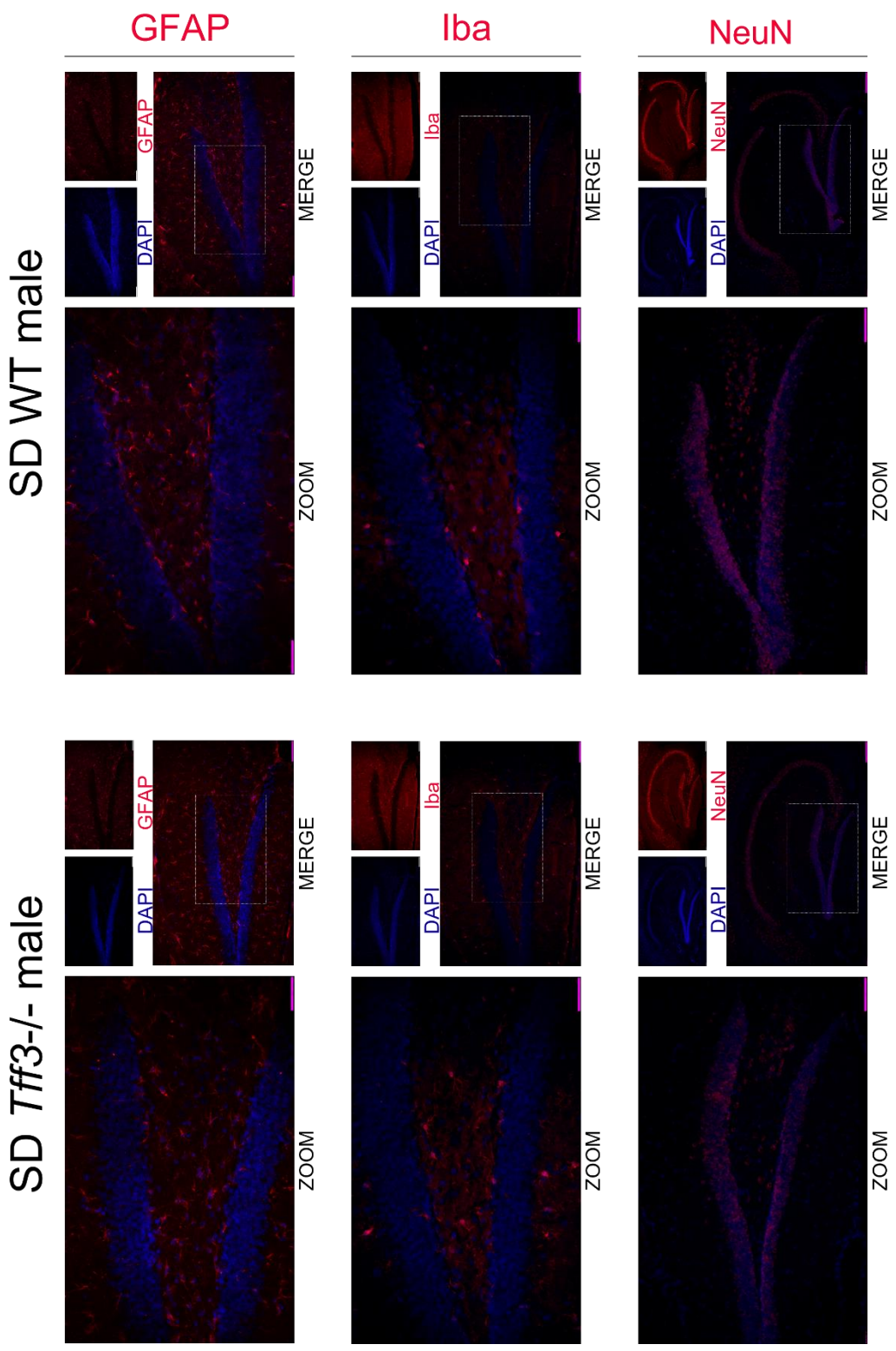

(b)

Figure 23. Caption on page 62.

Figure 23. The effects of Tff3 deficiency on cell morphology of specific cell type protein markers in hippocampi of (a) HFD and (b) SD male mice. Immunofluorescence images of dentate gyrus of hippocampus showing astrocytes labeled by GFAP (left panel), microglia labeled by Iba1 (middle panel), and mature neurons labelled by NeuN (right panel).

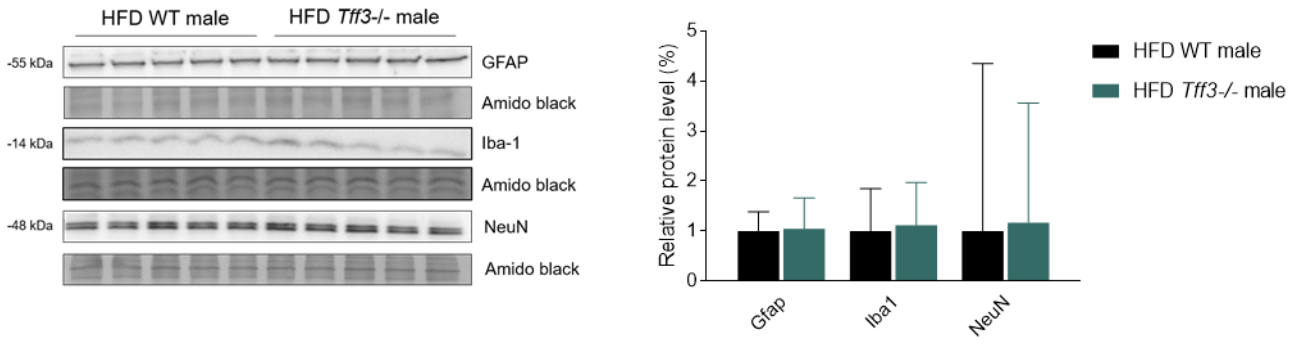

(a)

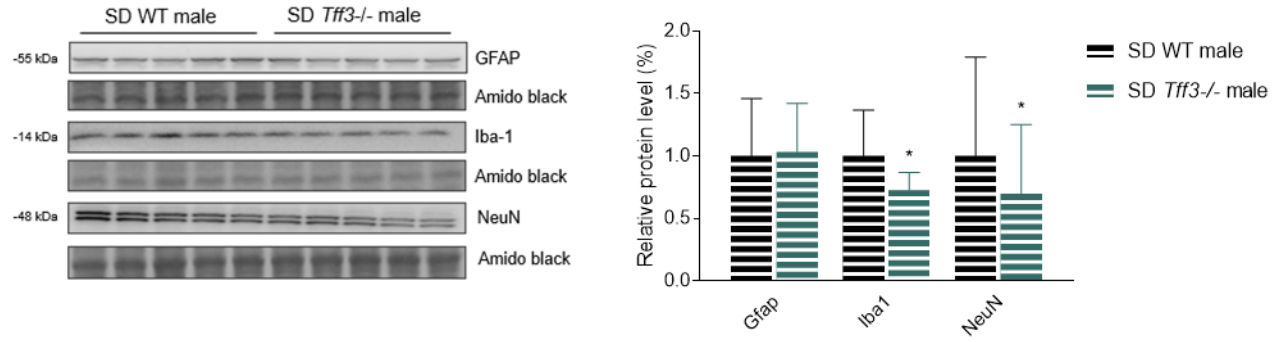

(b)

Figure 24. The effect of Tff3 deficiency on expression of specific cell type protein markers in hippocampi of (a) HFD and (b) SD exposed male mice. Protein levels of specific cell type markers GFAP (astrocytes), Iba1 (microglia) and NeuN (mature neurons) was determined by western blot (left) and associated protein quantification by densitometry (right). ImageJ was used to obtain the relative protein levels and they were normalized against the Amido black signal. Unpaired two-tailed Student's t- test was used for statistical analysis, and the results are shown as mean and SD. ** $p \leq 0.05$*

In female HFD mice, astrocytes were similar in both morphology (Figure 25a, left panel) and GFAP accumulation (Figure 26a). HFD *Tff3-/-* female mice had more activated microglia compared to WT female mice (Figure 25a, middle panel). This was followed by a slight increase in Iba1 protein levels in the hippocampus (Figure 26a). NeuN was slightly but not significantly increased in *Tff3-/-* females.

SD-fed mice appeared to have generally inactive astrocytes and microglia (Figures 23b and 25b, left and middle panels). Morphology and arrangement of cells showed no major differences between genotypes in male SD mice (Figure 23b). However, protein quantification showed a reduction in Iba1 and NeuN protein levels in the hippocampus of male SD *Tff3-/-* mice compared with WT mice (Figure 24b). SD female mice did not show statistically significant differences between genotypes (Figures 25a and 25b).

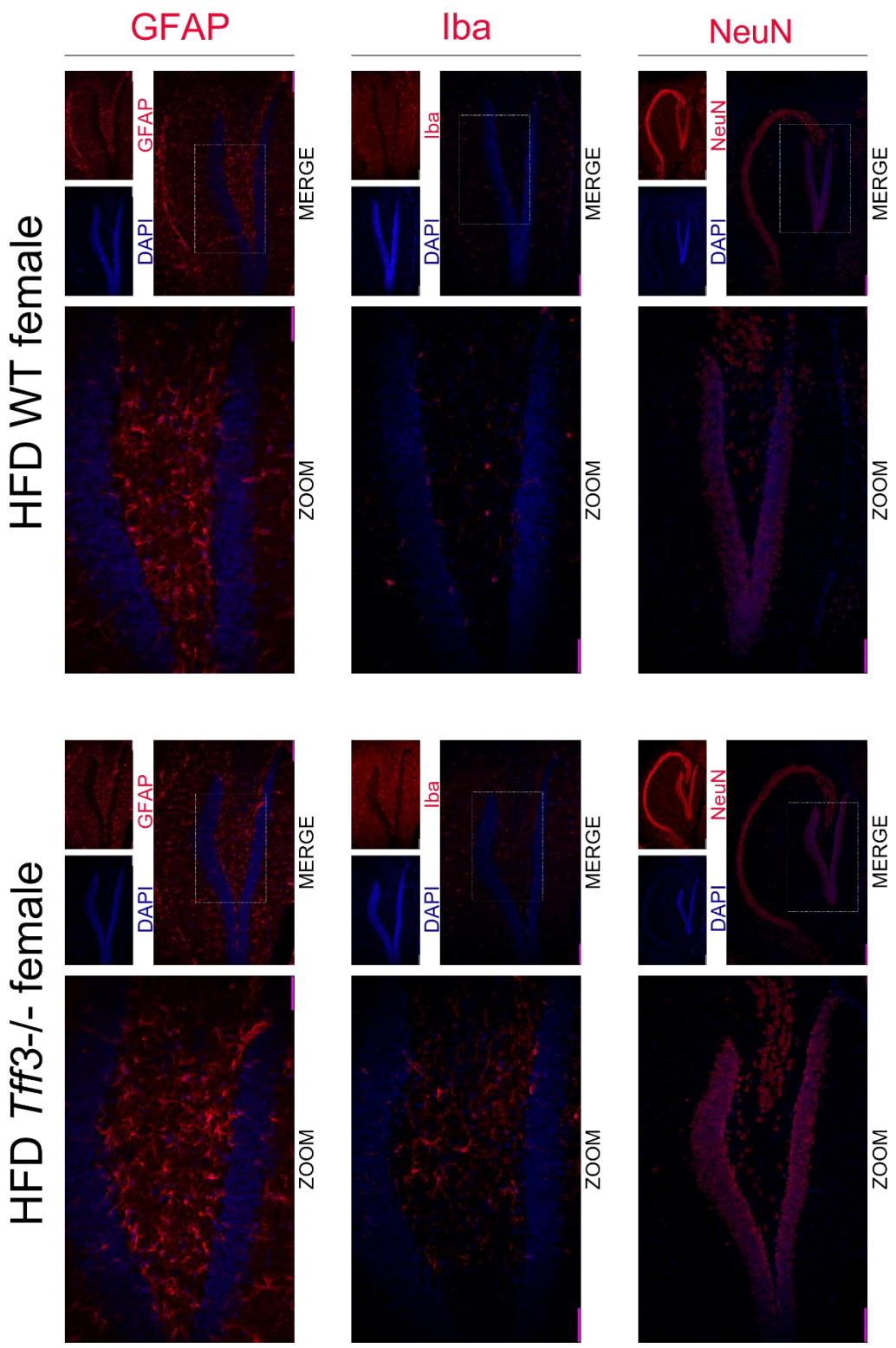

(a)

Figure 25. Caption on page 67.

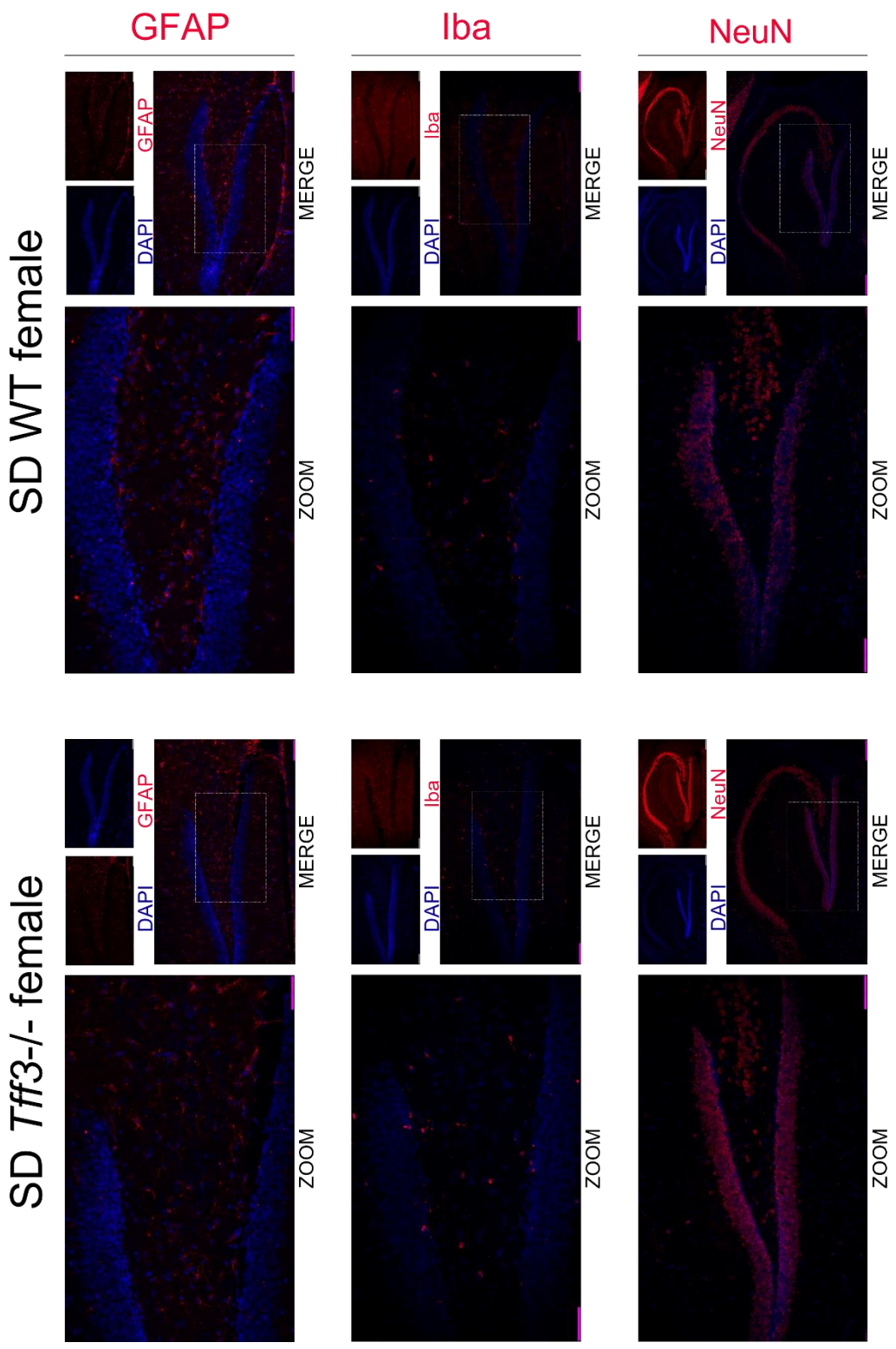

(b)

Figure 25. Caption on page 67.

Figure 25. The effect of Tff3 deficiency on cell morphology of specific cell type protein markers in hippocampi of (a) HFD and (b) SD male mice. Immunofluorescence images of dentate gyrus of hippocampus showing astrocytes labeled by GFAP (left panel), microglia labeled by Iba1 (middle panel), and mature neurons labeled by NeuN (right panel).

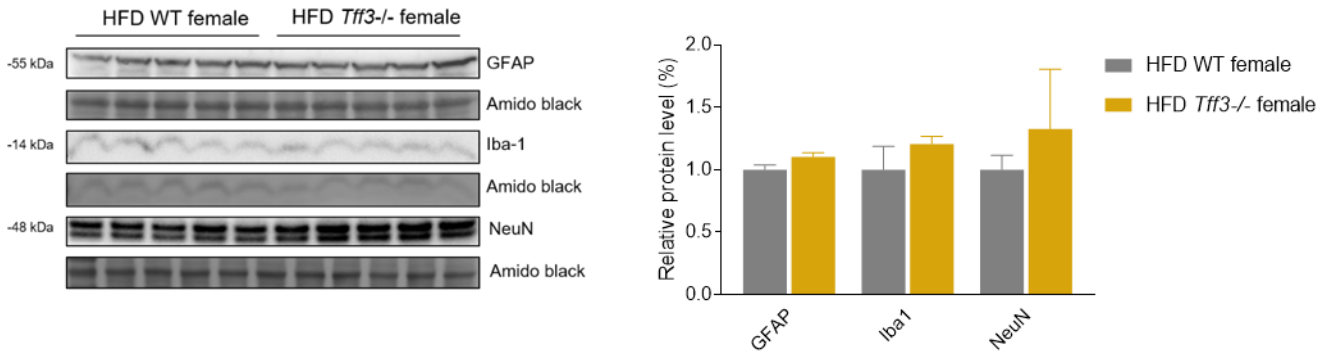

(a)

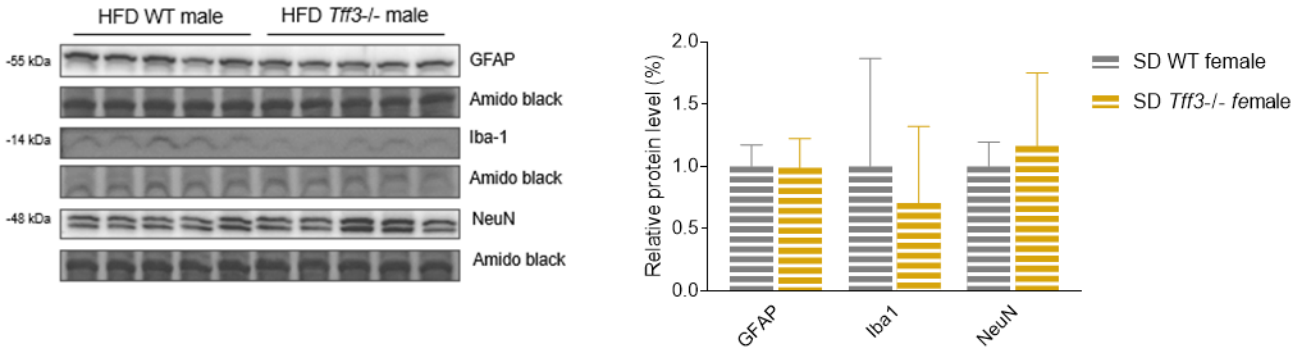

(b)

Figure 26. The effect of Tff3 deficiency on expression of specific cell protein markers in hippocampi of (a) HFD and (b) SD exposed female mice. Protein levels of specific cell type markers GFAP (astrocytes), Iba1 (microglia) and NeuN (mature neurons) was determined by western blot (left) and associated protein quantification by densitometry (right). ImageJ was used to obtain the relative protein levels and they were normalized against the Amido black signal. Unpaired two-tailed Student's t- test was used for statistical analysis, and the results are shown as mean and SD.

3.6.2 The effect of Tff3 absence on synaptic integrity and neurodegeneration

To determine whether Tff3 deficiency affects synaptic integrity, levels of Synaptosomal-Associated Protein, 25kDa (Snap-25), a marker of functional synapses, were determined by Western blot. No significant differences in Snap-25 protein levels were observed

between mice of genotype WT and genotype *Tff3-/-*, regardless of sex and diet (Figure 27).

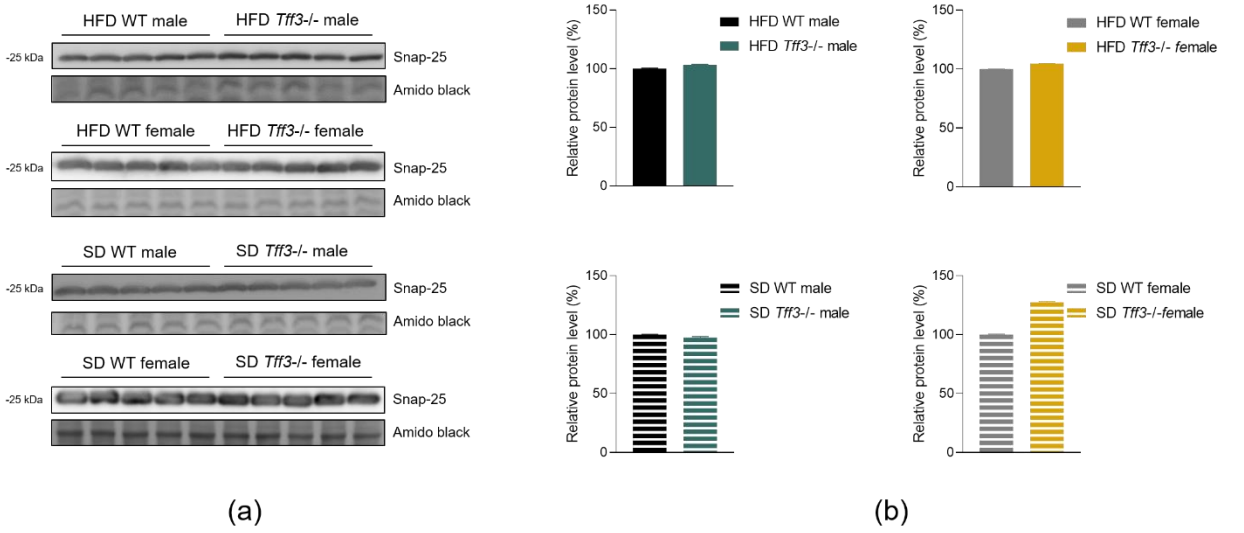

Figure 27. Protein accumulation of Snap-25 in the hippocampi of 40-week-old *Tff3-/-* and WT mice fed. (a) Blots showing Snap protein levels in the hippocampi of male HFD WT and HFD *Tff3-/-* mice (top panel), female HFD WT and HFD *Tff3-/-* mice (upper middle panel), male SD WT and SD *Tff3-/-* mice (lower middle panel), and female SD WT and SD *Tff3-/-* mice. Amido black staining was used as loading control. (b) Associated quantification of proteins by densitometry. ImageJ was used to obtain the relative protein levels and they were normalized against the Amido black signal. Unpaired two-tailed Student's t- test was used for statistical analysis, and the results are shown as mean and SD.

Brain sections were stained with Fluoro-Jade C to visualize degenerating neurons. While SD fed animals showed no signal (data not shown), hippocampi from HFD mice showed some signal (Figure 28).

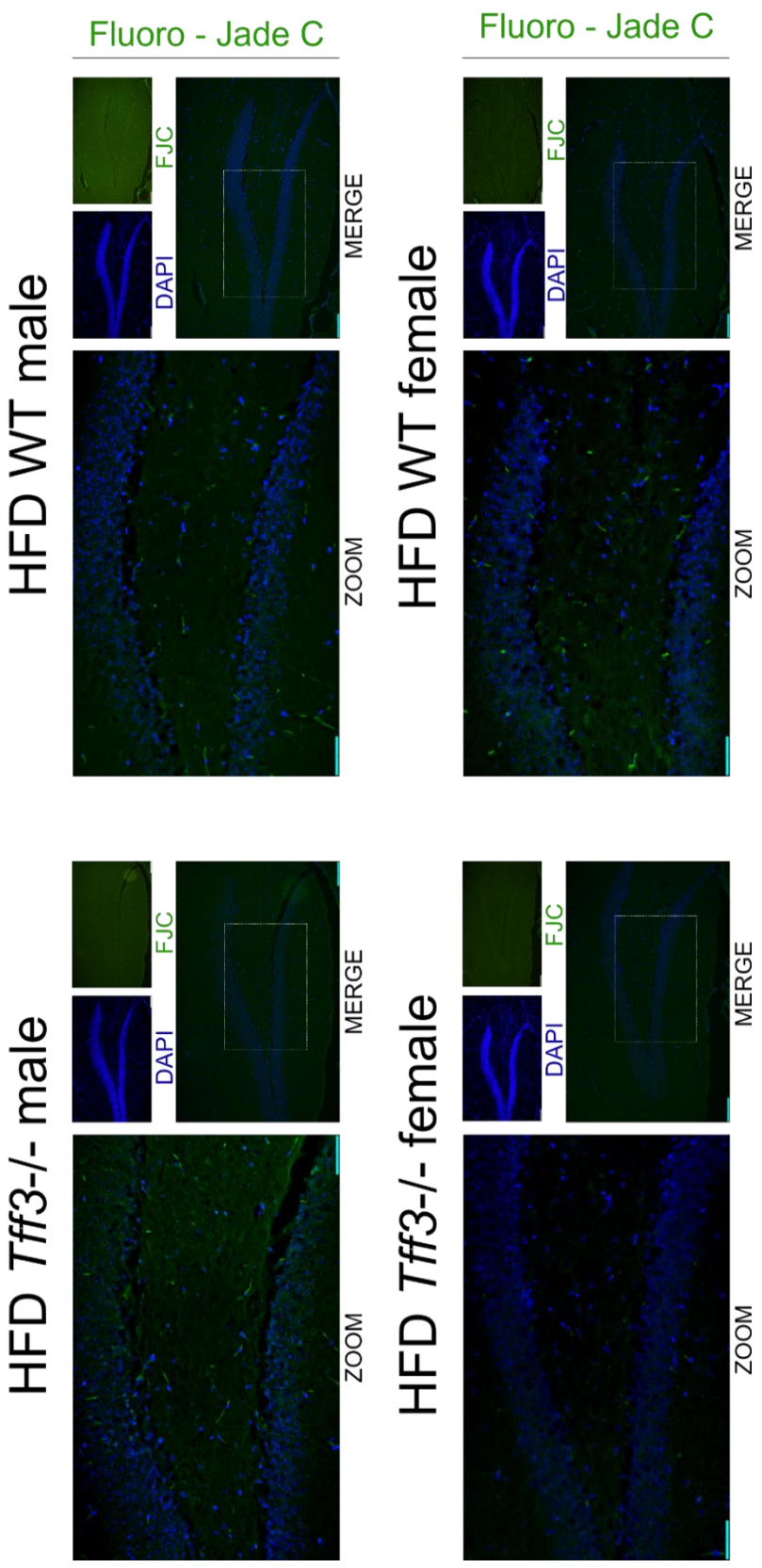

Figure 28. Caption on page 71.

Figure 28. The effect of the absence of Tff3 on degenerating neurons in hippocampus amid long term HFD consumption. Brain slices stained with FluoroJade C show degenerating neurons in dentate gyrus of hippocampus of 40-week-old HFD fed male and female WT and *Tff3-/-* mice.

4 Discussion

Metabolic and neurodegenerative diseases are a growing public health concern. They share signaling pathways that may help clarify the developmental mechanisms of these complex conditions. The Tff3 protein is involved in numerous metabolic processes (36,37,132,133,38,40–42,52,95,96,131), and it displayed a potential to be a biomarker for brain atrophy and ventricular expansion in Alzheimer's disease (112). Given the intertwining of metabolic and neuronal pathophysiology with the function of Tff3 protein, the question of its systemic effect in metabolic and neurodegenerative processes arises. Therefore, the aim of this study was to determine the systemic effect of Tff3 deficiency in C57BL6/N genotype mice exposed to chronic metabolic stress induced by HFD treatment. The focus was on overall metabolic status and liver and hippocampal integrity. To mimic the high-calorie, high-fat diet prevalent in modern lifestyle, a group of mice with genetic background C57BL6N were exposed to HFD for 8 months. This included WT and *Tff3*-/- mice of both sexes. Age- and sex-matched control mice were fed SD during the same period to account for any metabolic effect of Tff3 deficiency independent of the burden of fat overload.

4.1 The effect of Tff3 deficiency on body weight of mice

To determine whether Tff3 deficiency caused a differential overall response to stress induced by high energy intake, mice were weighed halfway through and at the end of HFD exposure. Male HFD WT mice weighed significantly less than male *Tff3-/-* mice at 21 weeks of age (17 weeks of HFD) (Figure 4a). Further HFD treatment narrowed these differences by 36 weeks of age (32 weeks of HFD) (Figure 4b). Age- and sex-matched SD-fed mice were weighed at the same age (Figure 4b) to determine if Tff3 deficiency itself was at the root of this distinction. No significant weight difference was observed between SD WT and *Tff3-/-* mice, regardless of age or sex. In B6.CAST-17 congenic mice, whose characteristics include significantly increased carbohydrate and total caloric

intake, compared with their C57BL/6 WT littermates, considerable upregulation of Tff3 was observed (134), indicating that Tff3 might have an impact on general energy intake. Here, the absence of Tff3 is shown to have a significant effect on weight only in combination with HFD treatment. This effect was dependent on the duration of the treatment, as it was attenuated by the end of it. Previously, more pronounced weight loss in *Tff3-/-* mice than WT mice after dextran sulphate sodium (DSS) treatment (15) and significantly lower body weight in *Tff3-/-* than WT mice after five months of SD (96) were reported. Later, it was shown that Tff3 deficiency had no effect on the weight of 12-week-old mice (38). It is important to note that these mice had a mixed genetic background (C57BL6J/Sv129) with unknown genetic recombination input, possibly contributing to phenotype. In this work, a new congenic *Tff3-/-* strain on the genetic background C57BL/6N without additional metabolically relevant mutations (39) was used. Since the body weight of mice is strongly influenced by many factors, including strain, age, sex, and diet, their complex interactions may explain the discrepancy between the results.

4.2 Differential Tff3 expression in the liver due to obesity or sex

The first time that Tff3 protein was associated with metabolic dysfunction was a study in which dramatically lower gene expression was observed in the livers of 7-week-old Tally-Ho mice, a model for T2D, compared with control mice (41). The same was observed in genetic models of obesity, ob/ob and db/db mice, and in mice in which obesity was induced by high-fat consumption (36,37), as well as in models of hepatic steatosis (132). This study confirmed that HFD intake reduced Tff3 expression in the livers of male WT mice (Figure 11a). There was virtually no difference in *Tff3* expression between HFD and SD female mice (Figure 11b). Further analysis revealed that female mice, both HFD- and SD-fed, showed exceptionally low Tff3 expression in the liver (Figure 11c and 11d).

The sexual dimorphism of Tff3 expression in the liver may be an additional factor in the differential regulation of disease processes in male and female individuals, as illustrated here by the differences between males and females in the majority of the data.

4.3 Protective effect of Tff3 deficiency on metabolic status of mice

The previously reported involvement of Tff3 in metabolic homeostasis (36,37,132,133,38,40–42,52,95,96,131) prompted metabolic testing. Metabolic tests were performed on *Tff3-/-* and WT mice of both sexes and under different nutritional conditions (Figures 5,6,8, and 9). The IPGTT performed on HFD mice at 21 weeks of age revealed that male HFD *Tff3-/-*mice utilized glucose from the blood faster than WT mice (Figure 5a). At 36 weeks of age, this difference diminishes to the point that, conversely, at 60' timepoint male HFD WT mice exhibit faster glucose utilization than their *Tff3-/-* counterparts (Figure 5e). In contrast, at 21 weeks of age, SD male mice showed no differences in glucose tolerance (Figure 5c). The differences appeared at 36 weeks of age, when male SD *Tff3-/-* mice showed better glucose tolerance than male SD WT mice (Figure 5g). It seems that male *Tff3-/-* mice are better able to maintain glucose tolerance when faced with stress, whether induced by HFD or ageing.

Female mice of both genotypes had very similar glucose tolerance, regardless of age or diet (Figures 5b, 5d, 5f, and 5h). The only exception was at the 30' time point in a test on 21-week-old female SD mice (Figure 5d). Here, *Tff3-/-* mice showed more rapid glucose uptake from the blood.

In IPITT, male HFD mice showed no differences between genotypes, regardless of age (Figures 8a and 8e). Female HFD *Tff3-/-* mice showed slightly better insulin tolerance than SD WT females, with significantly lower glucose levels 60' and 120' after insulin administration at 23 weeks of age (Figure 8b).

Standard diet - fed 23-week-old male *Tff3-/-* mice exhibited lower glucose level throughout the test (Figure 8c), while female SD *Tff3-/-*mice exhibited lower glucose levels at the beginning and the end of the test (Figure 8d). Interestingly, both male and female mice showed genotype related differences in fasting glucose levels (at 0') after 4 hours of fasting before IPITT (Figure 8c and 8d), whereas there were no differences between the same animals after 16 hours of fasting prior to IPGTT (Figures 5c and 5d). This shows

once again how each factor can influence metabolic regulation. At 38 weeks of age, the only difference remains at the end of the test (120') performed on male SD mice (Figure 8g).

Consistent with the trend in this study, Tff3 deficiency in 12-week-old mixed background mice on SD resulted in lower glucose levels compared to WT mice at 15' and 30' after both glucose and insulin administration (38). On the other hand, overexpression of Tff3 also improved glucose tolerance and insulin sensitivity in obese mice (genetic and diet-induced obesity models) (37,42). There are many unknowns surrounding Tff3, its complete function, its interactions, and its exact expression pattern. Moreover, many factors contribute to metabolic regulation and consequently to the outcome of metabolic tests. From this study alone it is clear that factors such as diet, age or fasting time, which is not yet standardized in animal research, can drastically alter the glucose levels. Additionally, there is the issue of genetic background and mutations in the are C57BL/6J strain which may affect metabolic homeostasis. This complex mixture of influences on metabolic regulation makes it difficult to determine the exact reason that the absence and overexpression of Tff3 result in similar effects.

Biochemical analysis of serum after 36 weeks of HFD was used as an indicator of general health status of mice (Figure 12). It revealed changes in levels of LDL, total cholesterol, ALT and ALP, which were lower in the serum of male *Tff3-/-* mice compared with male WT mice. This was not the case for Tff3- deficient mice on mixed genetic background (38). Overexpression of Tff3 in obese mice also did not have any effect on cholesterol levels (42). In rats with non-alcoholic steatohepatitis (NASH) - a progressive form of NAFLD, recombinant human Tff3 administration had a similar effect as here presented Tff3 deficiency, as it reduced the levels of serum markers of liver integrity ALT and ALP (34). Overall, it is difficult to conclude exact reasons for observed phenotypes in this complex metabolic model.

4.4 Tff3 deficiency ameliorates fatty liver phenotype

The complexity of metabolism is illustrated by the liver lipid homeostasis. Its imbalance leads to a variety of metabolic syndrome manifestations, including insulin resistance, type 2 diabetes, and fatty liver phenotype (135). The association is so close that recently a group of experts reached the consensus that metabolic (dysfunction) associated fatty liver disease (MAFLD) is a more appropriate term for heterogeneous pathogenesis hitherto known as non-alcoholic fatty liver disease (NAFLD) (136). Hepatic steatosis is a hallmark of metabolic disease and all but guaranteed under the stressful conditions of long-term exposure to HFD. Given the potentially deleterious effects of HFD on liver integrity and the fact that serum biochemistry points towards protective effects of Tff3 deficiency in the liver, the liver histomorphology was examined (Figures 13-15). Not surprisingly, HFD mice of both genotypes, exhibited signs of hepatic steatosis, but these were markedly reduced in the livers of HFD *Tff3-/-* mice of both sexes compared with HFD WT mice, as confirmed by fatty acid content analysis (Table 6). Although there was no evidence of steatosis, the livers of mice fed with SD showed some lipid accumulation, which was less in the livers of SD Tff3 mice of both sexes than in the livers of their WT counterparts (Figure 15). Lipid droplets of *Tff3-/-* mice seemed to be smaller compared to WT mice. In line with the work presented here, Tff3 was increased in the livers of *Cbs*-deficient mice, a model of genetic fatty liver (132). However, the same group showed a negative association between Tff3 and hepatic fat in in apoE-deficient mice consuming linoleic acid (LA)-containing diet.

Hepatic adenoviral overexpression of Tff3 in diabetic (db/db) and obese (ob/ob) mice showed a protective effect against hepatic steatosis (36). It was shown that it can upregulate the expression of PPAR α and thus promote fatty acid oxidation. Additionally, ChIP assay of mouse liver tissue showed that Tff3 can bind to the promotor region of PPARα. Tff3 deficient mice on mixed genetic background had an increased number of smaller lipid containing vesicles in the hepatocytes compared with WT mice on a standard diet (38). Lipid droplets are mobile and dynamic organelles with vital roles in the homeostasis of cellular metabolism and do not function as metabolically inactive lipid stores as previously thought (137). Lipid droplets have a hydrophobic core enclosed in a

phospholipid monolayer membrane (138). Phospholipid content of the membrane can affect the size of the droplets. It would be interesting to see if there is a connection between Tff3 and any of the factors influencing phospholipid composition of the membrane (139), synthesis, growth or catabolism of lipid droplets (140) or interactions between lipid droplets and other organelles (141). Tff3 shows an undeniable but varied effect on hepatic steatosis and further studies are necessary to explain the reasons behind the different directions of regulation.

Morphological differences were followed by quantitative differences in liver total fat content (Tables 6 And 7). *Tff3-/-* mice show reduced total liver fat compared to WT mice. both male and female mice, no matter the diet. Since it was shown that fatty acids may have a key role in the development of insulin resistance and type 2 diabetes (142), liver fat composition was analyzed. While HFD animals show similar fatty acid composition between genotypes, SD animals show some genotype related differences. In both male and female SD *Tff3-/-* mice level of total saturated fatty acid (SFA) content was significantly increased and of total monounsaturated fatty acids (MUFA) significantly decreased. The only specific significantly decreased SFA was palmitic acid (16:0) and the significantly increased MUFA was octadecanoic acid (18:1), of which oleic acid is the main representative. Tff3 knockout mice with mixed genetic background did not show the same for palmitic acid, but did for SFA, MUFA, and oleic acid, as well as several other FAs that were not altered here (38). Interestingly, palmitic acid was shown to have deleterious and oleic acid beneficial effects on insulin resistance and type 2 diabetes (143). In this regard, SD *Tff3-/-* male mice of this study had significantly better glucose tolerance and slightly better insulin response.

4.5 Tff3 deficiency affects the expression of genes involved in important pathophysiological processes in the liver

HFD uptake affects a variety of signaling pathways and processes underlying the pathophysiology of metabolic disorders. Genes involved in inflammation, fatty acid metabolism, apoptosis, endoplasmic reticulum stress, and oxidative stress were studied in liver tissue. Among all genes analyzed, several showed differential regulation between HFD mice of the two genotypes. When analyzed in SD mice, they showed similar expression between *Tff3-/-* and WT mice, meaning that the variation in their expression was due to HFD induced response and not Tff3 deficiency itself.

Pparγ expression was downregulated in HFD males and females of *Tff3-/-* genotype (Figure 16). Protein accumulation followed a downward trend but without reaching statistical significance (Figure 22). Pparγ is a transcription factor that regulates fatty acid storage and glucose metabolism. It is not abundantly expressed in the liver under normal conditions, but its hepatic expression has been shown to be upregulated in murine models of obesity and hepatic steatosis (144–153). Liver-specific deletion of Pparγ was shown to reduce liver steatosis in mice treated with HFD and ethanol (154). The link between Tff3 and Pparγ was first suggested because conjugated linoleic acid treatment induced their expression of mouse colitis-affected colon and human colonocyte cell line, while pre-treatment of the cells with a Pparγ inhibitor prevented the Tff3 induction (155). This interaction is also supported by the presence of potential PPARγ-binding sites in the promoter sequence of TFF3 and previous findings of PPARγ-dependent regulation of TFF2 in gastric epithelial cells (156). In addition, it has been suggested that Tff3 attenuates NAFLD via an increase in PPARα expression through direct binding to the PPARα promoter (36). *Pparα* mRNA level was unchanged in SD *Tff3-/-* mice.

The only significant change in cytokine levels in male mice was an increase in Il-6 expression in the absence of Tff3 (Figure 17a). On the protein level, the same trend was observed, but without statistical significance (Figure 22a). Il-6 is a cytokine involved,

among many others, in the pathophysiology of obesity and its comorbidities, although its exact role remains to be elucidated (157). Il-6 knockout mice develop obesity, insulin resistance, hepatic steatosis and inflammation, and worse phenotype than controls when subjected to HFD treatment, suggesting a protective role (158). In this study, it also seemed to have a protective role as its upregulation was observed in mice with a less pronounced obesity phenotype. In our previous work *Tff3-/-* male mice exhibited liver Il-6 mRNA increase in response to high salt burden (115), while there were also no differences between genotypes in mice on SD. Small interfering RNA (siRNA) - mediated downregulation of *Tff3* expression induced IL-6/JAK/STAT3 pathway and treatment with TFF3 inhibited it in thyroid cancer cells (159) and human bronchial epithelial cells (160). Another group reported a reciprocal relationship between the two (26). IL-6/STAT3 signaling initiated the expression of *Tff3* in biliary epithelial cells (BEC) and subsequently promoted proliferation and migration to facilitate wound healing in response to bile duct injury.

Overload of lipids, free fatty acids and cholesterol can trigger ER stress, which leads to unfolded protein response (UPR) to restore normal ER function (161). Among the ER stress markers, *sXbp1* was significantly upregulated in the livers of HFD male *Tff3-/-* mice compared to WT (Figure 19a). Tffs, including Tff3, have been associated with ER stress pathways before (113,162–166), but to my knowledge this is the first connection to *sXbp1*. SXbp1 is an active transcription factor, a product of cleaving Xbp1 by inositol-requiring protein 1 alpha (IRE1 α) (167), one of the three transmembrane stress sensors by which UPR is mediated (168). Hepatic sXbp1 has been identified as a transcription factor that regulates the expression of genes involved in lipid metabolism (169–171), as well as, glucose and insulin homeostasis (172,173). Xbp1 activity is significantly reduced in the liver of ob/ob mice compared with WT mice (172) and once restored, glucose homeostasis improves (172,174,175). Moreover, Xbp1- deficient mice develop glucose intolerance and systemic insulin resistance. (176). As mentioned previously, IRE -1α activates splicing of Xbp1, and liver-specific IRE -1α-null mice have been shown to develop severe fatty liver disease following ER stress induction (177). These findings suggest that Xbp1, albeit with unresolved molecular mechanism, may play a protective

role in the development of hepatic steatosis. The upregulation of sXbp1 mRNA expression in HFD male *Tff3-/-* mice compared to HFD WT mice shown in this work supports sXbp1 acting as a protective factor in the obesity-associated metabolic conditions.

Pparγ, Il-6 and Xbp1 have been shown to be interdependently related in many different contexts and directions: Pparγ can have an effect on Il-6 (178–184), Il-6 on Pparγ (185–187), Pparγ on Xbp1 (188), Xbp1 on Pparγ (177,189,190), Il-6 on Xbp1 (191–193), and Xbp1 on Il-6 (194,195,204,196–203). It is impossible to say without more extensive research, but perhaps they regulate each other through the same pathway. As previously mentioned, siRNA – mediated downregulation of *Tff3* is able to induce IL-6/JAK/STAT3 pathway(159,160), some of the Il-6-Xbp1 interactions mentioned also included STAT3 signaling (186,194,197,198), Pparγ was known to interact with STAT3, and Tff3 can regulate STAT3 at the promoter level (205). Taken together, this raises the question of whether STAT3 could be a common denominator in this potential signaling pathway.

In addition to *Pparγ* mentioned above, female mice displayed differences in *Cxcl*1, *Ccr2* (Figure 17b), and *Bag6* (Figure 18b) expression. Cxcl1 one reduction observed on mRNA level was present on protein level as well (Figure 22b). Cxcl1 acts as a chemoattractant for neutrophils (206). Hepatic infiltration of neutrophils is critical for the development of inflammatory liver disease and accelerates the NAFLD progression (207). Its expression was lower in the livers of HFD *Tff3-/-* females, which exhibited attenuated steatosis compared to HFD WT females. In our previous work *Tff3-/-* mice, albeit male, also had lower *Cxcl1* expression compared to WT mice upon the induction of ER stress, another stressful condition characterized by increased inflammation (208). Liver-specific deletion of Pparγ reduced hepatic steatosis and caused Cxcl1 upregulation (154). However, in several tissues, activation of Pparγ resulted in both an increase (209) and a decrease (210,211) in Cxcl1 expression.

Ccr2 mediates the recruitment of monocytes and macrophages to the site of inflammation by binding monocyte chemoattractant protein-1 (Mcp-1). Both were reduced in the livers

of *Tff3-/-* females compared to WT female, but only Ccr2 significantly (Figure 17b). Ccr2 deficiency ameliorated hepatic steatosis, improved glucose homeostasis and insulin sensitivity in obese mice (212). Ccr2 may trigger the expression of Ppar (213), while Pparγ was shown to have inhibitory effect on Ccr2 (214–216). It is possible that Pparγ is included in the regulation of these cytokines by Tff3.

Bag6 was upregulated in the liver of *Tff3-/-* female mice (Figure 18b). Bag6/Bat3/Scythe is a protein complex involved in apoptosis and membrane proteins quality control (164). Screening of the mouse cochlear cDNA library with a yeast-two-hybrid assay identified Bcl2-associated athanogene 6 (Bag6/Bat3/Scythe) as a potential Tff3 interactive partner (113).

Taken together, the results presented show that the Tff3 protein is involved in complex metabolic processes and its absence throughout the body appears to be a protective factor, as evidenced by the improvement in steatosis and glucose and insulin homeostasis (in some cases), as well as favorable expression profile of relevant genes in mice of the *Tff3-/-* genotype.

4.6 Astrocytes, microglia, and neurons in the absence of Tff3

Since the first report of Tff3 expression in the brain (98), it has been referred to as a neuropeptide and has been detected several times in different regions of the mammalian brain. It has been associated with many brain-related pathologies, including neurodegeneration (108,110–112). Obesity and HFD associated with metabolic syndrome have been linked to cognitive impairment, neuroinflammation, and eventually neurodegeneration. To elucidate the role of Tff3 in this context, we have determined whether its absence has effects on the hippocampus of mice exposed to HFD-induced stress.

The major cell types in the brain were visualized using common cell protein markers, which were also quantified. HFD treatment caused signs of neuroinflammation in male and female mice, as evidenced by activation of astrocytes and microglia (Figures 23a, and 25a) absent in SD mice (Figures 23b and 25b). Activation of astrocytes is characterized by their hypertrophy and increased expression of GFAP (217). Microglial activation can be recognized by increased soma size, shorter and thicker processes and increased Iba1 expression (218). Age- and sex- matched animals fed SD did not exhibit such activation (Figures 23b and 25b).

Astrocytes are the most abundant glial cells in the central nervous system (219) with a role in maintaining the homeostasis. They are involved in neuroinflammation, and their response may be inflammatory or immunosuppressive depending on the environment (220). Astrocyte activation is provoked by HFD (221–224). According to Arnold et al, Tff3 was found in vesicles within astrocytes in primary cultures from rat cortex, and its transcription was reduced by incubation with LPS. On the other hand, Tff3 was not synthesized by primary astrocytes from rat hippocampus (45). In this study, no genotype-related differences were observed in astrocytes, suggesting that Tff3 deficiency has no influence in this context (Figures 23-26)

Iba1, a marker for microglial cells, was altered by Tff3 deficiency in SD males. Male SD Tff3 -/- mice had significantly lower accumulation of Iba1 protein in the hippocampus (Figure 24b). Both male and female HFD mice showed activation of microglia, females less so (Figures 23a and 25a). This activation is not surprising, as it has been previously shown that HFD induces microglia activation (221,222,225–230). Interestingly, male HFD mice *Tff3-/-* mice appeared to have slightly less activated microglia (Figure 23a) while female HFD *Tff3-/-* mice exhibited more activation than their WT counterparts (Figure 25a). This may be because male Tff3-/- mice have lower microglia levels even in the absence of activation by HFD, preventing them from catching up with WT mice in the inflamed state. Activation of microglia is not only reflected in the morphological changes but is also accompanied by upregulation of Iba1 (45,218). Fu et al. reported the expression of Tff3 in primary rat hippocampal and cortical Iba-1-expressing cells and even showed co-localization of Iba1 and Tff3 in cortical cell culture. Microglia are characterized

by their rapid activation in response to even minor pathological challenges in the CNS. Recently, even middle-aged mice were found to exhibit some reactivity.

NeuN was also downregulated in the hippocampi of male SD *Tff3-/-* mice compared to WT mice (Figure 24b), indicating neuronal loss in Tff3 deficient males on SD. Tff3 was detected in the neurons of almost all brain regions in humans and rodents (44,46,47,97–101). It was expressed by and colocalized with microtubule-associated protein 2 (Map2) (another marker of neurons) in primary rat cortical and hippocampal cell cultures, as well as in the cerebellum of adult rats (45). It exerts protective effect on injured neurons in the ischemic cerebral tissue of mouse model of stroke (114). Taken together, this suggests an important role of Tff3 in neuron function, corroborated by the above presented finding.

4.7 The effects of Tff3 deficiency on one of the hallmarks of early neurodegeneration pathology and neurodegeneration itself

Since Tff3 has been associated with several neurodegenerative pathologies (108,110–112), the aim was to determine if Tff3 deficiency has impact on synaptic function as an early pathological event in neurodegeneration (231) and neurodegeneration itself. Synaptic function was assessed by quantifying Synaptosomal-Associated Protein, 25kDa (Snap-25), a marker of functional synapses (232,233). This marker was chosen among many because my research group found it was affected by Tff3 deficiency in the hippocampus of a different mouse model on shorter HFD regimen (unpublished data). The level of SNAP 25 was not affected by Tff3 deficiency, neither in SD nor HFD model of this study (Figure 27).

It is known that HFD can induce neurodegeneration (127). Brain sections were stained with FJC (234,235) and, indeed, HFD caused neuronal degeneration (Figure 28) in both *Tff3*-/- and WT mice. Interestingly, Fluoro-Jade C staining showed some elongated signals, seemingly in blood vessels. The signal in blood vessels could be due to inefficient perfusion, since FJC is an analogue of eosin and could stain blood cells (236). However,

both HFD and SD animal groups were perfused in the same way, and these signals weren't present in SD animals. Additionally, a recent study suggests that Thiazine Red positive platelet inclusions in the cerebral blood vessels are an early sign of disease in AD mouse model (237). Perhaps, HFD treatment induced similar platelet aggregation in cerebral blood vessels here, which made them harder to perfuse entirely than those without platelet aggregation in SD mice.

Taken together the data acquired by this study suggest a role of Tff3 in changes induced by HFD treatment, however it is still unclear.

4.8 Commentary on Sexual Dimorphism

The subject of sexual dimorphism in these data could be a whole different dissertation, so it was only briefly touched upon earlier in the thesis, but it is important to note that the sex of the animals was a very influential variable, which influenced the outcome of each experiment presented in this thesis. Sexual dimorphism is ubiquitous but has been largely ignored in biomedical research for years. The data presented here highlight the importance of including both sexes in research and clearly identifying the strain and sex of animal models or participants.

5 Conclusion

Whole-body deficiency of Tff3 resulted in a differential response of C57BL6/N mice to chronic metabolic stress induced by long-term HFD consumption, and the treatment caused *Tff3* reduction in the livers of WT animals, confirming a distinct role of Tff3 protein in metabolic processes. As hypothesized, the absence of Tff3 showed a protective effect on glucose homeostasis in and lipid regulation. Previous studies usually indicate a protective effect of its increased expression or its systemic administration. However, this study was the first to be performed in a *Tff3*-/- mouse on a pure C57BL/6N genetic background, which excluded the possibility of the influence of potential heterozygosity and metabolic mutations. Moreover, most previous research has been performed by specifically silencing or enhancing expression in one organ or cell culture, whereas in this model Tff3 is absent at the whole-organism level. Given its presence in the blood and its already demonstrated ability to act at distant sites, it is possible that interaction between different organ systems is a cause of the disparate results. The immense complexity of metabolism and the factors influencing it should also be considered. In this study, it was found that some differences that existed halfway through the experiment disappeared by the end of it.

Unexpectedly, genotypic differences in the hippocampus were virtually non-existent in a stressful environment, whereas subtle differences were present under standard conditions. A number of factors are involved in this overall interaction, which are likely to be turned on and off depending on external stimulus.

In addition, the influence of sexual dimorphism, which is not commonly addressed, was demonstrated, not only on the action of Tff3, but also on its expression in the liver.

All in all, this research has again demonstrated the important role of Tff3 in the organism and provides a good basis for a more detailed focus on the mechanistic explanations of the demonstrated phenotype. Furthermore, the observed sex differences and the different results of this study compared to previous studies demonstrate the importance of including both sexes in biomedical research and accurately describing the subjects.

6 References

1. Thim L. A new family of growth factor-like peptides 'Trefoil' disulphide loop structures as a common feature in breast cancer associated peptide (pS2), pancreatic spasmolytic polypeptide (PSP), and frog skin peptides (spasmolysins). FEBS Lett [Internet]. 1989 Jun 19 [cited 2022 Mar 8];250(1):85–90. Available from: https://onlinelibrary.wiley.com/doi/full/10.1016/0014-5793%2889%2980690-8

2. Carr MD. Proton NMR-Based Determination of the Secondary Structure of Porcine Pancreatic Spasmolytic Polypeptide: One of a New Family of "Trefoil" Motif Containing Cell Growth Factors. Biochemistry [Internet]. 1992 Feb 1 [cited 2022 Mar 18];31(7):1998–2004. Available from: https://pubs.acs.org/doi/abs/10.1021/bi00122a015

3. De A, Brown DG, Gorman MA, Carr M, Sanderson MR, Freemont PS. Crystal structure of a disulfide-linked "trefoil" motif found in a large family of putative growth factors. Proc Natl Acad Sci U S A [Internet]. 1994 [cited 2022 Mar 18];91(3):1084–8. Available from: https://www.pnas.org

4. Hoffmann W, Hauser F. The P-domain or trefoil motif: a role in renewal and pathology of mucous epithelia? Trends Biochem Sci. 1993 Jul 1;18(7):239–43.

5. Jørgensen KH, Thim L, Jacobsen HE. Pancreatic Spasmolytic Polypeptide (PSP): I. Preparation and initial chemical characterization of a new polypeptide from porcine pancreas. Regul Pept. 1982 Mar 1;3(3–4):207–19.

6. Kinoshita K, Taupin DR, Itoh H, Podolsky DK. Distinct Pathways of Cell Migration and Antiapoptotic Response to Epithelial Injury: Structure-Function Analysis of Human Intestinal Trefoil Factor. Mol Cell Biol [Internet]. 2000 [cited 2022 May 5];20(13):4680–90. Available from: https://journals.asm.org/journal/mcb

7. Suemori S, Lynch-Devaney K, Podolsky DK. Identification and characterization of rat intestinal trefoil factor: Tissue- and cell-specific member of the trefoil protein family. Proc Natl Acad Sci U S A [Internet]. 1991 [cited 2022 Mar 8];88(24):11017–

21. Available from: https://www.pnas.org

8. Aihara E, Engevik KA, Montrose MH. Trefoil Factor Peptides and Gastrointestinal Function. http://dx.doi.org/101146/annurev-physiol-021115-105447 [Internet]. 2017 Feb 13 [cited 2022 Jun 22];79:357–80. Available from: https://www.annualreviews.org/doi/abs/10.1146/annurev-physiol-021115-105447

9. Madsen J, Nielsen O, Tornøe I, Thim L, Holmskov U. Tissue localization of human trefoil factors 1, 2, and 3. J Histochem Cytochem. 2007;55(5):505–13.

10. Poulsom R, Wright NA. Trefoil peptides: A newly recognized family of epithelial mucin- associated molecules. Am J Physiol - Gastrointest Liver Physiol. 1993;265(2 28-2).

11. Hanby AM, Poulsom R, Elia G, Singh S, Longcroft JM, Wright NA. The expression of the trefoil peptides pS2 and human spasmolytic polypeptide (hSP) in 'gastric metaplasia' of the proximal duodenum: Implications for the nature of 'gastric metaplasia.' J Pathol [Internet]. 1993 Mar 1 [cited 2022 Jun 23];169(3):355–60. Available from: https://onlinelibrary.wiley.com/doi/full/10.1002/path.1711690313

12. Podolsky DK, Lynch-Devaney K, Stow JL, Oates P, Murgue B, DeBeaumont M, et al. Identification of human intestinal trefoil factor. Goblet cell-specific expression of a peptide targeted for apical secretion. J Biol Chem [Internet]. 1993 Mar 25 [cited 2022 Jun 23];268(9):6694–702. Available from: https://linkinghub.elsevier.com/retrieve/pii/S0021925818533056

13. Wright NA, Poulsom R, Stamp GWH, Hall PA, Jeffery RE, Longcroft JM, et al. Epidermal growth factor (EGF/URO) induces expression of regulatory peptides in damaged human gastrointestinal tissues. J Pathol [Internet]. 1990 Dec 1 [cited 2022 Jun 23];162(4):279–84. Available from: https://onlinelibrary.wiley.com/doi/full/10.1002/path.1711620402

14. Nakov R. New markers in ulcerative colitis. Clin Chim Acta. 2019 Oct 1;497:141–6.

15. Mashimo H, Wu DC, Podolsky DK, Fishman MC. Impaired Defense of Intestinal Mucosa in Mice Lacking Intestinal Trefoil Factor. Science (80-) [Internet]. 1996 Oct

11 [cited 2022 Mar 16];274(5285):262–5. Available from: https://www.science.org/doi/abs/10.1126/science.274.5285.262

16. Taupin D, Podolsky DK. TREFOIL FACTORS : INITIATORS OF MUCOSAL HEALING. 2003;4(September).

17. Wright NA, Hoffmann W, Otto WR, Rio MC, Thim L. Rolling in the clover: trefoil factor family (TFF)-domain peptides, cell migration and cancer. FEBS Lett [Internet]. 1997 May 19 [cited 2022 Oct 13];408(2):121–3. Available from: https://onlinelibrary.wiley.com/doi/full/10.1016/S0014-5793%2897%2900424-9

18. Masiakowski P, Breathnach R, Bloch J, Gannon F, Krust A, Chambon P. Cloning of cDNA sequences of hormone-regulated genes from the MCF-7 human breast cancer cell line. Nucleic Acids Res [Internet]. 1982 Dec 20 [cited 2022 Mar 8];10(24):7895–903. Available from: https://academic.oup.com/nar/article/10/24/7895/2379131

19. Muskett FW, May FEB, Westley BR, Feeney J. Solution Structure of the Disulfide-Linked Dimer of Human Intestinal Trefoil Factor (TFF3): The Intermolecular Orientation and Interactions Are Markedly Different from Those of Other Dimeric Trefoil Proteins. Biochemistry. 2003;42(51):15139–47.

20. Chinery R, Poulsom R, Cox HM. The gene encoding mouse intestinal trefoil factor: structural organization, partial sequence analysis and mapping to murine chromosome 17q. Gene. 1996 Jun 1;171(2):249–53.

21. Kayademir T, Rosewell I, Blin N, Gött P. Genomic structure of the mouse trefoil factor (Tff) gene cluster in 17q. GeneScreen [Internet]. 2000 May 1 [cited 2022 May 5];1(1):15–9. Available from: https://onlinelibrary.wiley.com/doi/full/10.1046/j.1466-9218.2000.00004.x

22. Seib T, Blin N, Hilgert K, Seifert M, Theisinger B, Engel M, et al. The Three Human Trefoil Genes TFF1, TFF2, and TFF3 Are Located within a Region of 55 kb on Chromosome 21q22.3. Genomics. 1997 Feb 15;40(1):200–2.

23. Ribieras S, Lefèbvre O, Tomasetto C, Rio MC. Mouse Trefoil Factor genes:

genomic organization, sequences and methylation analyses. Gene. 2001 Mar 21;266(1–2):67–75.

24. Mashimo H, Podolsky DK, Fishman MC. Structure and Expression of Murine Intestinal Trefoil Factor: High Evolutionary Conservation and Postnatal Expression. Biochem Biophys Res Commun. 1995 May 5;210(1):31–7.

25. Svanes K, Ito S, Takeuchi K, Silen W. Restitution of the surface epithelium of the in vitro frog gastric mucosa after damage with hyperosmolar sodium chloride. Morphologic and physiologic characteristics. Gastroenterology. 1982;82(6):1409–26.

26. Jiang GX, Zhong XY, Cui YF, Liu W, Tai S, Wang ZD, et al. IL-6/STAT3/TFF3 signaling regulates human biliary epithelial cell migration and wound healing in vitro. Mol Biol Rep. 2010;37(8):3813–8.

27. Taupin DR, Kinoshita K, Podolsky DK. Intestinal trefoil factor confers colonic epithelial resistance to apoptosis. Proc Natl Acad Sci U S A. 2000;97(2):799–804.

28. Kjellev S. The trefoil factor family - Small peptides with multiple functionalities. Cell Mol Life Sci. 2009 Apr;66(8):1350–69.

29. Beck PL, Wong JF, Li Y, Swaminathan S, Xavier RJ, Devaney KL, et al. Chemotherapy- and Radiotherapy-Induced Intestinal Damage Is Regulated by Intestinal Trefoil Factor. Gastroenterology. 2004;126(3):796–808.

30. Carrasco R, Pera M, May FEB, Westley BR, Martinez A, Morales L. Trefoil factor family peptide 3 prevents the development and promotes healing of ischemia-reperfusion injury in weanling rats. J Pediatr Surg. 2004 Nov 1;39(11):1693–700.

31. Meyer zum Büschenfelde D, Tauber R, Huber O. TFF3-peptide increases transepithelial resistance in epithelial cells by modulating claudin-1 and -2 expression. Peptides. 2006 Dec 1;27(12):3383–90.

32. Xu LF, Teng X, Guo J, Sun M. Protective effect of intestinal trefoil factor on injury of intestinal epithelial tight junction induced by platelet activating factor. Inflammation [Internet]. 2012 Feb [cited 2022 Jun 22];35(1):308–15. Available from:

https://link.springer.com/article/10.1007/s10753-011-9320-x

33. Buda A, Jepson MA, Pignatelli M. Regulatory Function of Trefoil peptides (TFF) on Intestinal Cell Junctional Complexes. http://dx.doi.org/103109/154190612012748326 [Internet]. 2012 Oct [cited 2022 Jun 22];19(5–6):63–8. Available from: https://www.tandfonline.com/doi/abs/10.3109/15419061.2012.748326

34. Wang Y, Liang K, Kong W. Intestinal Trefoil Factor 3 Alleviates the Intestinal Barrier Function Through Reducing the Expression of TLR4 in Rats with Nonalcoholic Steatohepatitis. Arch Med Res. 2019 Jan 1;50(1):2–9.

35. Lin N, Xu L fen, Sun M. The protective effect of trefoil factor 3 on the intestinal tight junction barrier is mediated by toll-like receptor 2 via a PI3K/Akt dependent mechanism. Biochem Biophys Res Commun. 2013 Oct 11;440(1):143–9.

36. Wu X, Zheng H, Yang R, Luan X, Zhang L, Jin Q, et al. Mouse trefoil factor 3 ameliorated high-fat-diet-induced hepatic steatosis via increasing peroxisome proliferator-activated receptor-α-mediated fatty acid oxidation. 2019 Sep 1 [cited 2021 Jun 28];317(3):E436–45. Available from: https://pubmed.ncbi.nlm.nih.gov/31211621/

37. Xue Y, Shen L, Cui Y, Zhang H, Chen Q, Cui A, et al. Tff3, as a Novel Peptide, Regulates Hepatic Glucose Metabolism. 2013 Sep 23 [cited 2021 Jun 29];8(9). Available from: www.plosone.org

38. Bujak M, Bujak ITT, Sobočanec S, Mihalj M, Novak S, Cosić A, et al. Trefoil Factor 3 Deficiency Affects Liver Lipid Metabolism. Cell Physiol Biochem [Internet]. 2018 Jun 1 [cited 2021 Aug 31];47(2):827–41. Available from: https://www.karger.com/Article/FullText/490039

39. Šešelja K, Bazina I, Welss J, Schicht M, Paulsen F, Bijelić N, et al. Effect of Tff3 deficiency and ER stress in the liver. Int J Mol Sci [Internet]. 2019 Sep 1 [cited 2021 Jun 15];20(18):4389. Available from: www.mdpi.com/journal/ijms

40. Zhu Y, Zhao S, Deng Y, Gordillo R, Ghaben AL, Shao M, et al. Hepatic GALE

Regulates Whole-Body Glucose Homeostasis by Modulating Tff3 Expression. Diabetes [Internet]. 2017 Nov 1 [cited 2021 Aug 31];66(11):2789–99. Available from: https://diabetes.diabetesjournals.org/content/66/11/2789

41. Brown AC, Olver WI, Donnelly CJ, May ME, Naggert JK, Shaffer DJ, et al. Searching QTL by gene expression: analysis of diabesity. 2005 [cited 2021 Jun 28]; Available from: http://www.biomedcentral.com/1471-2156/6/12

42. Ge H, Gardner J, Wu X, Rulifson I, Wang J, Xiong Y, et al. Trefoil factor 3 (TFF3) is regulated by food intake, improves glucose tolerance and induces mucinous metaplasia. PLoS One [Internet]. 2015 Jun 17 [cited 2021 Jun 29];10(6):e0126924. Available from: https://journals.plos.org/plosone/article?id=10.1371/journal.pone.0126924

43. Belovari T, Bijelić N, Levak MT, Lončar MB. Trefoil factor family peptides TFF1 and TFF3 in the nervous tissues of developing mouse embryo. Bosn J Basic Med Sci [Internet]. 2015 Feb 1 [cited 2022 Oct 11];15(1):33–7. Available from: https://www.bjbms.org/ojs/index.php/bjbms/article/view/251

44. Bernstein H-G, Dobrowolny H, Trübner K, Steiner J, Bogerts B, Hoffmann W. Differential regional and cellular distribution of TFF3 peptide in the human brain. Amin Acids 2015 475 [Internet]. 2015 Feb 18 [cited 2021 Aug 31];47(5):1053–63. Available from: https://link.springer.com/article/10.1007/s00726-015-1938-9

45. Fu T, Stellmacher A, Znalesniak EB, Dieterich DC, Kalbacher H, Hoffmann W. Tff3 is Expressed in Neurons and Microglial Cells. Cell Physiol Biochem [Internet]. 2014 Jan 13 [cited 2021 Aug 31];34(6):1912–9. Available from: https://www.karger.com/Article/FullText/366389

46. Hinz M, Schwegler H, Chwieralski CE, Laube G, Linke R, Pohle W, et al. Trefoil factor family (TFF) expression in the mouse brain and pituitary: changes in the developing cerebellum. Peptides. 2004 May 1;25(5):827–32.

47. Jagla W, Wiede A, Dietzmann K, Rutkowski K, Hoffmann W. Co-localization of TFF3 peptide and oxytocin in the human hypothalamus. FASEB J [Internet]. 2000

Jun 1 [cited 2021 Aug 31];14(9):1126–31. Available from: https://faseb.onlinelibrary.wiley.com/doi/full/10.1096/fasebj.14.9.1126

48. Arnold P, Rickert U, Helmers AK, Spreu J, Schneppenheim J, Lucius R. Trefoil factor 3 shows anti-inflammatory effects on activated microglia. Cell Tissue Res [Internet]. 2016 Jul 1 [cited 2022 Oct 11];365(1):3–11. Available from: https://link.springer.com/article/10.1007/s00441-016-2370-5

49. Paulsen F, Varoga D, Paulsen A, Tsokos M. Trefoil factor family (TFF) peptides of normal human Vater's ampulla. Cell Tissue Res 2005 3211 [Internet]. 2005 May 21 [cited 2022 Nov 3];321(1):67–74. Available from: https://link.springer.com/article/10.1007/s00441-005-1131-7

50. Srivatsa G, Giraud AS, Ulaganathan M, Yeomans ND, Dow C, Nicoll AJ. Biliary epithelial trefoil peptide expression is increased in biliary diseases. Histopathology [Internet]. 2002 Mar 1 [cited 2022 Nov 3];40(3):261–8. Available from: https://onlinelibrary.wiley.com/doi/full/10.1046/j.1365-2559.2002.01347.x

51. Sasaki M, Ikeda H, Ohira S, Ishikawa A, Nakanuma Y. Expression of trefoil factor family 1, 2, and 3 peptide is augmented in hepatolithiasis. Peptides. 2004 May 1;25(5):763–70.

52. Jackerott M, Lee YC, Møllgård K, Kofod H, Jensen J, Rohleder S, et al. Trefoil Factors Are Expressed in Human and Rat Endocrine Pancreas: Differential Regulation by Growth Hormone. Endocrinology [Internet]. 2006 Dec 1 [cited 2021 Aug 31];147(12):5752–9. Available from: https://academic.oup.com/endo/article/147/12/5752/2500833

53. Winkel L, Bagge A, Larsen L, Haase TN, Rasmussen M, Lykke J, et al. Trefoil factor 3 in perinatal pancreas is increased by gestational low protein diet and associated with accelerated β-cell maturation. Islets. 2018 May;10(3):e1472186.

54. Jahan R, Ganguly K, Smith LM, Atri P, Carmicheal J, Sheinin Y, et al. Trefoil factor(s) and CA19.9: A promising panel for early detection of pancreatic cancer. EBioMedicine [Internet]. 2019;42:375–85. Available from:

https://www.sciencedirect.com/science/article/pii/S2352396419302014

55. Cook GA, Familari M, Thim L, Giraud AS. The trefoil peptides TFF2 and TFF3 are expressed in rat lymphoid tissues and participate in the immune response. FEBS Lett. 1999;456(1):155–9.

56. Baus-Loncar M, Kayademir T, Takaishi S, Wang T. Trefoil factor family 2 deficiency and immune response. Cell Mol Life Sci. 2005 Dec;62(24):2947–55.

57. Kont V, Laan M, Kisand K, Merits A, Scott HS, Peterson P. Modulation of Aire regulates the expression of tissue-restricted antigens. Mol Immunol. 2008 Jan;45(1):25–33.

58. Hauser F, Poulsom R, Chinery R, Rogers LA, Hanby AM, Wright NA, et al. hP1.B, a human P-domain peptide homologous with rat intestinal trefoil factor, is expressed also in the ulcer-associated cell lineage and the uterus. Proc Natl Acad Sci [Internet]. 1993 Aug 1 [cited 2022 Nov 3];90(15):6961–5. Available from: https://www.pnas.org/doi/abs/10.1073/pnas.90.15.6961

59. Jagla W, Wiede A, Hinz M, Dietzmann K, Gülicher D, Gerlach KL, et al. Secretion of TFF-peptides by human salivary glands. Cell Tissue Res 1999 2981 [Internet]. 1999 [cited 2022 Oct 16];298(1):161–6. Available from: https://link.springer.com/article/10.1007/s004419900087

60. Wiede A, Jagla W, Welte T, Köhnlein T, Busk H, Hoffmann W. Localization of TFF3, a New Mucus-associated Peptide of the Human Respiratory Tract. https://doi.org/101164/ajrccm15949804149 [Internet]. 2012 Dec 14 [cited 2022 Nov 3];159(4 I):1330–5. Available from: www.atsjournals.org

61. Kutta H, Steven P, Varoga D, Paulsen FP. TFF peptides in the human false vocal folds of the larynx. Peptides. 2004 May 1;25(5):811–8.

62. Dos E, Silva S, Ulrich M, Do È Ring G, Botzenhart K, Go Èttt P, et al. Trefoil factor family domain peptides in the human respiratory tract. [cited 2022 Nov 3]; Available from: https://onlinelibrary.wiley.com/doi/10.1002/

63. Ahmed ARH, Griffiths AB, Tilby MT, Westley BR, May FEB. TFF3 is a normal breast

epithelial protein and is associated with differentiated phenotype in early breast cancer but predisposes to invasion and metastasis in advanced disease. Am J Pathol. 2012 Mar;180(3):904–16.

64. Barrera GJ, Sanchez G, Gonzalez JE. Trefoil factor 3 isolated from human breast milk downregulates cytokines (IL8 and IL6) and promotes human beta defensin (hBD2 and hBD4) expression in intestinal epithelial cells HT-29. Bosn J Basic Med Sci. 2012;12(4):256–64.

65. Wiede A, Hinz M, Canzler E, Franke K, Quednow C, Hoffmann W. Synthesis and localization of the mucin-associated TFF-peptides in the human uterus. Cell Tissue Res 2000 3031 [Internet]. 2001 [cited 2022 Nov 3];303(1):109–15. Available from: https://link.springer.com/article/10.1007/s004410000297

66. Rinnert M, Hinz M, Buhtz P, Reiher F, Lessel W, Hoffmann W. Synthesis and localization of trefoil factor family (TFF) peptides in the human urinary tract and TFF2 excretion into the urine. Cell Tissue Res [Internet]. 2010;339(3):639–47. Available from: https://doi.org/10.1007/s00441-009-0913-8

67. Du T, Luo H, Qin H, Wang F, Wang Q, Xiang Y, et al. Circulating Serum Trefoil Factor 3 (TFF3) Is Dramatically Increased in Chronic Kidney Disease. PLoS One [Internet]. 2013 Nov 25;8(11):e80271. Available from: https://doi.org/10.1371/journal.pone.0080271

68. Tanaka K, Sugiyama H, Yamanari T, Mise K, Morinaga H, Kitagawa M, et al. Renal expression of trefoil factor 3 mRNA in association with tubulointerstitial fibrosis in IgA nephropathy. Nephrology [Internet]. 2018 Sep 1;23(9):855–62. Available from: https://doi.org/10.1111/nep.13444

69. Astor BC, Köttgen A, Hwang S-J, Bhavsar N, Fox CS, Coresh J. Trefoil factor 3 predicts incident chronic kidney disease: a case-control study nested within the Atherosclerosis Risk in Communities (ARIC) study. Am J Nephrol. 2011;34(4):291–7.

70. Yamanari T, Sugiyama H, Tanaka K, Morinaga H, Kitagawa M, Onishi A, et al. Urine

Trefoil Factors as Prognostic Biomarkers in Chronic Kidney Disease. Seki G, editor. Biomed Res Int [Internet]. 2018;2018:3024698. Available from: https://doi.org/10.1155/2018/3024698

71. Krüger K, Schmid S, Paulsen F, Ignatius A, Klinger P, Hotfiel T, et al. Trefoil Factor 3 (TFF3) Is Involved in Cell Migration for Skeletal Repair. Int J Mol Sci. 2019 Sep;20(17).

72. Rösler S, Haase T, Claassen H, Schulze U, Schicht M, Riemann D, et al. Trefoil factor 3 is induced during degenerative and inflammatory joint disease, activates matrix metalloproteinases, and enhances apoptosis of articular cartilage chondrocytes. Arthritis Rheum. 2010 Mar;62(3):815–25.

73. Bijelić N, Belovari T, Baus Lončar M. Trefoil factor family protein 3 (TFF3) is present in cartilage during endochondral ossification in the developing mouse fetus. Acta Histochem [Internet]. 2013;115(3):204–8. Available from: https://www.sciencedirect.com/science/article/pii/S006512811200092X

74. Paulsen FP, Schaudig U, Fabian A, Ehrich D, Sel S. TFF peptides and mucins are major components of dacryoliths. Graefe's Arch Clin Exp Ophthalmol. 2006 Sep;244(9):1160–70.

75. Schulze U, Sel S, Paulsen FP. Trefoil factor family peptide 3 at the ocular surface. A promising therapeutic candidate for patients with dry eye syndrome? Dev Ophthalmol. 2010;45:1–11.

76. Schulze U, Hampel U, Sel S, Contreras-Ruiz L, Schicht M, Dieckow J, et al. Trefoil factor family peptide 3 (TFF3) is upregulated under experimental conditions similar to dry eye disease and supports corneal wound healing effects in vitro. Invest Ophthalmol Vis Sci. 2014 May;55(5):3037–42.

77. Lubka M, Shah AA, Blin N, Baus-Lončar M. The intestinal trefoil factor (Tff3), also expressed in the inner ear, interacts with peptides contributing to apoptosis. J Appl Genet. 2009;50(2):167–71.

78. Lubka M, Müller M, Baus-Loncar M, Hinz M, Blaschke K, Hoffmann W, et al. Lack

of Tff3 peptide results in hearing impairment and accelerated presbyacusis. Cell Physiol Biochem Int J Exp Cell Physiol Biochem Pharmacol. 2008;21(5–6):437–44.

79. See Hag Lee, Seung Hoon Lee, Byung Hoon Oh, Heung Man Lee, Jong Ouck Choi, Kwang Yoon Jung. Expression of mRNA of Trefoil Factor Peptides in Human Nasal Mucosa. http://dx.doi.org/101080/00016480152602320 [Internet]. 2009 [cited 2022 Nov 3];121(7):849–53. Available from: https://www.tandfonline.com/doi/abs/10.1080/00016480152602320

80. Mihalj M, Bujak M, Butković J, Zubčić Ž, Tolušić Levak M, Čes J, et al. Differential Expression of TFF1 and TFF3 in Patients Suffering from Chronic Rhinosinusitis with Nasal Polyposis. Int J Mol Sci. 2019 Nov;20(21).

81. Aamann L, Vestergaard EM, Grønbæk H. Trefoil factors in inflammatory bowel disease. World J Gastroenterol [Internet]. 2014 [cited 2022 Oct 16];20(12):3223–30. Available from: https://www.wjgnet.com/1007-9327/full/v20/i12/3223.htm

82. Jahan R, Shah A, Kisling SG, Macha MA, Thayer S, Batra SK, et al. Odyssey of trefoil factors in cancer: Diagnostic and therapeutic implications. Biochim Biophys Acta - Rev Cancer. 2020 Apr 1;1873(2):188362.

83. Yang Y, Lin Z, Lin Q, Bei W, Guo J. Pathological and therapeutic roles of bioactive peptide trefoil factor 3 in diverse diseases: recent progress and perspective. Cell Death Dis. 2022;13(1):1–14.

84. Wright NA. Interaction of trefoil family factors with mucins: clues to their mechanism of action? Gut [Internet]. 2001 Mar 1 [cited 2022 Oct 16];48(3):293–4. Available from: https://gut.bmj.com/content/48/3/293

85. Yu H, He Y, Zhang X, Peng Z, Yang Y, Zhu R, et al. The Rat IgGFcγBP and Muc2 C-Terminal Domains and TFF3 in Two Intestinal Mucus Layers Bind Together by Covalent Interaction. PLoS One [Internet]. 2011 [cited 2022 Oct 16];6(5):e20334. Available from: https://journals.plos.org/plosone/article?id=10.1371/journal.pone.0020334

86. Dignass A, Lynch-Devaney K, Kindon H, Thim L, Podolsky DK. Trefoil peptides promote epithelial migration through a transforming growth factor β-independent pathway. J Clin Invest. 1994;94(1):376–83.

87. Hoffmann W. Trefoil factor family (TFF) peptides and their diverse molecular functions in mucus barrier protection and more: Changing the paradigm. Int J Mol Sci. 2020;21(12):1–20.

88. Houben T, Harder S, Schlüter H, Kalbacher H, Hoffmann W. No Title. 2019 Oct 1 [cited 2021 Jun 29];20(20):5000. Available from: www.mdpi.com/journal/ijms

89. Yang Y, Lin Z, Lin Q, Bei W, Guo J. Pathological and therapeutic roles of bioactive peptide trefoil factor 3 in diverse diseases: recent progress and perspective. Cell Death Dis 2022 131 [Internet]. 2022 Jan 17 [cited 2022 Oct 16];13(1):1–14. Available from: https://www.nature.com/articles/s41419-022-04504-6

90. Rodrigues S, Nguyen Q-D, Faivre S, Bruyneel E, Thim L, Westley B, et al. Activation of cellular invasion by trefoil peptides and src is mediated by cyclooxygenase- and thromboxane A2 receptor-dependent signaling pathways. FASEB J. 2001 Jul;15(9):1517–28.

91. Loos M, De Creus A, Thim L, Remaut E, Rottiers P. Murine Trefoil Factor 3 Does not Directly Modulate LPS-Mediated Dendritic Cell Function. Scand J Immunol [Internet]. 2007 Jul 1 [cited 2022 Oct 16];66(1):35–42. Available from: https://onlinelibrary.wiley.com/doi/full/10.1111/j.1365-3083.2007.01944.x

92. Dieckow J, Brandt W, Hattermann K, Schob S, Schulze U, Mentlein R, et al. CXCR4 and CXCR7 mediate TFF3-induced cell migration independently from the ERK1/2 signaling pathway. Investig Ophthalmol Vis Sci. 2016 Jan 1;57(1):56–65.

93. Barrera Roa GJ, Sanchez Tortolero G. Trefoil factor 3 (TFF3) from human breast milk activates PAR-2 receptors, of the intestinal epithelial cells HT-29, regulating cytokines and defensins. Bratislava Med J. 2016;117(6):332–9.

94. Belle NM, Ji Y, Herbine K, Wei Y, Park JH, Zullo K, et al. TFF3 interacts with LINGO2 to regulate EGFR activation for protection against colitis and

gastrointestinal helminths. Nat Commun [Internet]. 2019 Dec 1 [cited 2021 Jun 29];10(1):1–13. Available from: https://doi.org/10.1038/s41467-019-12315-1

95. Fueger PT, Schisler JC, Lu D, Babu DA, Mirmira RG, Newgard CB, et al. Trefoil Factor 3 Stimulates Human and Rodent Pancreatic Islet β-Cell Replication with Retention of Function. Mol Endocrinol [Internet]. 2008 May 1 [cited 2021 Aug 31];22(5):1251–9. Available from: https://academic.oup.com/mend/article/22/5/1251/2660979

96. Shah AA, Leidinger P, Keller A, Wendschlag A, Backes C, Baus-Loncar M, et al. The intestinal factor Tff3 and a miRNA network regulate murine caloric metabolism. 2011 [cited 2021 Aug 31];8(1). Available from: https://www.tandfonline.com/doi/abs/10.4161/rna.8.1.13687

97. Probst JC, Skutella T, Müller-Schmid A, Jirikowski GF, Hoffmann W. Molecular and cellular analysis of rP1.B in the rat hypothalamus: In situ hybridization and immunohistochemistry of a new P-domain neuropeptide. Mol Brain Res. 1995 Nov 1;33(2):269–76.

98. Probst JC, Zetzsche T, Weber M, Theilemann P, Skutella T, Landgraf R, et al. Human intestinal trefoil factor is expressed in human hypothalamus and pituitary: evidence for a novel neuropeptide. FASEB J [Internet]. 1996 Nov 1 [cited 2021 Aug 31];10(13):1518–23. Available from: https://faseb.onlinelibrary.wiley.com/doi/full/10.1096/fasebj.10.13.8940297

99. Griepentrog T, Bauer M, Hornstein C, Sauer H, Jirikowski GF. Coexistence of intestinal trefoil factor (hITF) and oxytocin in magnocellular neurons in the human hypothalamus. Horm Metab Res. 2000;32(4):121–4.

100. Schwarz H, Jagla W, Wiede A, Hoffmann W. Ultrastructural co-localization of TFF3-peptide and oxytocin in the neural lobe of the porcine pituitary. Cell Tissue Res. 2001;305(3):411–6.

101. Pereira PL, Magnol L, Sahún I, Brault V, Duchon A, Prandini P, et al. A new mouse model for the trisomy of the Abcg1-U2af1 region reveals the complexity of the

combinatorial genetic code of down syndrome. Hum Mol Genet. 2009;18(24):4756–69.

102. Shi HS, Yin X, Song L, Guo QJ, Luo XH. Neuropeptide Trefoil factor 3 improves learning and retention of novel object recognition memory in mice. Behav Brain Res. 2012 Feb 1;227(1):265–9.

103. Zhu W-L, Qin J, Xu Y, Mi J, Wang J, Hou J, et al. Enhanced antidepressant-like effects of the macromolecule trefoil factor 3 by loading into negatively charged liposomes. Int J Nanomedicine [Internet]. 2014 Nov 12 [cited 2022 Oct 15];9(1):5247–57. Available from: https://www.dovepress.com/enhanced-antidepressant-like-effects-of-the-macromolecule-trefoil-fact-peer-reviewed-fulltext-article-IJN

104. Li J, Luo Y, Zhang R, Shi H, Zhu W, Shi J. Neuropeptide Trefoil Factor 3 Reverses Depressive-Like Behaviors by Activation of BDNF-ERK-CREB Signaling in Olfactory Bulbectomized Rats. Int J Mol Sci 2015, Vol 16, Pages 28386-28400 [Internet]. 2015 Nov 30 [cited 2021 Aug 31];16(12):28386–400. Available from: https://www.mdpi.com/1422-0067/16/12/26105/htm

105. Schwarzberg H, Kalbacher H, Hoffmann W. Differential Behavioral Effects of TFF Peptides: Injections of Synthetic TFF3 Into the Rat Amygdala. Pharmacol Biochem Behav. 1999 Jan 1;62(1):173–8.

106. Wu P, Shi HS, Luo YX, Zhang RX, Li JL, Shi J, et al. Neuropeptide trefoil factor 3 attenuates naloxone-precipitated withdrawal in morphine-dependent mice. Psychopharmacology (Berl). 2014;231(24):4659–68.

107. Wu P, Shi H-S, Luo Y-X, Zhang R-X, Li J-L, Shi J, et al. Neuropeptide trefoil factor 3 attenuates naloxone-precipitated withdrawal in morphine-dependent mice. Psychopharmacol 2014 23124 [Internet]. 2014 May 14 [cited 2021 Aug 31];231(24):4659–68. Available from: https://link.springer.com/article/10.1007/s00213-014-3615-1

108. Gardiner EJ, Cairns MJ, Liu B, Beveridge NJ, Carr V, Kelly B, et al. Gene

expression analysis reveals schizophrenia-associated dysregulation of immune pathways in peripheral blood mononuclear cells. J Psychiatr Res. 2013 Apr 1;47(4):425–37.

109. Hashimoto JG, Forquer MR, Tanchuck MA, Finn DA, Wiren KM. Importance of genetic background for risk of relapse shown in altered prefrontal cortex gene expression during abstinence following chronic alcohol intoxication. Neuroscience. 2011 Jan 26;173:57–75.

110. Kriks S, Shim JW, Piao J, Ganat YM, Wakeman DR, Xie Z, et al. Dopamine neurons derived from human ES cells efficiently engraft in animal models of Parkinson's disease. Nature. 2011;480(7378):547–51.

111. Zou J, Chen Z, Liang C, Fu Y, Wei X, Lu J, et al. Trefoil factor 3, cholinesterase and homocysteine: Potential predictors for Parkinson's disease dementia and vascular parkinsonism dementia in advanced stage. Aging Dis. 2018 Feb 1;9(1):51–65.

112. Paterson R, Bartlett J, Blennow K, Fox N, Neuroimaging Initiative D, Shaw L, et al. Cerebrospinal fluid markers including trefoil factor 3 are associated with neurodegeneration in amyloid-positive individuals. Transl Psychiatry [Internet]. 2014 [cited 2021 Jun 28];4:419. Available from: www.nature.com/tp

113. Lubka M, Shah AA, Blin N. The intestinal trefoil factor (Tff3), also expressed in the inner ear , interacts with peptides contributing to apoptosis. 2009;50(2):167–71.

114. Liu SQ, Roberts D, Zhang B, Ren Y, Zhang L-Q, Wu YH. Trefoil Factor 3 as an Endocrine Neuroprotective Factor from the Liver in Experimental Cerebral Ischemia/Reperfusion Injury. PLoS One [Internet]. 2013 Oct 18 [cited 2021 Aug 31];8(10):e77732. Available from: https://journals.plos.org/plosone/article?id=10.1371/journal.pone.0077732

115. Kozina N, Mihaljević Z, Lončar MB, Mihalj M, Mišir M, Radmilović MD, et al. Impact of High Salt Diet on Cerebral Vascular Function and Stroke in Tff3−/−/C57BL/6N Knockout and WT (C57BL/6N) Control Mice. Int J Mol Sci 2019, Vol 20, Page 5188

[Internet]. 2019 Oct 19 [cited 2022 Oct 2];20(20):5188. Available from: https://www.mdpi.com/1422-0067/20/20/5188/htm

116. Sigmund CD. Viewpoint: Are Studies in Genetically Altered Mice Out of Control? Arterioscler Thromb Vasc Biol [Internet]. 2000 [cited 2022 Aug 26];20(6):1425–9. Available from: https://www.ahajournals.org/doi/abs/10.1161/01.atv.20.6.1425

117. Mekada K, Abe K, Murakami A, Nakamura S, Nakata H, Moriwaki K, et al. Genetic differences among C57BL/6 substrains. Exp Anim. 2009;58(2):141–9.

118. Toye AA, Lippiat JD, Proks P, Shimomura K, Bentley L, Hugill A, et al. A genetic and physiological study of impaired glucose homeostasis control in C57BL/6J mice. Diabetologia [Internet]. 2005 Apr 24 [cited 2022 Jul 12];48(4):675–86. Available from: https://link.springer.com/article/10.1007/s00125-005-1680-z

119. Ronchi JA, Figueira TR, Ravagnani FG, Oliveira HCF, Vercesi AE, Castilho RF. A spontaneous mutation in the nicotinamide nucleotide transhydrogenase gene of C57BL/6J mice results in mitochondrial redox abnormalities. Free Radic Biol Med. 2013 Oct 1;63:446–56.

120. Tan C, Tuch BE, Tu J, Brown SA. Role of NADH Shuttles in Glucose-Induced Insulin Secretion From Fetal β-Cells. Diabetes [Internet]. 2002 Oct 1 [cited 2022 Oct 16];51(10):2989–96. Available from: https://diabetesjournals.org/diabetes/article/51/10/2989/25259/Role-of-NADH-Shuttles-in-Glucose-Induced-Insulin

121. Rawle DJ, Le TT, Dumenil T, Bishop C, Yan K, Nakayama E, et al. Widespread discrepancy in Nnt genotypes and genetic backgrounds complicates granzyme A and other knockout mouse studies. Elife. 2022 Feb 1;11.

122. Rogner UC, Avner P. Congenic mice: cutting tools for complex immune disorders. Nat Rev Immunol 2003 33 [Internet]. 2003 [cited 2022 Nov 28];3(3):243–52. Available from: https://www.nature.com/articles/nri1031

123. De la Monte SM, SM de la M. No Title. 2014 Dec 1 [cited 2021 Aug 26];24(12):1954–60. Available from: https://pubmed.ncbi.nlm.nih.gov/25088942/

124. S C, A M, Brandt R, Chinnathambi S, Chatterjee S, Mudher A. Alzheimer's Disease and Type 2 Diabetes: A Critical Assessment of the Shared Pathological Traits. 2018 Jun 8 [cited 2021 Aug 26];(JUN):383. Available from: www.frontiersin.org

125. Moran C, Phan TG, Chen J, Blizzard L, Beare R, Venn A, et al. Brain Atrophy in Type 2 Diabetes Regional distribution and influence on cognition. 2013 [cited 2021 Aug 26]; Available from: http://care.diabetesjournals.org/lookup/suppl/doi:10

126. Jayaraman A, Pike CJ. PATHOGENESIS OF TYPE 2 DIABETES AND INSULIN RESISTANCE (RM WATANABE, SECTION EDITOR) Alzheimer's Disease and Type 2 Diabetes: Multiple Mechanisms Contribute to Interactions.

127. Kim D-G, Krenz A, Toussaint LE, Maurer KJ, Robinson S-A, Yan A, et al. Non-alcoholic fatty liver disease induces signs of Alzheimer's disease (AD) in wild-type mice and accelerates pathological signs of AD in an AD model. 2015;

128. Intraperitoneal glucose tolerance test (IPGTT) Protocol - IMPReSS [Internet]. [cited 2022 Aug 2]. Available from: https://www.mousephenotype.org/impress/ProcedureInfo?action=list&procID=531

129. Haj FG. Intraperitoneal Insulin Tolerance Test. Mouse Metab Phenotyping Centers. 2012;5–6.

130. Park PW, Goins RE. In Situ Preparation of Fatty Acid Methyl Esters for Analysis of Fatty Acid Composition in Foods. J Food Sci [Internet]. 1994 Nov 1 [cited 2021 Sep 1];59(6):1262–6. Available from: https://onlinelibrary.wiley.com/doi/full/10.1111/j.1365-2621.1994.tb14691.x

131. Sun W, Qin J, Shan R-F, Zhu Y-A, Zhu H-Y. Elevated serum levels of trefoil factor 3 are correlated with severity of sepsis patients. Int J Clin Exp Pathol [Internet]. 2016 [cited 2022 Apr 26];9(8):8122–31. Available from: www.ijcep.com/

132. Guillén N, Navarro MA, Arnal C, Noone E, Arbonés-Mainar JM, Acín S, et al. Microarray analysis of hepatic gene expression identifies new genes involved in steatotic liver. Physiol Genomics [Internet]. 2009 May [cited 2022 Sep 16];37(3):187–98. Available from:

https://journals.physiology.org/doi/10.1152/physiolgenomics.90339.2008

133. Roa JB, Tortolero GS, Gonzalez E. Trefoil factor 3 (TFF3) expression is regulated by insulin and glucose. J Heal Sci [Internet]. 2013 Apr 15 [cited 2021 Aug 31];3(1):1–12. Available from: https://www.jhsci.ba/ojs/index.php/jhsci/article/view/123

134. Kumar KG, Smith Richards BK. Transcriptional Profiling of Chromosome 17 Quantitative Trait Loci for Carbohydrate and Total Calorie Intake in a Mouse Congenic Strain Reveals Candidate Genes and Pathways. Lifestyle Genomics [Internet]. 2008 Jun [cited 2022 Sep 6];1(4):155–71. Available from: https://www.karger.com/Article/FullText/113657

135. Targher G, Corey KE, Byrne CD, Roden M. The complex link between NAFLD and type 2 diabetes mellitus — mechanisms and treatments. Nat Rev Gastroenterol Hepatol. 2021;0123456789.

136. Eslam M, Sanyal AJ, George J, Sanyal A, Neuschwander-Tetri B, Tiribelli C, et al. MAFLD: A Consensus-Driven Proposed Nomenclature for Metabolic Associated Fatty Liver Disease. Gastroenterology [Internet]. 2020 May 1 [cited 2022 Sep 12];158(7):1999-2014.e1. Available from: http://www.gastrojournal.org/article/S0016508520301712/fulltext

137. Farese R V., Walther TC. Lipid Droplets Finally Get a Little R-E-S-P-E-C-T. Cell [Internet]. 2009 Nov 25 [cited 2022 Sep 16];139(5):855–60. Available from: http://www.cell.com/article/S0092867409014172/fulltext

138. Tauchi-Sato K, Ozeki S, Houjou T, Taguchi R, Fujimoto T. The surface of lipid droplets is a phospholipid monolayer with a unique fatty acid composition. J Biol Chem [Internet]. 2002 Nov 15 [cited 2022 Sep 16];277(46):44507–12. Available from: http://www.jbc.org/article/S0021925819718067/fulltext

139. Onal G, Kutlu O, Gozuacik D, Dokmeci Emre S. Lipid Droplets in Health and Disease. Lipids Heal Dis 2017 161 [Internet]. 2017 Jun 29 [cited 2022 Sep 16];16(1):1–15. Available from:

https://lipidworld.biomedcentral.com/articles/10.1186/s12944-017-0521-7

140. Mashek DG. Hepatic lipid droplets: A balancing act between energy storage and metabolic dysfunction in NAFLD. Mol Metab. 2021 Aug 1;50:101115.

141. Olzmann JA, Carvalho P. Dynamics and functions of lipid droplets. Nat Rev Mol Cell Biol 2018 203 [Internet]. 2018 Dec 6 [cited 2022 Sep 20];20(3):137–55. Available from: https://www.nature.com/articles/s41580-018-0085-z

142. Shetty SS, Kumari S. Fatty acids and their role in type-2 diabetes (Review). Exp Ther Med [Internet]. 2021 Jul 1 [cited 2022 Sep 9];22(1):1–6. Available from: http://www.spandidos-publications.com/10.3892/etm.2021.10138/abstract

143. Palomer X, Pizarro-Delgado J, Barroso E, Vázquez-Carrera M. Palmitic and Oleic Acid: The Yin and Yang of Fatty Acids in Type 2 Diabetes Mellitus. Trends Endocrinol Metab [Internet]. 2018 Mar 1 [cited 2022 Sep 11];29(3):178–90. Available from: http://www.cell.com/article/S1043276017301704/fulltext

144. Vidal-Puig A, Jimenez-Liñan M, Lowell BB, Hamann A, Hu E, Spiegelman B, et al. Regulation of PPAR gamma gene expression by nutrition and obesity in rodents. J Clin Invest. 1996 Jun 1;97(11):2553–61.

145. Edvardsson U, Bergström M, Alexandersson M, Bamberg K, Ljung B, Dahllöf B. Rosiglitazone (BRL49653), a PPAR-selective agonist, causes peroxisome proliferator-like liver effects in obese mice. J Lipid Res. 1999;40:1177–84.

146. Memon RA, Tecott LH, Nonogaki K, Beigneux A, Moser AH, Grunfeld C, et al. Up-Regulation of Peroxisome Proliferator-Activated Receptors (PPAR-α) and PPAR-γ Messenger Ribonucleic Acid Expression in the Liver in Murine Obesity: Troglitazone Induces Expression of PPAR-γ-Responsive Adipose Tissue-Specific Genes in the Liver of Obese Diabetic Mice*This work was supported by grants from the Research Service of the Department of Veterans Affairs (to C.G. and K.R.F.), NIH Grant DK-49448 (to C.G.), and Merck Research Laboratories (to L.H.T. and K.N.). Endocrinology [Internet]. 2000 Nov 1 [cited 2022 Sep 30];141(11):4021–31. Available from: https://academic.oup.com/endo/article/141/11/4021/2987575

147. Costet P, Legendre C, Moré J, Edgar A, Galtier P, Pineau T. Peroxisome Proliferator-activated Receptor α-Isoform Deficiency Leads to Progressive Dyslipidemia with Sexually Dimorphic Obesity and Steatosis. J Biol Chem. 1998 Nov 6;273(45):29577–85.

148. Rahimian R, Masih-Khan E, Lo M, Van Breemen C, McManus BM, Dubé GP. Hepatic over-expression of peroxisome proliferator activated receptor γ2 in the ob/ob mouse model of non-insulin dependent diabetes mellitus. Mol Cell Biochem 2001 2241 [Internet]. 2001 [cited 2022 Sep 30];224(1):29–37. Available from: https://link.springer.com/article/10.1023/A:1011927113563

149. Gavrilova O, Haluzik M, Matsusue K, Cutson JJ, Johnson L, Dietz KR, et al. Liver Peroxisome Proliferator-activated Receptor γ Contributes to Hepatic Steatosis, Triglyceride Clearance, and Regulation of Body Fat Mass. J Biol Chem. 2003 Sep 5;278(36):34268–76.

150. Inoue M, Ohtake T, Motomura W, Takahashi N, Hosoki Y, Miyoshi S, et al. Increased expression of PPARγ in high fat diet-induced liver steatosis in mice. Biochem Biophys Res Commun. 2005 Oct 14;336(1):215–22.

151. Greenstein AW, Majumdar N, Yang P, Subbaiah P V., Kineman RD, Cordoba-Chacon J. Hepatocyte-specific, PPARγ-regulated mechanisms to promote steatosis in adult mice. J Endocrinol [Internet]. 2017 Jan 1 [cited 2022 Sep 30];232(1):107–21. Available from: https://joe.bioscientifica.com/view/journals/joe/232/1/107.xml

152. Yamazaki T, Shiraishi S, Kishimoto K, Miura S, Ezaki O. An increase in liver PPARγ2 is an initial event to induce fatty liver in response to a diet high in butter: PPARγ2 knockdown improves fatty liver induced by high-saturated fat. J Nutr Biochem. 2011 Jun 1;22(6):543–53.

153. Boelsterli UA, Bedoucha M. Toxicological consequences of altered peroxisome proliferator-activated receptor γ (PPARγ) expression in the liver: insights from models of obesity and type 2 diabetes. Biochem Pharmacol. 2002 Jan 1;63(1):1–10.

154. Wang W, Xu MJ, Cai Y, Zhou Z, Cao H, Mukhopadhyay P, et al. Inflammation is independent of steatosis in a murine model of steatohepatitis. Hepatology [Internet]. 2017 Jul 1 [cited 2022 Oct 5];66(1):108–23. Available from: https://onlinelibrary.wiley.com/doi/full/10.1002/hep.29129

155. Borniquel S, Jädert C, Lundberg JO. Dietary Conjugated Linoleic Acid Activates PPARγ and the Intestinal Trefoil Factor in SW480 Cells and Mice with Dextran Sulfate Sodium-Induced Colitis. J Nutr [Internet]. 2012 Dec 1 [cited 2022 Sep 22];142(12):2135–40. Available from: https://academic.oup.com/jn/article/142/12/2135/4630760

156. Shimada T, Koitabashi A, Kuniyoshi T, Hashimoto T, Yoshiura K, Yoneda M, et al. Up-regulation of TFF expression by PPARγ ligands in gastric epithelial cells. Aliment Pharmacol Ther [Internet]. 2003 Jul [cited 2022 Sep 23];18(1):119–25. Available from: https://onlinelibrary.wiley.com/doi/full/10.1046/j.1365-2036.18.s1.14.x

157. Kern L, Mittenbühler MJ, Vesting AJ, Ostermann AL, Wunderlich CM, Wunderlich FT. Obesity-induced TNFα and IL-6 signaling: The missing link between obesity and inflammation- driven liver and colorectal cancers. Cancers (Basel). 2019;11(1):1–21.

158. Matthews VB, Allen TL, Risis S, Chan MHS, Henstridge DC, Watson N, et al. Interleukin-6-deficient mice develop hepatic inflammation and systemic insulin resistance. Diabetologia. 2010;53(11):2431–41.

159. Xin Y, Shang X, Sun X, Liu Y, Xu G, Xue G. Trefoil Factor 3 Inhibits Thyroid Cancer Cell Progression Related to IL-6/JAK/STAT3 Signaling Pathway. Evidence-based Complement Altern Med. 2021;2021.

160. Chwieralski CE, Reinhold D, Thim L, Hoffmann W. Protein Kinase C and ERK Activation Are Required for TFF- peptide-stimulated Bronchial Epithelial Cell Migration and Tumor Necrosis Factor-α-induced Interleukin-6 (IL-6) and IL-8 Secretion. J Biol Chem. 2002 May 24;277(21):18440–6.

161. Lebeaupin C, Vallée D, Hazari Y, Hetz C, Chevet E, Bailly-Maitre B. Endoplasmic reticulum stress signalling and the pathogenesis of non-alcoholic fatty liver disease. J Hepatol. 2018 Oct 1;69(4):927–47.

162. Torres L, Karam SM, Wendling C, Chenard M, Kershenobich D, Tomasetto C, et al. TreFoil Factor 1 (TFF1 / pS2) Deficiency Activates the Unfolded Protein Response. 2002;8(5):273–82.

163. Baus-loncar M, Schmid J, Lalani E, Goodlad RA, Stamp GWH, Blin N. Cellular Physiology and Biochemistr y Biochemistry Trefoil Factor 2 (Tff2) Deficiency in Murine Digestive Tract Influences the Immune System. 2005;31–42.

164. Desmots F, Russell HR, Michel D, Mckinnon PJ. Scythe Regulates Apoptosis-inducing Factor Stability during. 2008;283(6):3264–71.

165. Ren C, Dokter-fokkens J, Lozano SF, Zhang Q, Haan BJ De, Zhang H, et al. Lactic Acid Bacteria May Impact Intestinal Barrier Function by Modulating Goblet Cells. 2018;1700572:1–14.

166. Asada R, Saito A, Kawasaki N, Kanemoto S, Iwamoto H, Oki M, et al. The Endoplasmic Reticulum Stress Transducer OASIS Is involved in the Terminal Differentiation of Goblet Cells in the Large Intestine * □. 2012;287(11):8144–53.

167. Park SM, Kang T Il, So JS. Roles of XBP1s in transcriptional regulation of target genes. Biomedicines. 2021;9(7):1–26.

168. Wang S, Kaufman RJ. The impact of the unfolded protein response on human disease. 2012;197(7):857–67.

169. Lee AH, Scapa EF, Cohen DE, Glimcher LH. Regulation of hepatic lipogenesis by the transcription factor XBP1. Science (80-) [Internet]. 2008 Jun 13 [cited 2021 Jun 29];320(5882):1492–6. Available from: http://science.sciencemag.org/

170. Zhang Z, Qian Q, Li M, Shao F, Ding WX, Lira VA, et al. The unfolded protein response regulates hepatic autophagy by sXBP1-mediated activation of TFEB. Autophagy. 2020;17(8):1–15.

171. Herrema H, Zhou Y, Zhang D, Lee J, Hernandez MAS, Shulman GI, et al. XBP1s is an anti-lipogenic protein∗?s. J Biol Chem. 2016;291(33):17394–404.

172. Park SW, Zhou Y, Lee J, Lu A, Sun C, Chung J, et al. The regulatory subunits of PI3K, p85α and p85B, interact with XBP-1 and increase its nuclear translocation. Nat Med. 2010;16(4):429–37.

173. Zhou Y, Lee J, Reno CM, Sun C, Park SW, Chung J, et al. Regulation of glucose homeostasis through a XBP-1-FoxO1 interaction. Nat Med [Internet]. 2011 Mar 13 [cited 2021 Jun 29];17(3):356–65. Available from: https://www.nature.com/articles/nm.2293

174. Park SW, Herrema H, Salazar M, Cakir I, Cabi S, Basibuyuk Sahin F, et al. BRD7 regulates XBP1s' activity and glucose homeostasis through its interaction with the regulatory subunits of PI3K. Cell Metab. 2014;20(1):73–84.

175. Lee J, Sun C, Zhou Y, Lee J, Gokalp D, Herrema H, et al. P38 MAPK-mediated regulation of Xbp1s is crucial for glucose homeostasis. Nat Med. 2011;17(10):1251–60.

176. Cortex P. Esearch rticle. 2003;302(November):1181–5.

177. Zhang K, Wang S, Malhotra J, Hassler JR, Back SH, Wang G, et al. The unfolded protein response transducer lRE1Î ± prevents ER stress-induced hepatic steatosis. EMBO J. 2011;30(7):1357–75.

178. Morán-Salvador E, Titos E, Rius B, González-Périz A, García-Alonso V, López-Vicario C, et al. Cell-specific PPARγ deficiency establishes anti-inflammatory and anti-fibrogenic properties for this nuclear receptor in non-parenchymal liver cells. J Hepatol [Internet]. 2013 Nov 1 [cited 2022 Oct 4];59(5):1045–53. Available from: http://www.journal-of-hepatology.eu/article/S0168827813004406/fulltext

179. Marion-Letellier R, Butler M, Déchelotte P, Playford RJ, Ghosh S. Comparison of cytokine modulation by natural peroxisome proliferator–activated receptor γ ligands with synthetic ligands in intestinal-like Caco-2 cells and human dendritic cells—potential for dietary modulation of peroxisome proliferator–activated recept. Am J

Clin Nutr [Internet]. 2008 Apr 1 [cited 2022 Oct 1];87(4):939–48. Available from: https://academic.oup.com/ajcn/article/87/4/939/4633319

180. Liu Y, Shi J, Lu J, Meng G, Zhu H, Hou Y, et al. Activation of peroxisome proliferator-activated receptor-γ potentiates pro-inflammatory cytokine production, and adrenal and somatotropic changes of weaned pigs after Escherichia coli lipopolysaccharide challenge. http://dx.doi.org/101177/1753425908102014 [Internet]. 2009 May 27 [cited 2022 Oct 1];15(3):169–78. Available from: https://journals.sagepub.com/doi/10.1177/1753425908102014

181. Wanichkul T, Han S, Huang RP, Sidell N. Cytokine regulation by peroxisome proliferator-activated receptor gamma in human endometrial cells. Fertil Steril. 2003 Mar 1;79(3 SUPPL. 1):763–9.

182. Heming M, Gran S, Jauch SL, Fischer-Riepe L, Russo A, Klotz L, et al. Peroxisome proliferator-activated receptor-γ modulates the response of macrophages to lipopolysaccharide and glucocorticoids. Front Immunol. 2018 May 8;9(MAY):893.

183. Patzer A, Zhao Y, Stöck I, Gohlke P, Herdegen T, Culman J. Peroxisome proliferator-activated receptorsγ (PPARγ) differently modulate the interleukin-6 expression in the peri-infarct cortical tissue in the acute and delayed phases of cerebral ischaemia. Eur J Neurosci [Internet]. 2008 Nov 1 [cited 2022 Oct 1];28(9):1786–94. Available from: https://onlinelibrary.wiley.com/doi/full/10.1111/j.1460-9568.2008.06478.x

184. Peng Y, Liu H, Liu F, Wang H, Liu Y, Duan S. Inhibitory effect of PPAR-Gamma activator on IL-6 and mPGES protein expression in PBMC induced by homocysteine. Hemodial Int [Internet]. 2005 Oct [cited 2022 Oct 4];9(SUPPL. 1):S15–20. Available from: https://onlinelibrary.wiley.com/doi/full/10.1111/j.1542-4758.2005.01165.x

185. Li L, Huang C, Yin H, Zhang X, Wang D, Ma C, et al. Interleukin-6 mediated exercise-induced alleviation of adiposity and hepatic steatosis in mice. BMJ Open Diabetes Res Care [Internet]. 2021 Apr 1 [cited 2022 Oct 4];9(1):e001431. Available from: https://drc.bmj.com/content/9/1/e001431

186. PITULIS NEA, PAPAGEORGIOU E, TENTA R, LEMBESSIS P, KOUTSILIERIS M. IL-6 and PPARγ Signalling in Human PC-3 Prostate Cancer Cells. Anticancer Res [Internet]. 2009 Jun 1;29(6):2331 LP – 2337. Available from: http://ar.iiarjournals.org/content/29/6/2331.abstract

187. Zhang Y, Huo Y, He W, Liu S, Li H, Li L. Visfatin is regulated by interleukin-6 and affected by the PPAR-γ pathway in BeWo cells. Mol Med Rep [Internet]. 2019 Jan 1 [cited 2022 Oct 4];19(1):400–6. Available from: http://www.spandidos-publications.com/10.3892/mmr.2018.9671/abstract

188. Maganti A V., Tersey SA, Syed F, Nelson JB, Colvin SC, Maier B, et al. Peroxisome Proliferator-activated Receptor-γ Activation Augments the β-Cell Unfolded Protein Response and Rescues Early Glycemic Deterioration and β Cell Death in Non-obese Diabetic Mice. J Biol Chem. 2016 Oct 21;291(43):22524–33.

189. Cho YM, Kwak SN, Joo NS, Kim DH, Lee AH, Kim KS, et al. X-box binding protein 1 is a novel key regulator of peroxisome proliferator-activated receptor γ2. FEBS J [Internet]. 2014 Nov 1 [cited 2022 Oct 1];281(22):5132–46. Available from: https://onlinelibrary.wiley.com/doi/full/10.1111/febs.13052

190. Cho YM, Kim DH, Lee KH, Jeong SW, Kwon OJ. The IRE1α-XBP1s pathway promotes insulin-stimulated glucose uptake in adipocytes by increasing PPARγ activity. Exp Mol Med 2018 508 [Internet]. 2018 Aug 15 [cited 2022 Oct 4];50(8):1–15. Available from: https://www.nature.com/articles/s12276-018-0131-0

191. Ayaub EA, Tandon K, Padwal M, Imani J, Patel H, Dubey A, et al. IL-6 mediates ER expansion during hyperpolarization of alternatively activated macrophages. Immunol Cell Biol [Internet]. 2019 Feb 1 [cited 2022 Oct 5];97(2):203–17. Available from: https://onlinelibrary.wiley.com/doi/full/10.1111/imcb.12212

192. Savic S, Ouboussad L, Dickie LJ, Geiler J, Wong C, Doody GM, et al. TLR dependent XBP-1 activation induces an autocrine loop in rheumatoid arthritis synoviocytes. J Autoimmun. 2014 May 1;50:59–66.

193. Wen XY, Stewart AK, Sooknanan RR, Henderson G, Hawley T, Reimold AM, et al.

Identification of c-myc promoter-binding protein and X-box binding protein 1 as interleukin-6 target genesin human multiple myeloma cells. Int J Oncol [Internet]. 1999 Jul 1 [cited 2022 Oct 5];15(1):173–8. Available from: http://www.spandidos-publications.com/10.3892/ijo.15.1.173/abstract

194. Fang P, Xiang L, Huang S, Jin L, Zhou G, Zhuge L, et al. IRE1α-XBP1 signaling pathway regulates IL-6 expression and promotes progression of hepatocellular carcinoma. Oncol Lett [Internet]. 2018 Oct 1 [cited 2022 Oct 5];16(4):4729–36. Available from: http://www.spandidos-publications.com/10.3892/ol.2018.9176/abstract

195. Bohnert KR, Goli P, Roy A, Sharma AK, Xiong G, Gallot YS, et al. The Toll-Like Receptor/MyD88/XBP1 Signaling Axis Mediates Skeletal Muscle Wasting during Cancer Cachexia. Mol Cell Biol [Internet]. 2019 Aug [cited 2022 Oct 5];39(15). Available from: https://journals.asm.org/doi/10.1128/MCB.00184-19

196. Martinon F, Chen X, Lee AH, Glimcher LH. TLR activation of the transcription factor XBP1 regulates innate immune responses in macrophages. Nat Immunol 2010 115 [Internet]. 2010 Mar 28 [cited 2022 Oct 5];11(5):411–8. Available from: https://www.nature.com/articles/ni.1857

197. Argemí J, Kress TR, Chang HCY, Ferrero R, Bértolo C, Moreno H, et al. X-box Binding Protein 1 Regulates Unfolded Protein, Acute-Phase, and DNA Damage Responses During Regeneration of Mouse Liver. Gastroenterology. 2017 Apr 1;152(5):1203-1216.e15.

198. Chen C, Zhang X. IRE1α-XBP1 pathway promotes melanoma progression by regulating IL-6/STAT3 signaling. J Transl Med [Internet]. 2017 Feb 21 [cited 2022 Oct 5];15(1):1–9. Available from: https://translational-medicine.biomedcentral.com/articles/10.1186/s12967-017-1147-2

199. Lyu X, Zhang M, Li G, Cai Y, Li G, Qiao Q. Interleukin-6 production mediated by the IRE1-XBP1 pathway confers radioresistance in human papillomavirus-negative oropharyngeal carcinoma. Cancer Sci [Internet]. 2019 Aug 1 [cited 2022 Oct 5];110(8):2471–84. Available from:

https://onlinelibrary.wiley.com/doi/full/10.1111/cas.14094

200. Niederreiter L, Fritz TMJ, Adolph TE, Krismer AM, Offner FA, Tschurtschenthaler M, et al. ER stress transcription factor Xbp1 suppresses intestinal tumorigenesis and directs intestinal stem cells. J Exp Med [Internet]. 2013 Sep 23 [cited 2022 Oct 5];210(10):2041–56. Available from: www.jem.org/cgi/doi/10.1084/jem.20122341

201. Mo ZT, Zheng J, Liao Y ling. Icariin inhibits the expression of IL-1β, IL-6 and TNF-α induced by OGD/R through the IRE1/XBP1s pathway in microglia. https://doi.org/101080/1388020920211991959 [Internet]. 2021 [cited 2022 Oct 5];59(1):1473–9. Available from: https://www.tandfonline.com/doi/abs/10.1080/13880209.2021.1991959

202. Iwakoshi NN, Lee AH, Vallabhajosyula P, Otipoby KL, Rajewsky K, Glimcher LH. Plasma cell differentiation and the unfolded protein response intersect at the transcription factor XBP-1. Nat Immunol 2003 44 [Internet]. 2003 Mar 3 [cited 2022 Oct 5];4(4):321–9. Available from: https://www.nature.com/articles/ni907

203. Choi S, Snider JM, Olakkengil N, Lambert JM, Anderson AK, Ross-Evans JS, et al. Myristate-induced endoplasmic reticulum stress requires ceramide synthases 5/6 and generation of C14-ceramide in intestinal epithelial cells. FASEB J [Internet]. 2018 Oct 1 [cited 2022 Oct 5];32(10):5724–36. Available from: https://onlinelibrary.wiley.com/doi/full/10.1096/fj.201800141R

204. Xu G, Liu K, Anderson J, Patrene K, Lentzsch S, Roodman GD, et al. Expression of XBP1s in bone marrow stromal cells is critical for myeloma cell growth and osteoclast formation. Blood [Internet]. 2012 May 3 [cited 2022 Oct 5];119(18):4205–14. Available from: https://ashpublications.org/blood/article/119/18/4205/30092/Expression-of-XBP1s-in-bone-marrow-stromal-cells

205. Sun Y, Wang L, Zhou Y, Mao X, Deng X. Human Trefoil Factor 3 induces the transcription of its own promoter through STAT3. Sci Reports 2016 61 [Internet]. 2016 Jul 25 [cited 2022 Oct 2];6(1):1–8. Available from: https://www.nature.com/articles/srep30421

206. Cummings CJ, Martin TR, Frevert CW, Quan JM, Wong VA, Mongovin SM, et al. Expression and function of the chemokine receptors CXCR1 and CXCR2 in sepsis. J Immunol. 1999 Feb;162(4):2341–6.

207. Hwang S, Yun H, Moon S, Cho YE, Gao B. Role of Neutrophils in the Pathogenesis of Nonalcoholic Steatohepatitis. Front Endocrinol (Lausanne). 2021 Oct 11;12:1318.

208. Zhang K, Kaufman RJ. From endoplasmic-reticulum stress to the inflammatory response. Nat 2008 4547203 [Internet]. 2008 Jul 1 [cited 2022 Oct 10];454(7203):455–62. Available from: https://www.nature.com/articles/nature07203

209. Ferreira BL, Ramirez-Moral I, Otto NA, Salomão R, de Vos AF, van der Poll T. The PPAR-γ agonist pioglitazone exerts proinflammatory effects in bronchial epithelial cells during acute Pseudomonas aeruginosa pneumonia. Clin Exp Immunol [Internet]. 2022 May 12 [cited 2022 Oct 5];207(3):370–7. Available from: https://academic.oup.com/cei/article/207/3/370/6494535

210. Keshamouni VG, Arenberg DA, Reddy RC, Newstead MJ, Anthwal S, Standiford TJ. PPAR-γ Activation Inhibits Angiogenesis by Blocking ELR+CXC Chemokine Production in Non-small Cell Lung Cancer. Neoplasia. 2005 Mar 1;7(3):294–301.

211. Remels AHV, Langen RCJ, Gosker HR, Russell AP, Spaapen F, Voncken JW, et al. PPARγ inhibits NF-κB-dependent transcriptional activation in skeletal muscle. Am J Physiol - Endocrinol Metab [Internet]. 2009 Jul [cited 2022 Oct 5];297(1):174–83. Available from: https://journals.physiology.org/doi/10.1152/ajpendo.90632.2008

212. Weisberg SP, Hunter D, Huber R, Lemieux J, Slaymaker S, Vaddi K, et al. CCR2 modulates inflammatory and metabolic effects of high-fat feeding. J Clin Invest [Internet]. 2006 Jan 4 [cited 2022 Oct 6];116(1):115–24. Available from: http://www.jci.org

213. Bartneck M, Koppe C, Fech V, Warzecha KT, Kohlhepp M, Huss S, et al. Roles of

CCR2 and CCR5 for Hepatic Macrophage Polarization in Mice With Liver Parenchymal Cell-Specific NEMO Deletion. Cell Mol Gastroenterol Hepatol. 2021 Jan 1;11(2):327–47.

214. Barlic J, Zhang Y, Foley JF, Murphy PM. Oxidized lipid-driven chemokine receptor switch, CCR2 to CX3CR1, mediates adhesion of human macrophages to coronary artery smooth muscle cells through a peroxisome proliferator-activated receptor γ-dependent pathway. Circulation [Internet]. 2006 Aug 22 [cited 2022 Oct 5];114(8):807–19. Available from: https://www.ahajournals.org/doi/abs/10.1161/CIRCULATIONAHA.105.602359

215. Han KH, Chang MK, Boullier A, Green SR, Li A, Glass CK, et al. Oxidized LDL reduces monocyte CCR2 expression through pathways involving peroxisome proliferator–activated receptor γ. J Clin Invest. 2000 Sep 15;106(6):793–802.

216. Chen Y, Green SR, Ho J, Li A, Almazan F, Quehenberger O. The mouse CCR2 gene is regulated by two promoters that are responsive to plasma cholesterol and peroxisome proliferator-activated receptor γ ligands. Biochem Biophys Res Commun. 2005 Jun 24;332(1):188–93.

217. Haim L Ben, Carrillo-de Sauvage MA, Ceyzériat K, Escartin C. Elusive roles for reactive astrocytes in neurodegenerative diseases. Front Cell Neurosci. 2015 Aug 3;9(AUGUST):278.

218. Ito D, Imai Y, Ohsawa K, Nakajima K, Fukuuchi Y, Kohsaka S. Microglia-specific localisation of a novel calcium binding protein, Iba1. Mol Brain Res. 1998 Jun 1;57(1):1–9.

219. Jennes L. Cytology of the Central Nervous System. Conn's Transl Neurosci. 2017 Jan 1;1–10.

220. Colombo E, Farina C. Astrocytes: Key Regulators of Neuroinflammation. Trends Immunol. 2016 Sep 1;37(9):608–20.

221. Koga S, Kojima A, Kuwabara S, Yoshiyama Y. Immunohistochemical analysis of tau phosphorylation and astroglial activation with enhanced leptin receptor

expression in diet-induced obesity mouse hippocampus. Neurosci Lett. 2014 Jun 13;571:11–6.

222. Yu M, Huang H, Dong S, Sha H, Wei W, Liu C. High mobility group box-1 mediates hippocampal inflammation and contributes to cognitive deficits in high-fat high-fructose diet-induced obese rats. Brain Behav Immun. 2019 Nov 1;82:167–77.

223. Heneka MT, Kummer MP, Latz E. Innate immune activation in neurodegenerative disease. Nat Rev Immunol 2014 147 [Internet]. 2014 Jun 25 [cited 2022 Oct 11];14(7):463–77. Available from: https://www.nature.com/articles/nri3705

224. Tsai SF, Wu HT, Chen PC, Chen YW, Yu M, Wang TF, et al. High-fat diet suppresses the astrocytic process arborization and downregulates the glial glutamate transporters in the hippocampus of mice. Brain Res. 2018 Dec 1;1700:66–77.

225. Vinuesa A, Bentivegna M, Calfa G, Filipello F, Pomilio C, Bonaventura MM, et al. Early Exposure to a High-Fat Diet Impacts on Hippocampal Plasticity: Implication of Microglia-Derived Exosome-like Extracellular Vesicles. Mol Neurobiol [Internet]. 2019 Jul 1 [cited 2022 Oct 11];56(7):5075–94. Available from: https://link.springer.com/article/10.1007/s12035-018-1435-8

226. Boitard C, Etchamendy N, Sauvant J, Aubert A, Tronel S, Marighetto A, et al. Juvenile, but not adult exposure to high-fat diet impairs relational memory and hippocampal neurogenesis in mice. Hippocampus [Internet]. 2012 Nov [cited 2022 Oct 11];22(11):2095–100. Available from: https://pubmed.ncbi.nlm.nih.gov/22593080/

227. Zhuang H, Yao X, Li H, Li Q, Yang C, Wang C, et al. Long-term high-fat diet consumption by mice throughout adulthood induces neurobehavioral alterations and hippocampal neuronal remodeling accompanied by augmented microglial lipid accumulation. Brain Behav Immun. 2022 Feb 1;100:155–71.

228. Kang EB, Koo JH, Jang YC, Yang CH, Lee Y, Cosio-Lima LM, et al. Neuroprotective Effects of Endurance Exercise Against High-Fat Diet-Induced Hippocampal

Neuroinflammation. J Neuroendocrinol [Internet]. 2016 May 1 [cited 2022 Oct 11];28(5). Available from: https://pubmed.ncbi.nlm.nih.gov/26991447/

229. Ledreux A, Wang X, Schultzberg M, Granholm AC, Freeman LR. Detrimental effects of a high fat/high cholesterol diet on memory and hippocampal markers in aged rats. Behav Brain Res. 2016 Oct 1;312:294–304.

230. Jeon BT, Jeong EA, Shin HJ, Lee Y, Lee DH, Kim HJ, et al. Resveratrol Attenuates Obesity-Associated Peripheral and Central Inflammation and Improves Memory Deficit in Mice Fed a High-Fat Diet. Diabetes [Internet]. 2012 Jun [cited 2022 Oct 11];61(6):1444. Available from: /pmc/articles/PMC3357272/

231. Soria Lopez JA, González HM, Léger GC. Alzheimer's disease. Handb Clin Neurol. 2019 Jan 1;167:231–55.

232. Sutphen CL, McCue L, Herries EM, Xiong C, Ladenson JH, Holtzman DM, et al. Longitudinal decreases in multiple cerebrospinal fluid biomarkers of neuronal injury in symptomatic late onset Alzheimer's disease. Alzheimer's Dement [Internet]. 2018 Jul 1 [cited 2022 Oct 11];14(7):869–79. Available from: https://onlinelibrary.wiley.com/doi/full/10.1016/j.jalz.2018.01.012

233. Brinkmalm A, Brinkmalm G, Honer WG, Frölich L, Hausner L, Minthon L, et al. SNAP-25 is a promising novel cerebrospinal fluid biomarker for synapse degeneration in Alzheimer's disease. Mol Neurodegener [Internet]. 2014 Nov 23 [cited 2022 Oct 11];9(1):53. Available from: https://molecularneurodegeneration.biomedcentral.com/articles/10.1186/1750-1326-9-53

234. Schmued LC, Albertson C, Slikker W. Fluoro-Jade: a novel fluorochrome for the sensitive and reliable histochemical localization of neuronal degeneration. Brain Res. 1997 Mar 14;751(1):37–46.

235. Schmued LC, Stowers CC, Scallet AC, Xu L. Fluoro-Jade C results in ultra high resolution and contrast labeling of degenerating neurons. Brain Res. 2005 Feb 21;1035(1):24–31.

236. Fluoro-Jade C (FJC) Ready-to-Dilute Staining Kit for identifying Degenerating Neurons [Internet]. [cited 2022 Nov 8]. Available from: https://www.biosensis.com/fluoro-jade-c-fjc-ready-to-dilute-staining-kit-for-identifying-degenerating-neurons.html

237. Kniewallner KM, Wenzel D, Humpel C. Thiazine Red+ platelet inclusions in Cerebral Blood Vessels are first signs in an Alzheimer's Disease mouse model. Sci Rep [Internet]. 2016;6(1):28447. Available from: https://doi.org/10.1038/srep28447

7 Summary

Tff3 is a small secretory protein ubiquitous in distribution and function. It is secreted mainly by goblet cells of the intestine, where it plays a role in mucosal restitution, but has been detected in most organs, including liver and brain. It is involved in several pathologies, including metabolic and neurological disorders. A reduction of Tff3 in the liver of Tally-Ho mice, models of "diabesity," was found in the early stages of the disease. This was later confirmed in other models of obesity. Many studies showed an effect of Tff3 on some features of the metabolic disorder. Deregulation of Tff3 was also found in neurodegenerative diseases. This was most striking in the CSF of AD patients, where it was markedly reduced and associated with the severity of brain atrophy and ventricular expansion. Tff3 showed a neuroprotective effect, and ability to cross blood-brain barrier.

It is known from previous research that HFD ingestion induces features of the metabolic syndrome, such as impaired glucose metabolism and insulin signaling and hepatic steatosis. In addition, it has been shown that such exposure can cause changes in the brain ranging from neuroinflammation to neurodegeneration

In this study, newly developed congenic *Tff3-/-* mice on a C57Bl/6N genetic background and appropriate WT controls were exposed to an 8-month HFD treatment. During this time, they were subjected to metabolic tests, while serum, liver, and brain were collected at the end of the experiment and analyzed.

HFD induced *Tff3* reduction and some features of the metabolic syndrome. Tff3 knockout mice generally exhibited a protective metabolic phenotype. This was reflected in better glucose utilization in metabolic tests, lower blood biochemical parameters associated with fatty liver, an improved fatty liver phenotype, and a favorable gene expression profile of markers for relevant pathophysiological processes

The hippocampus of all animals exposed to HFD showed some degree of inflammation. Differences in the levels of major cell types between genotypes were noted in only in the animals on SD, where the male Tff3-/- mice showed slightly lower levels of microglia and neuron protein markers. HFD treatment counterbalanced these differences.

The results reported in this dissertation identify Tff3 as an important player in metabolic regulation and provide the basis for further research into its role and a possible mechanistic explanation for the observed phenotype.

8 Sažetak

8.1 Uvod

Trefoil factor 3 je mali sekretorni protein sa širokom distribucijom i funkcijom. Uglavnom se izlučuje iz crijevnih vrčastih stanica gdje ima ulogu u restituciji sluznice, ali je otkriven u većini organa, uključujući jetru i mozak. Uključen je u razne patologije, uključujući metaboličke i neurološke poremećaje. Smanjenje Tff3 u jetri Tally Ho miševa, modela "dijabetesa", primijećeno je u ranim fazama poremećaja, što je kasnije potvrđeno u drugim modelima pretilosti. Mnoga su istraživanja pokazala učinak Tff3 na značajke metaboličkog poremećaja. Deregulacija Tff3 zabilježena je i kod neurodegenerativnih bolesti. Ponajviše u likvoru bolesnika s AD-om, gdje je bio izrazito smanjen i povezan s razinom atrofije mozga i ventrikularne ekspanzije. Tff3 je pokazao neuroprotektivni učinak i može prijeći krvno-moždanu barijeru.

Dobro je poznata činjenica iz prijašnjih istraživanja da visokomasna prehrana izaziva značajke metaboličkog sindroma, kao što su poremećeni metabolizam glukoze i inzulinska signalizacija, te steatoza jetre. Osim toga, pokazalo se da takav stres može izazvati promjene u mozgu, u rasponu od neuroinflamacije do neurodegeneracije.

8.2 Cilj istraživanja

Cilj ovog istraživanja bio je miševima inducirati kronični stres pomoću visokomasne prehrane s ciljem uzrokovanja obilježja metaboličkog sindroma i promjena u mozgu i pratiti odgovor. Krajnji cilj je bio pratiti ima li razlika u odgovoru između *Tff3*-/- miševa u odnosu na miševe divljeg tipa na razini metabolizma i integriteta jetre i mozga kao centralnih organa metaboličkih i neurodegenerativnih poremećaja.

8.3 Materijali i metode

U ovom istraživanju korišten je novorazvijeni kongenični *Tff3*-/- mišji soj na C57Bl/6N genetskoj pozadini i odgovarajuće WT kontrole. Životinje oba spola hranjene su visokomasnom hranom od odvajanja od majke s 4 tjedna do žrtvovanja s 40 tjedana. U svrhu kontrole jesu li promatrane promjene ovisne o odgovoru na stres ili uzrokovane samim nedostatkom Tff3 skupina životinja jednakog sastava hranjena je standardnom prehranom. Životinje su podvrgnute metaboličkim testovima (test tolerancije glukoze ili inzulina) na polovici i kraju pokusa. Nakon 8 mjeseci visokomasne prehrane životinje su žrtvovane te su prikupljeni serum i tkiva jetre i mozga za daljnje analize. U serumu su određeni standardni biokemijski parametri. Jetra je analizirana histomorfološki, određen je sastav i količina masti pomoću HPLC-a i genski profil markera metabolizma masnih kiselina, upale, apoptoze, stresa endoplazmatskog retikuluma i oksidativnog stresa.Ti procesi relevantni su i deregulirani u većini patofizioloških događaja u organizmu. U jetri životinja divljeg tipa provjerena je razina ekspresije Tff3. Mozak, točnije hipokampus, je proučavan uz pomoć imunofluorescencije i kvantifikacije Western blot metodom proteina markera astrocita, mikroglija i neurona u hipokampusu. Dodatno, kvantifikacijom Snap 25 proteina provjeren je integritet sinapsi, a bojanjem Fluoro Jade C bojom procijenjena je razina neurodegeneracije u hipokampusu.

8.4 Rezultati

Na polovici pokusa pri vaganju, mužjaci *Tff3*-/- genotipa težili su znatno manje nego WT mužjaci. Također su se pokazali bolji na testu tolerancije glukoze. Daljnjim unosom masne hrane približili su se WT mužjacima u spomenutim vrijednostima. Ženke nisu pokazivale značajne razlike. Visokomasna prehrana uzrokovala je smanjenje Tff3 ekspresije u jetri WT mužjaka, dok je u jetri ženki ekspresija Tff3 bila zanemariva bez obzira na prehranu. U vidu metabolizma masti *Tff3*-/- miševi općenito su pokazali povoljniji metabolički fenotip. *Tff3*-/- miševi oba spola pokazali su smanjeni masni fenotip

u jetri i morfološki i količinom masti u jetri. Kod mužjaka je to bilo izraženije i dodatno praćeno smanjenim biokemijskim parametrima koju ukazuju na oštećenje jetre. Životinje oba spola pokazale su smanjenje Pparγ ekspresije. Genski profil markera ostalih stresom induciranih procesa bili su različiti kod mužjaka i ženki. U hipokampusu su primijećene promjene u vidu neuroinflamacije, bez nekih značajnih razlika.među genotipovima. Interesantna je činjenica da su kod mužjaka na standardnoj prehrani postojale razlike koje su uklonjene masnom prehranom. Iba1 i NeuN, makreri mikroglija i neurona bili su sniženi u hipokampusu *Tff3-/-* mužjaka. Masna prehrana je uzrokovala je degeneraciju neurona koja je izostala kod životinja na standardnoj prehrani, kao efekt starenja .

8.5 Rasprava i zaključak.

Analizom dobivenih rezultata može se sa sigurnošću potvrditi uloga Tff3 proteina u metabolizmu. U ovom istraživanju u kontekstu metabolizma nedostatak Tff3 pokazao je zaštitni učinak, iako prijašnja istraživanja mahom ukazuju na zaštitni učinak njegove povećane ekspresije ili sistemske primjene. Međutim, ovo istraživanje je rađeno po prvi put na *Tff3*-/- mišu čistog genetskog porijekla čime je otklonjena mogućnost utjecaja potencijalne heterozigotnosti i mutacija relevantnih za metabolizam. Nadalje, većina dosadašnjih istraživanja je rađena specifičnim stišavanjem ili pojačavanjem ekspresije u jednom organu ili kulturi stanica dok je kod ovog moda riječ o nedostatku Tff3 na razini cijelog organizma. Ako se uzme u obzir njegova pojavnost u krvi i već pokazana mogućnost djelovanja na udaljenim mjestima, moguće je da je interakcija između različitih sustava dio uzroka različitih nalaza. Također treba uzeti u obzir neizmjernu kompleksnost metabolizma i faktora koji utječu na njega. I u ovom istraživanju vidjelo se da su neke razlike koje su postojale na pola puta do kraja pokusa nestale. S druge stane genotipske razlike u mozgu pokazale su se relativno suptilnima u stresnom okruženju, a postoje u standardnim uvjetima. U cijeloj toj interakciji sudjeluje niz faktora koji se vjerojatno uključuju i isključuju u ovisnosti o vanjskim faktorima. Dodatno ponovo je pokazan utjecaj spolnog dimorfizma, ne samo na djelovanje Tff3 nego i na njegovi ekspresiju u jetri. Sve

u svemu, ovo istraživanje još jednom je pokazalo važnu ulogu Tff3 u organizmu u predstavlja dobre temelje za preciznije usmjeravanje na mehanistička objašnjenja pokazanog fenotipa. Dodatno, primijećene spolne razlike i različiti nalazi ovog od dosadašnjih istraživanja ukazuju na važnost uključivanja oba spola u biomedicinska istraživanja i detaljnog opisivanja pokusnih subjekata.